Geology and Geophysics

Early Triassic fossil plants from the Transantarctic Mountains

Gregory J. Retallack, *Department of Geological Sciences, University of Oregon*

Although fossil plants of Triassic and Permian age have been known from the Transantarctic Mountains since 1914 and continue to be collected actively (Bose, Taylor, and Taylor 1990) and early Triassic vertebrates also are known (Retallack and Hammer 1996), until now no fossil plants of Early Triassic age have been reported from the Transantarctic Mountains other than wood and root traces. Assemblages dominated by *Dicroidium zuberi* near Mount Bumstead in the central Transantarctic Mountains (figure 1; Townrow 1967a) are superficially similar to Early Triassic floras, but associated fossil plants such as Yabeiella (Boucher 1995) indicate a Late Triassic age (Retallack 1977; Bose et al. 1990). Supposed "Glossopteris" (more likely Gontriglossa or Linguifolium) and *Dicroidium odontopteroides* "from beds high on Allan Nunatak" (Rigby and Schopf 1969) are from the Middle Triassic Lashly Formation (Bose et al. 1990; Retallack, Krull, and Robinson 1995). Recently, an Early Triassic flora was reported from the Prince Charles Mountains of East Antarctica (McLoughlin, Lindström, and Drinnan 1997). This account reports other Early Triassic plants from the central Transantarctic Mountains.

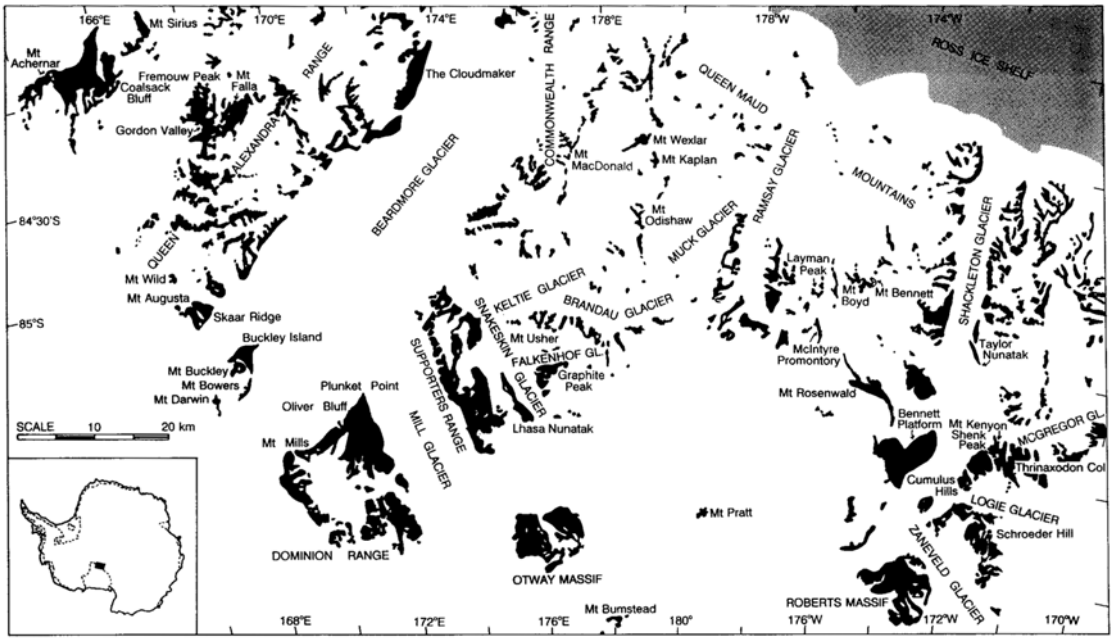

Figure 1. Location of Early Triassic fossil plant localities in the Beardmore and Shackleton Glacier areas of the central Transantarctic Mountains.

Newly discovered plant fragments from the downfaulted block east of Mount Rosenwald (figure 1), north of the central Shackleton Glacier (85°2.094'S 178°29.518'W) are dominated by *Dicroidium zuberi*, but these fossils have thick (coriaceous), rounded, and wide rhomboidal pinnules characteristic of Early Triassic varieties of this species (figures 2B-C and 3C-D). Associated with one of these fragments (figures 2C and 3D) is a large seed like those associated with Early Triassic D. zuberi from eastern Australia (Retallack 1977). Also found were leafy stems of the equisetalean *Phyllotheca brookvalensis* (figures 3A and B; Townrow 1955) and short conifer shoots referable to Pagiophyllum sp. indet. (figures 2D and 3F). The conifer shoots are similar in shape and dimorphism of leaves to those of *Voltziopsis angusta*, but cuticles or cones are needed to support such an identification (Townrow 1967b). These fragments were found in a siltstone lense within a paleochannel sandstone of a sequence of red paleosols of the Fremouw Formation (at sampling level 19 of Collinson and Elliot (1984); 1 meter (m) in section of Retallack, Krull, and Robinson 1996).

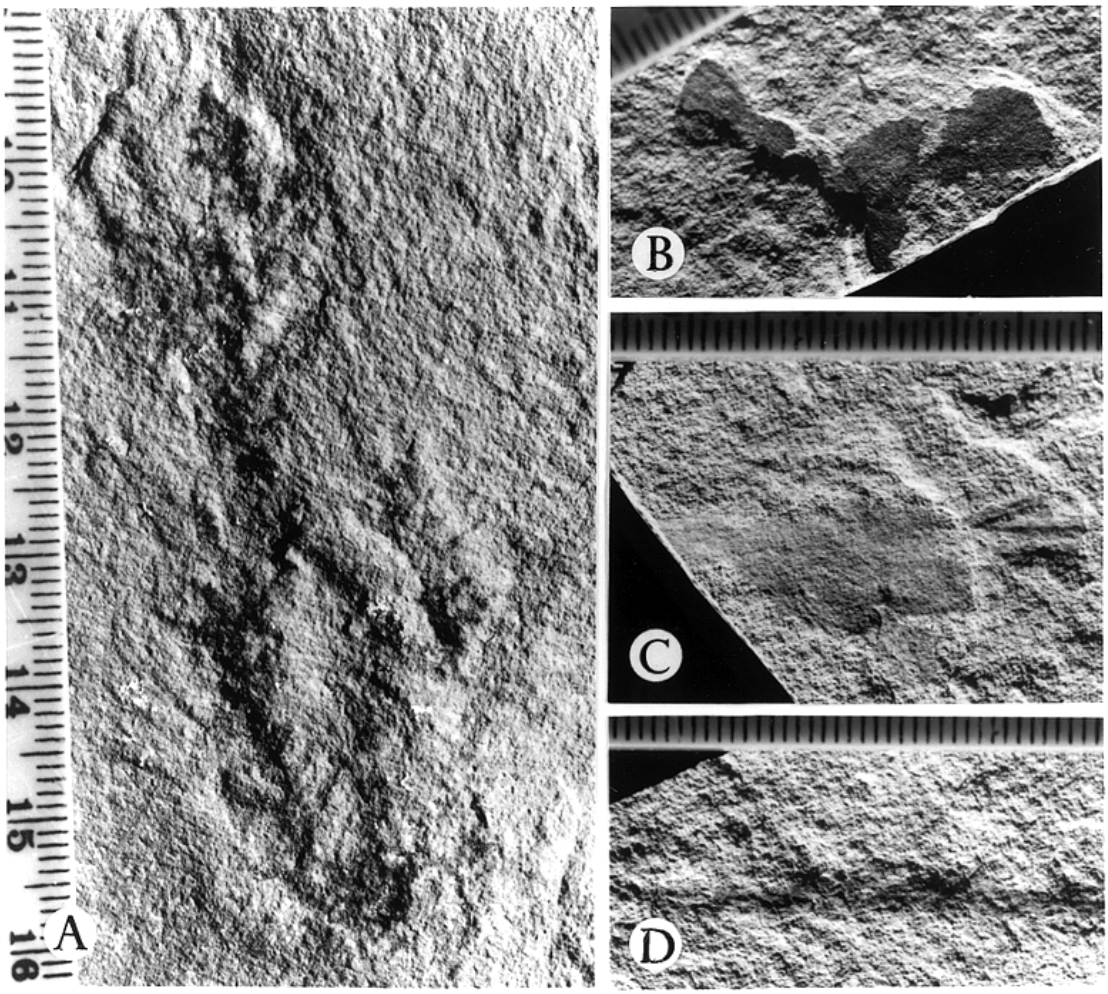

Figure 2. Photographs of Early Triassic plant fragments from the central Transantarctic Mountains:* A, Voltziopsis africanus *shoot with cones (F35143A);* B–C, Dicroidium zuberi, *leaf fragments (F35140A and F35140C, respectively); and* D, Pagiophyllum *sp. indet. (F35139B) from Graphite Peak (*A*) and Mount Rosenwald (*B–D*). Specimen numbers are for the Condon Collection, University of Oregon. Scales in each frame are graduated in millimeters.

The stratigraphic position of red beds within the Fremouw Formation is better understood on Graphite Peak (figure 1) in the nearby Beardmore Glacier area (85°2.99'S 172°21.65'E). Here, red beds of the Fremouw Formation are 129–230 m above the base of the formation, which is the local Permian–Triassic boundary (Retallack et al. 1996). Early Triassic reptiles including *Lystrosaurus murrayi*, *Thrinaxodon liorhinus*, and *Prolacerta broomi* have been found at Graphite peak 24–25 m above the base of the Fremouw Formation, and the labyrinthodont *Austrobrachyops jenseni* 83 m above the base (Retallack and Hammer 1996). Unidentified bone fragments also were found 146 m above the base of the Fremouw Formation at a stratigraphic level similar to that of fossil reptiles of the Cynognathus zone in Gordon Valley, about 300 m above the base of the Fremouw Formation on the other side of the Beardmore Glacier (Hammer 1995). Fossil plant fragments were recently found in the lower Fremouw Formation. These include locally abundant remains of cones and foliar spurs of the conifer *Voltziopsis africana* at 55 m above the base of the Fremouw Formation (figures 2A and 3G). Although cones and some foliar spurs agree in external form with this species, other shoots show more copious branching than is typical for this species (Townrow 1967b) and may represent a separate species. Fragments of Early Triassic *Dicroidium zuberi* with rounded pinnules (figure 3E) like those of Mount Rosenwald also were found below red beds of the Fremouw Formation, 110 m above its base. Fragments of the Middle Triassic seed fern *Dicroidium odontopteroides* were first encountered at 302 m above the base of the Fremouw Formation (Condon Collection specimen F35145), associated with a distinctive assemblage of green clayey paleosols identical to those associated with this and other Middle Triassic fossil plants in southern Victoria Land (Retallack et al. 1995).

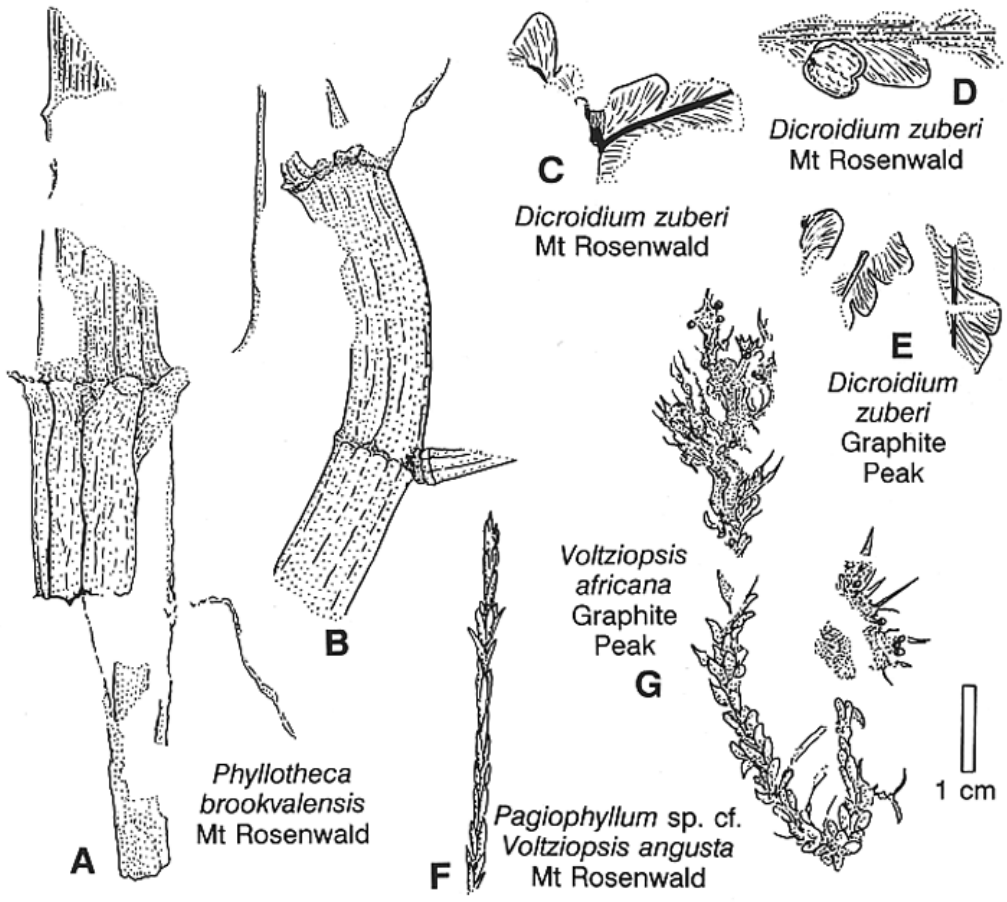

Figure 3. Sketches of Early Triassic plant fragments from the central Transantarctic Mountains:* A–B, Phyllotheca brookvalensis *leafy shoots (F35138A and F35138B, respectively);* C–E, Dicroidium zuberi, *leaf fragments (F35140A, F35140C, and F35144, respectively);* F, Pagiophyllum *sp. indet. (F35139B);* G, Voltziopsis africanus *shoot with cones (F35143A), from Mount Rosenwald (*A–D, F*) and Graphite Peak (*E *and* G*). Specimen numbers are for the Condon Collection, University of Oregon. All drawn to same scale (lower right).

All of the Early Triassic fossil plants reported here from the lower Fremouw Formation of the central Transantarctic Mountains are similar to fossils better known from the Narrabeen Group of the Sydney Basin, Australia (Retallack 1977, 1980). There is no sign of *Dicroidium hughesii* or other plants of diverse, formerly subtropical, Early Triassic floras of Western Australia, India, or South Africa (Retallack 1996). As for the Sydney Basin, the central Transantarctic Mountains were probably within the cool, humid woodland biome during the Early Triassic (Retallack 1997).

I thank E.S. Krull, S.E. Robinson, and S.M. Norman for assistance in the field, and D. Elliot and K. Kililea for logistic assistance. Work was funded by National Science Foundation grant OPP 93-15228.

References

Bose, M.N., T.N. Taylor, and E.L. Taylor. 1990. Gondwana floras of India and Antarctica—A survey and appraisal. In T.N. Taylor and E.L. Taylor (Eds.), *Antarctic paleobiology*. New York: Springer.

Boucher, L.D. 1995. Morphometric and paleobiogeographic analysis of *Dicroidium* from the Triassic of Gondwana. (Unpublished Ph.D. thesis, Ohio State University, Columbus, Ohio.)

Collinson, J.W., and D.H. Elliot. 1984. Triassic stratigraphy of the Shackleton Glacier area. In M.D. Turner and J.F. Splettstoesser (Eds.), *Geology of the central Transantarctic Mountains* (Antarctic Research Series, Vol. 36). Washington, D.C.: American Geophysical Union.

Hammer, W.R. 1995. New therapsids from the upper Fremouw Formation (Triassic) of Antarctica. *Journal of Vertebrate Paleontology*, 15(1), 105–112.

McLoughlin, S., S. Lindström, and A.M. Drinnan. 1997. Gondwanan floristic and sedimentological trends during the Permian–Triassic transition: New evidence from the Amery Group, northern Prince Charles Mountains, East Antarctica. *Antarctic Science*, 9(3), 281–298.

Retallack, G.J. 1977. Reconstructing Triassic vegetation of the eastern Australasia: A new approach to the biostratigraphy of Gondwanaland. *Alcheringa*, 1, 247–277.

Retallack, G.J. 1980. Late Carboniferous to Middle Triassic megafossil floras from the Sydney Basin. In C. Herbert and R.J. Helby (Eds.), *A guide to the Sydney Basin* (Bulletin of the Geological Survey of New South Wales, Vol. 26). Sydney, Australia: Geological Survey of New South Wales.

Retallack, G.J. 1996. An early Triassic fossil flora from Culvida Soak, Canning Basin, western Australia. *Journal of the Royal Society of Western Australia*, 78, 57–66.

Retallack, G.J. 1997. Palaeosols in the upper Narrabeen Group of New South Wales as evidence of Early Triassic palaeoenvironments without exact modern analogues. *Australian Journal of Earth Sciences*, 44, 185–201.

Retallack, G.J., and W.R. Hammer. 1996. Paleoenvironment of the Triassic therapsid *Lystrosaurus* in the central Transantarctic Mountains, Antarctica. *Antarctic Journal of the U.S.*, 31(2), 33–35.

Retallack, G.J., E.S. Krull, and S.E. Robinson. 1995. Permian and Triassic paleosols and paleoenvironments of southern Victoria Land. *Antarctic Journal of the U.S.*, 30(5), 33–36.

Retallack, G.J., E.S. Krull, and S.E. Robinson. 1996. Permian and Triassic paleosols and paleoenvironments of the central Transantarctic Mountains. *Antarctic Journal of the U.S.*, 31(2), 29–32.

Rigby, J.F., and J.M. Schopf. 1969. Stratigraphic implications of antarctic paleobotanical studies. In A.J. Amos (Ed.), *Gondwana stratigraphy*. Paris: UNESCO.

Townrow, J.A. 1955. On some species of *Phyllotheca*. *Journal and Proceedings of the Royal Society of New South Wales*, 89(1), 39–63.

Townrow, J.A. 1967a. Fossil plants from Allan and Carapace Nunataks and from the upper Mill and Shackleton Glaciers, Antarctica. *New Zealand Journal of Geology and Geophysics*, 10(2), 456–473.

Townrow, J.A. 1967b. On *Voltziopsis*, a southern conifer of Lower Triassic age. *Papers and Proceedngs of the Royal Society of Tasmania*, 101, 173–188.

The Kerguelen Archipelago: A 40-million-year record of volcanism derived from the Kerguelen Mantle Plume

Frederick A. Frey *and* Kirsten Nicolaysen, *Department of Earth, Atmospheric and Planetary Sciences, Massachusetts Institute of Technology*

Dominique Weis, *Department of Earth Sciences and Environment, Université Libre de Bruxelles, Brussels, Belgium*

Throughout Earth history, there have been brief intervals of massive magmatism. Two early Cretaceous examples are the Ontong Java and Kerguelen Plateaus, on the Pacific and Antarctic Plates, respectively. The rapid formation of these very large [approximately 2×10^6 square kilometers (km^2)], submarine volcanic provinces demonstrates that energy transfer from the Earth's interior is episodic, and it is likely that such large eruptions had environmental consequences (Coffin and Eldholm 1994). A plausible mechanism for formation of these plateaus is decompression melting of a mantle plume, a buoyant parcel of the Earth's mantle that is thermally and geochemically distinct from its surrounding mantle. For the past 115 million years or so, the Kerguelen Plume has been a prolific magma source that created major bathymetric features on the eastern Indian Ocean seafloor, the Ninetyeast and Broken Ridges on the Indian Plate, and the submarine Kerguelen Plateau with its superimposed islands on the Antarctic Plate (figure 1). A collaborative effort involving researchers from the United States, Belgium, and France and the multinational Ocean Drilling Program is focused on the approximately 115-million-year volcanic record derived from the Kerguelen Plume. This plume is particularly important because

- it is unusually long-lived;
- all aspects of plume-related volcanism are accessible for study (i.e., the Kerguelen Plateau, which is associated with plume initiation, and the Ninetyeast Ridge, a chain of volcanoes that formed as the Indian Plate subsequently migrated northward over the spatially fixed plume);
- the Kerguelen and Heard Islands on the Antarctic Plate (figure 1) provide access to the recent volcanic record; and
- lavas associated with this plume have a distinctive geochemical signature that may reflect recycling of crust into the deep mantle.

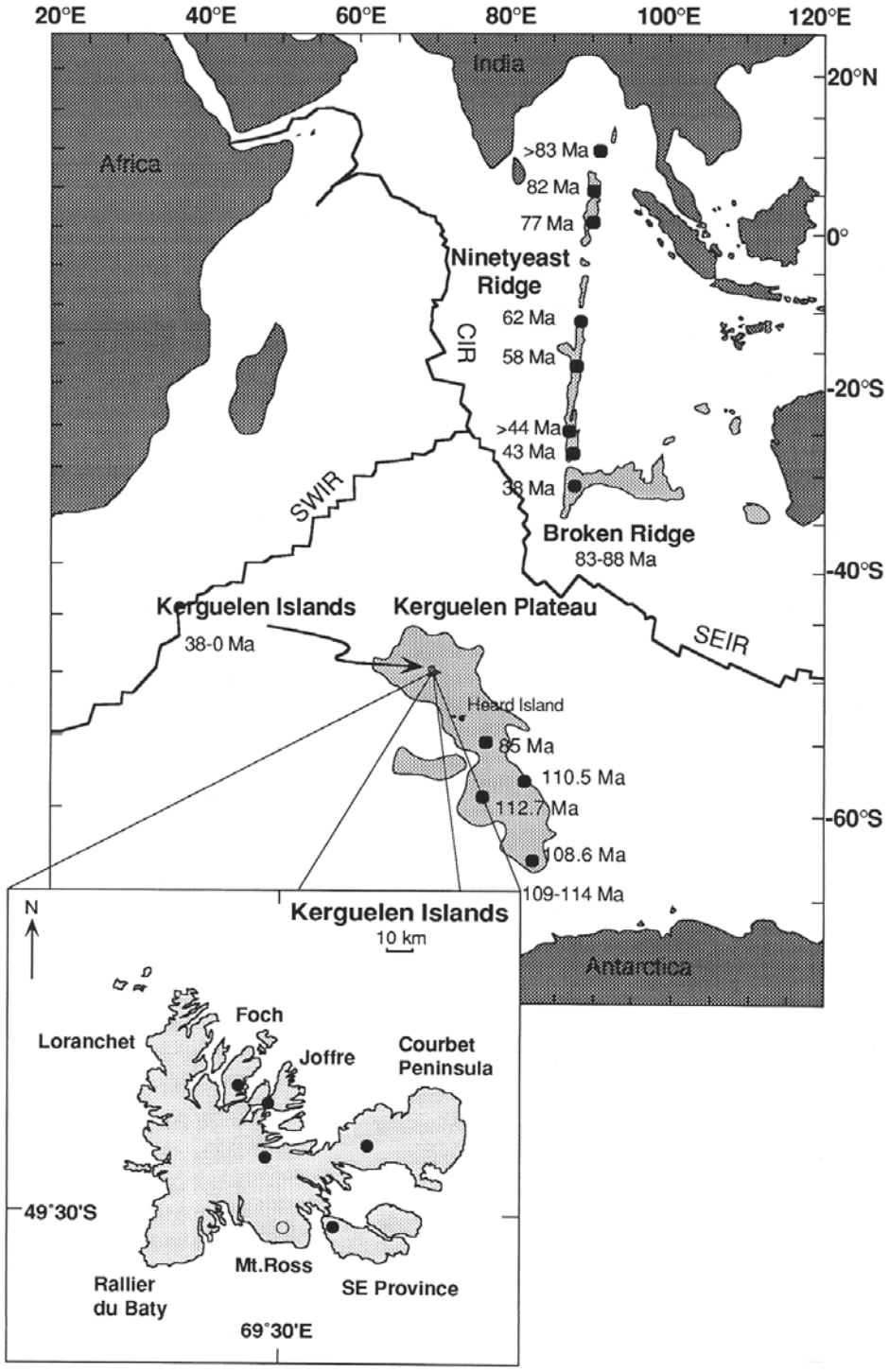

Figure 1. Bathymetric features of the eastern Indian Ocean seafloor, which are attributed to the Kerguelen Plume; specifically the Ninetyeast and Broken Ridges on the Indian Plate and Kerguelen Plateau with Kerguelen Archipelago and Heard Island on the Antarctic Plate. Solid circles indicate sites where basement basalts were recovered by drilling and the indicated basement ages reflect the results of Duncan (1991) and Coffin et al. (in preparation). Inset shows the Kerguelen Archipelago with the location of the studied flood basalt sections (solid circles) and Mount Ross, the youngest volcanic edifice (Weis et al. 1998). (Ma denotes million years.)

Plume-derived magmas provide information about processes occurring in the Earth's mantle that cannot be obtained from the study of volcanism associated with diverging and converging plates. For the Kerguelen Plume, the islands on the Kerguelen Plateau are the only part of the volcanic record that is readily accessible. This project focused on the flood basalt that forms the Kerguelen Archipelago. Lava flows from kilometer-thick sections show spatial and temporal variations in geochemical characteristics. Such data are used to understand the role of post-melting crustal processes, determine the variability of magma flux from the mantle, determine changes in depth and extent of melting, evaluate the geochemical heterogeneity of the plume, and determine changes in proportions between two or more geochemically distinct magma sources.

Important results arising from the study of five lava sections (figure 1 inset) are as follows.

- The upper kilometer of flood basalt ranges in age from about 23 to 30 million years old (figure 2), thereby indicating that the flood basalt did not form in a brief interval at approximately 40 million years when the plume was coincident with the newly formed Southeast Indian Ridge. Compared to the magma supply rate that formed the Ninetyeast Ridge and Kerguelen Plateau, the magma eruption rate during formation of the Kerguelen Archipelago was low (Coffin, Pringle, and Storey in preparation).
- The lava compositions (Yang et al. 1998), the 20-km-thick crustal section with lower crustal seismic velocities similar to those of mafic cumulate rocks (Charvis et al. 1995), and the abundance of gabbroic xenoliths, which originated as cumulates (Grégoire et al. 1994), show that the mantle-derived magmas cooled and partially crystallized while ascending slowly through the crust.
- Although depleted mantle with characteristically low strontium-87/strontium-86 ($^{87}Sr/^{86}Sr$) and high neodymium-143/neodymimum-144 ($^{143}Nd/^{144}Nd$) (see the Southeast Indian Ridge field in figure 3) was postulated to be an important source component during early formation of the archipelago, most of the uppermost archipelago crust has relatively high $^{87}Sr/^{86}Sr$ (approximately 0.7052) and low $^{143}Nd/^{144}Nd$ (approximately 0.5126) (figure 3). Lavas from parts of the older Ninetyeast Ridge and Kerguelen Plateau have similar isotopic ratios (figure 3). We infer that these relatively high $^{87}Sr/^{86}Sr$ and low $^{143}Nd/^{144}Nd$ ratios are the signature of the Kerguelen Plume.
- From west to east across the archipelago, the lavas decrease in age (figure 2), increase in alkalinity, and the clinopyroxene/plagioclase ratio in the fractionating mineral assemblage increases. These trends are consistent with a temporal decrease in extent of melting and increasing mean pressure of mineral/melt fractionation.

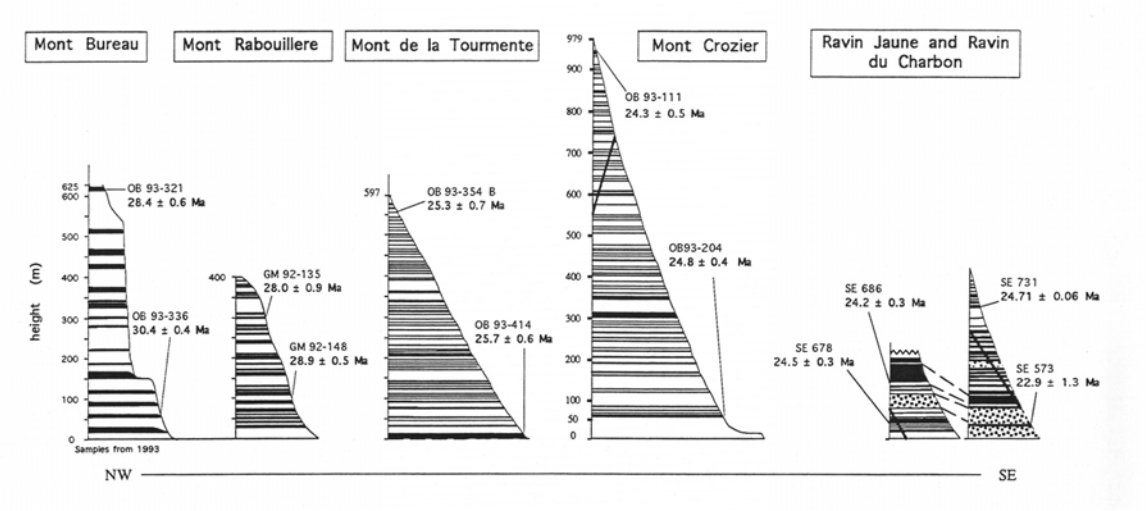

Figure 2. This preliminary figure from Nicolaysen et al. (1996) shows that each lava section formed in less than 2 million years, and that there is a general decrease in age from about 30 million years in the northwest to about 23 million years in the southeast. (m denotes meter; Ma denotes million years.)

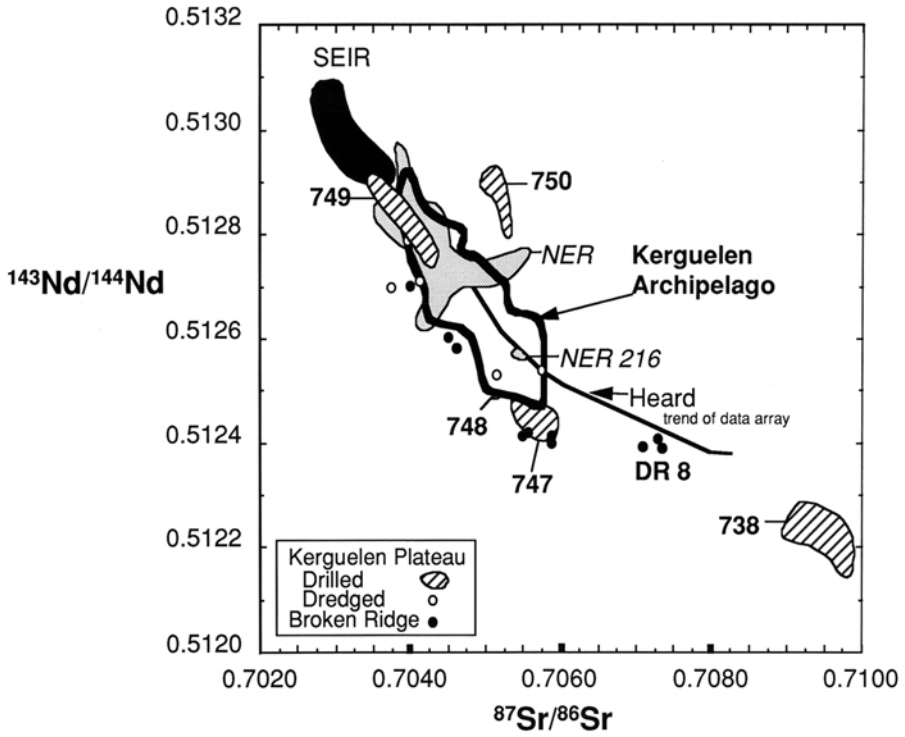

Figure 3. $^{143}Nd/^{144}Nd$ versus $^{87}Sr/^{86}Sr$ showing the fields for basaltic lavas from the Southeast Indian Ridge (SEIR), Kerguelen Archipelago, Ninetyeast Ridge (NER), Broken Ridge (BR), and Kerguelen Plateau (KP). Important results are that all lavas related to the Kerguelen Plume are offset from the SEIR field. Although the field for the Kerguelen Archipelago is quite large, more than 80 percent of the 115 analyzed lavas have $^{143}Nd/^{144}Nd=0.51259\pm5$ and $^{87}Sr/^{86}Sr=0.70515\pm12$. Many lavas from the NER, BR, and KP have similar ratios. Lavas from site 738 on the KP and Dr 8 from BR are offset to extreme isotopic ratios that require a continental component in their source. Evidence for such a component is also found in some Heard Island lavas (Barling, Goldstein, and Nicholls 1994) but not in Kerguelen Archipelago lavas. Data sources are Mahoney et al. (1995); Weis et al. (1993, 1998); Yang et al. (1998).

This research was supported by National Science Foundation grants OPP 94-17774 and EAR 96-14532 and Belgian grant FNRS 1.5.019.95F. Geologic field efforts in the Kerguelen Archipelago are supported by the French Institut Français pour la Recherche et la Technologie Polaires with the leadership of Professor A. Giret (University Jean Monnet, Saint-Etienne, France). H.-J. Yang (United States), and D. Damasceno (Belgium) have also made important contributions to this research effort.

References

Barling, J., S.L. Goldstein, and I.A. Nicholls. 1994. Geochemistry of Heard Island (southern Indian Ocean): Characterization of an enriched mantle component and implications for enrichment of the sub-Indian ocean mantle. *Journal of Petrology*, 35, 1017–1053.

Charvis, P., M. Recq, S. Operto, and D. Brefort. 1995. Deep structure of the northern Kerguelen Plateau and hotspot-related activity. *Geophysical Journal International*, 122, 899–924.

Coffin, M., and O. Eldholm. 1994. Large igneous provinces: Crustal structure, dimensions, and external consequences. *Reviews of Geophysics*, 32, 1–36.

Coffin, M.F., M.S. Pringle, and M.S. Storey. In preparation. Kerguelen hotspot magma output since 130 Ma.

Duncan, R.A. 1991. Age distribution of volcanism along aseismic ridges in the eastern Indian Ocean. In J. Weissel, J. Peirce, E. Taylor, J. Alt, et al. (Eds.), *Proceedings of the Ocean Drilling Program, scientific results* (Vol. 121). College Station, Texas: Ocean Drilling Program.

Grégoire, M., N. Mattielli, C. Nicollet, J.Y. Cotin, H. Leyrit, D. Weis, N. Shimizu, and A. Giret. 1994. Oceanic mafic granulite xenoliths from the Kerguelen archipelago. *Nature*, 367, 360–363.

Mahoney, J., W. Jones, F.A. Frey, V. Salters, D. Pyle, and H. Davies. 1995. Geochemical characteristics of lavas from Broken Ridge, the Naturaliste Plateau and Southernmost Kerguelen Plateau: Early volcanism of the Kerguelen hotspot. *Chemical Geology*, 120, 315–345.

Nicolaysen, K., F.A. Frey, K. Hodges, D. Weis, A. Giret, and H. Leyrit. 1996. $^{40}Ar/^{39}Ar$ geochronology of flood basalts forming the Kerguelen Archipelago. *EOS, Transactions of the American Geophysical Union*, 77(46), fall meeting supplement, F824.

Weis, D., F.A. Frey, A. Giret, and J.M. Cantagrel. 1998. Geochemical characteristics of the youngest volcano (Mount Ross) in the Kerguelen Archipelago: Inferences for magma flux, lithosphere assimilation and composition of the Kerguelen Plume. *Journal of Petrology*, 39, 973–994.

Weis, D., F.A. Frey, H. Leyrit, and I. Gautier. 1993. Kerguelen Archipelago revisited: Geochemical and isotopic study of the Southeast Province lavas. *Earth and Planetary Science Letters*, 118, 101–119.

Yang, H.-J., F.A. Frey, D. Weis, A. Giret, D. Pyle, and G. Michon. 1998. Petrogenesis of the flood basalts forming the northern Kerguelen Archipelago: Implications for the Kerguelen Plume. *Journal of Petrology*, 39(4), 711–748.

Geodetic field work at Palmer Station, Antarctica

Gunter Reppchen, *Department Of Surveying And Cartography, Hochschule für Technik und Wirtschaft Dresden (FH), University Of Applied Sciences, Dresden*

German Global Positioning System (GPS) campaign for researching of tectonic plate movements

The area of the Antarctic Peninsula and the adjacent Southern Ocean with its micro-plates is one of the geodynamical active regions of the world. Geodynamical deformations, resulting from plate motions at the plate boundaries, can be determined by geodetic measurements across the plate boundaries. In 1995 and 1998, two Scientific Committee on Antarctic Research (SCAR) Epoch GPS campaigns were carried out in Antarctica and on the neighboring continents in order to fit the Antarctic plate into the global pattern of plate kinematics. Fourteen countries took part in this research program. The Technical University of Dresden, Germany, was responsible for coordination and data analysis.

The main objectives of these GPS campaigns were

- to create a continent-wide geodetic reference net with a connection to the International Terrestrial Reference Frame (ITRF) in order to analyze the tectonic plate movements relative to neighboring continental plates.
- to determine sea-level changes and changes in the surface heights of ice sheets.

Altogether 45 GPS stations were used around Antarctica and the neighboring continents. Some of stations were part of the permanent tracking system in the southern hemisphere. On the Peninsula, 16 new measuring points were marked. Trimble equipments were used on most of them.

The first measurements in 1995 resulted in the coordinate set for all of the GPS stations. To get plausible results, four different types of GPS analysis software were used:

- Bernese software (University of Bern)
- Gipsy (GPS Inferred Positioning System)
- Geonap (Geodetic Navstar Positioning)
- Gamit (GPS at Massachusetts Institute of Technology).

The movement-rate vectors are the results of the repeated measurements 1998.

Figure 1. Permanent tracking Ashtech GPS station PALM

The United States has been involved in the GPS Campaigns in 1995 and 1998 at Palmer Station on the Antarctic Peninsula. The SCAR GPS point PAL 1 is situated about 300 meters to the east of the station. PAL 1 moves 13 millimeters per year to the north and 15 millimeters per year to the east (Dietrich 2000).

Since spring 1997, Palmer Station has been equipped with a permanent tracking Ashtech Z-12 GPS receiver. The name of the reference point is PALM (figure 1). The installation of this permanent receiver is an important scientific contribution to studying plate tectonics. With 21 days of simultaneous observations during the GAP 98 epoch campaign on the sites PAL 1 and PALM, a high precision geodetic tie between the two antennas was realized. Both tracking stations received the data from 21 January 1998 to 10 February 1998. The calibration data between PAL 1 and PALM and the analysis of the position of PAL 1 relative to PALM was reported to the U.S. Geological Survey.

Final coordinates (ITRF 96 epoch 1998.1) :

PALM :	Latitude	64° 46' 30,3272'' South
	Longitude	64° 03' 04,0481'' West
	Ellips. height	31,050 m (antenna phase centre)
PAL 1 :	Latitude	64° 46' 25,6230'' South
	Longitude	64° 02' 47,7683'' West
	Ellips. height	40,556 m (marker)

Space vector from PAL 1 to PALM :

Δ Latitude : + 145,680 m
Δ Longitude : + 215,143 m
Δ Height : - 9,506 m

Tide gauge measurements at Palmer Station

Tide gauge observations in Antarctica are needed for developing new geoid models for the region to reduce ellipsoidal heights (GPS data) to orthometric heights (mean sea level). At Palmer Station, the automatical tide gauge is located on the pier at a depth of about 2 meters. The GPS centres PAL 1 and the GPS point BC 4 near PALM were connected with the surface of the ocean by leveling. The measurements were repeated 37 times between 22 January 1998 and 9 February 1998 and reduced by measurements from the tide gauge at the corresponding Universal Time Coordinated (UTC).

The results are the elevations of PAL 1, PALM and BC 4 above mean sea level (msl).

- Elevation above msl :

PAL 1 : + 25.464 m = b_1

PALM : + 15.958 m = b_2 (antenna phase center) The height b_2 was calculated, not measured.

BC 4 : + 14.051 m = b_3

Figure 2 shows the elevation of msl above the ellipsoid.

The difference u (figure 2) between ellipsoid and msl amounts to 15.10 meters. The Earth Gravity Model (EGM) 96 (Lemoine 1998), however, gives a height of 14.68 meters for the same region. The difference of 0.42 meters between these measurements and the EGM 96 occurs because, lacking enough reliable gravity measurements for Antarctica, the latter produces imprecise data. Consequently, the Earth Gravity Model

cannot be relied on at this geographical latitude.

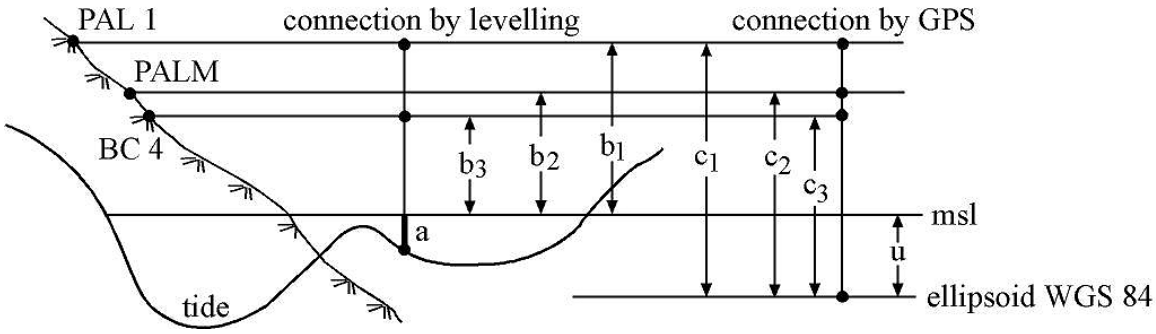

Figure 2. Relationship between tide gauge, GPS measurements and msl

a…tide correction ***b_1; b_2; b_3…elevation above msl***

u…msl above ellipsoid ***c_1; c_2; c_3…GPS heights***

Two geodetic benchmarks were made on Humble and Torgerson islands to support the biological investigations (figure 3).

Figure 3: Leveling on Torgerson Island. The background shows Palmer Station

The elevations above msl of the markers at Humble and Torgerson islands are +11.95 meters and +18.22 meters, respectively.

Contribution of global change

The effects of climate change in the Antarctic Peninsula region can be shown by comparing the ice edges of a glacier over a period of some years.

The ice edge of the glacier Marr Ice Piedmont on Anvers Island was measured in 1987 by U.S. scientists. During the GPS Campaigns 1995 and 1998, the German GPS observer determined the position of the ice edge by a tacheometric survey.

The ice edges are documented in the Palmer Station Site Plan (1 inch equals 200 feet).

The data reveal that the glacier is pulling back as a speed of approximately 30 feet per year. That means the mass balance between snow accumulation and melting has been negative in the last 10 years. As it withdraws, the glacier exposes areas of brown stone. These areas emit additional heat. In the austral summer of 1998 the track path over the glacier had to be displaced several times because the glacier melted significantly.

The author would like to thank the U.S. National Science Foundation, Office of Polar Programs, for support of the SCAR GPS Campaign 1998 at Palmer Station. Special thanks are directed to the "crew" of Palmer Station. Many thanks to Ron Nugent and Lou Graham for technical and administrative support. Many thanks to William Fraser for the productive team work between different scientific disciplines, to Randolph Sliester for the boat course, which was necessary for going by Zodiak to the islands. Thanks to Kevin Bliss, the science technician, who supported the GPS measurement and the tide gauge measurement with additional data .

References:

Dietrich, R. Deutsche Beiträge zu GPS-Kampagnen des Scientific Committee on Antarctic Research (SCAR), 1995-1998. ("German Contributions to the GPS-Campaigns of the SCAR 1995-1998"), Deutsche Geodätische Kommission (German Geodetic Commission), Volume B, number 310, pp. 11-20

Lemoine, F. The Development of the Joint NASA GSFC and the National Imagery and Mapping Agency (NIMA) Geopotential Model EGM96. NASA/TP-1998-206861

Magnetic properties of a sediment core from Andvord Drift

Emily K. Youcha *and* Stefanie Brachfeld, *Institute for Rock Magnetism, University of Minnesota, Minneapolis, MN, 55455*

United States Antarctic Program (USAP) Cruise 99-03 of the research ship *Nathaniel B. Palmer* collected several sediment cores from the western Antarctic Peninsula to examine the natural degree of environmental variability in this region during the Holocene (Domack et al. 1999). Here we examine variations in three magnetic parameters along an approximately 3-meter sediment core (Kasten core KC18C), which reflect the composition, grain size, and concentration of magnetic material in the sediments. The purpose of this magnetic study is to characterize the sediment magnetic mineral assemblage and to understand the local sedimentation processes that generate the assemblage.

Core NBP 99-03 KC18C was collected at the mouth of Andvord Bay (figure 1), at a water depth of approximately 427.7 m (64° 46.342, 62° 49.746). This core samples Andvord Drift, which was discovered and mapped during USAP cruise 98-02 of the U.S. research ship *Lawrence M. Gould* (Harris et al. 1999). Subsamples were collected from the core for rock-magnetic analyses performed at the Institute for Rock Magnetism (IRM), University of Minnesota.

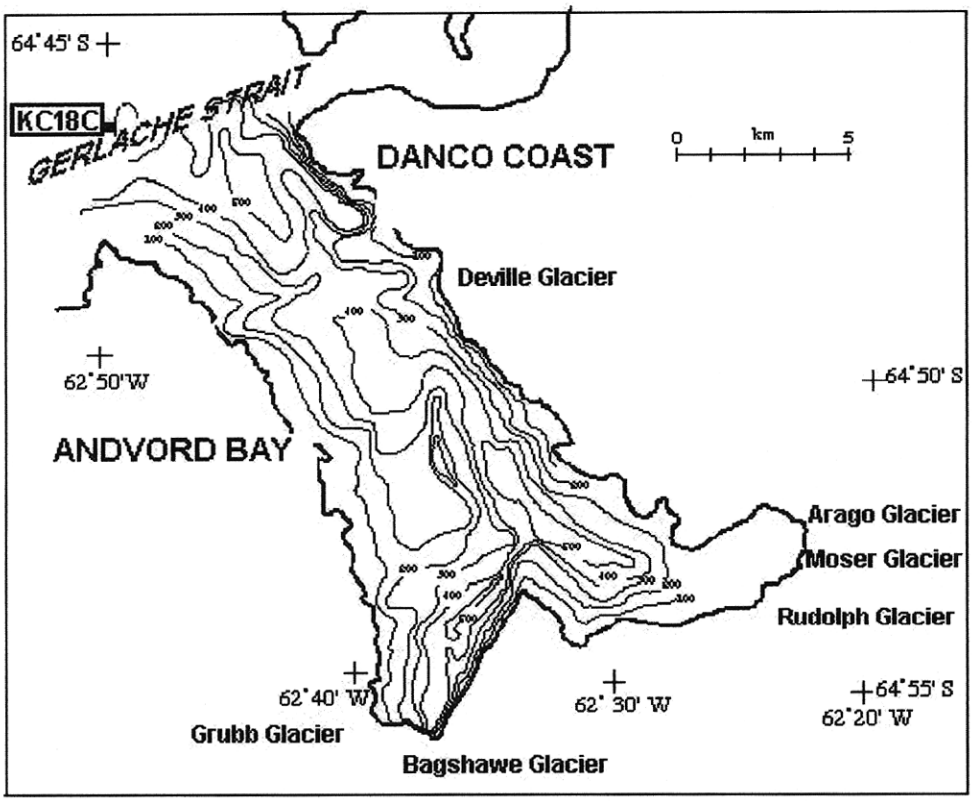

Figure 1. Location of core NBP99-03 KC18C (redrawn after Domack et al., 1993).

Magnetic susceptibility (figure 2) is used as a measure of the concentration of magnetic material. Variations in the concentration of magnetic material, usually derived from terrigenous sources, can be caused by variable dilution by biogenic sediment such as organic carbon or silica. KC18C displays higher average values from 0 to 126 cm followed by a shift to lower values below 126 cm. The high susceptibility interval from 0-126 cm indicates a higher concentration of magnetic minerals, and the low susceptibility interval from 126-266 cm represents a lower concentration likely in response to variations in biogenic silica.

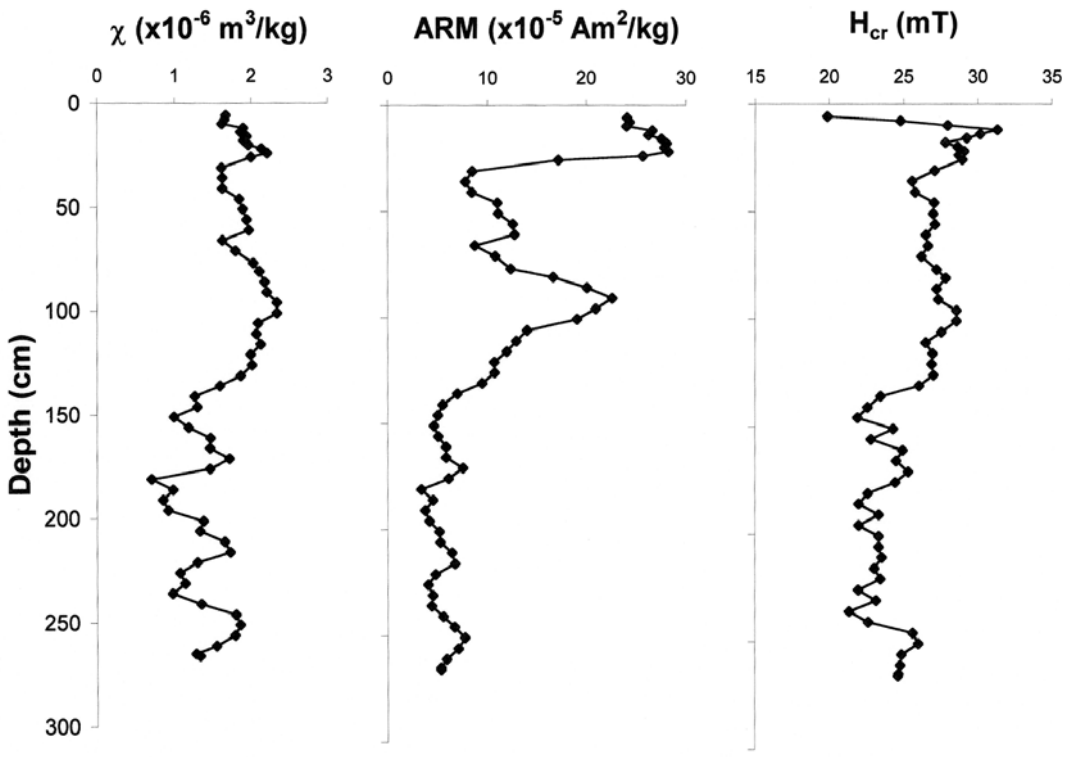

Figure 2. The variations in mass-normalized magnetic susceptibility (χ), anhysteretic remanent magnetization (ARM), and coercivity of remanence (Hcr) down core KC18C. The decrease in all three parameters indicates a change in the magnetic mineral assemblage at 126 cm.

Anhysteretic remanent magnetization (ARM) is a parameter that is sensitive to the concentration of small stable-single-domain (SSD) and pseudo-single-domain (PSD) grains (0.03 to 1 micron and 1 to 10 microns, respectively for magnetite). In addition, paramagnetic (clays) and diamagnetic (silica) material contributes nothing to ARM. Again, we see a change at approximately 126 cm where the ARM decreases (figure 2). There are also two high peaks in ARM around 25 and 90 cm just as there are for susceptibility.

Hysteresis loop parameters were determined for each sample to monitor variations in magnetic grain size down the core. The coercivity of remanence (H_{cr}) (figure 2) shows a clear decrease at 126 cm, which indicates a shift from relatively finer grains in the top half of the core to relatively courser multi-domain (MD) grains at greater depths. These shifts could be a result of dissolution of the finer grains, leaving a course residual assemblage. The shift in grain size may also suggest a change in the provenance, to a source rock with finer-grained magnetic particles.

Magnetic mineralogy was examined using the temperature-dependence of magnetic properties. The low temperature measurements indicate a clear magnetite Verwey transition at 120 K throughout the entire core (figure 3). Additionally, Curie temperature measurements from several depths throughout the core also indicate magnetite as the primary magnetic mineral, with a Curie temperature of 575°C.

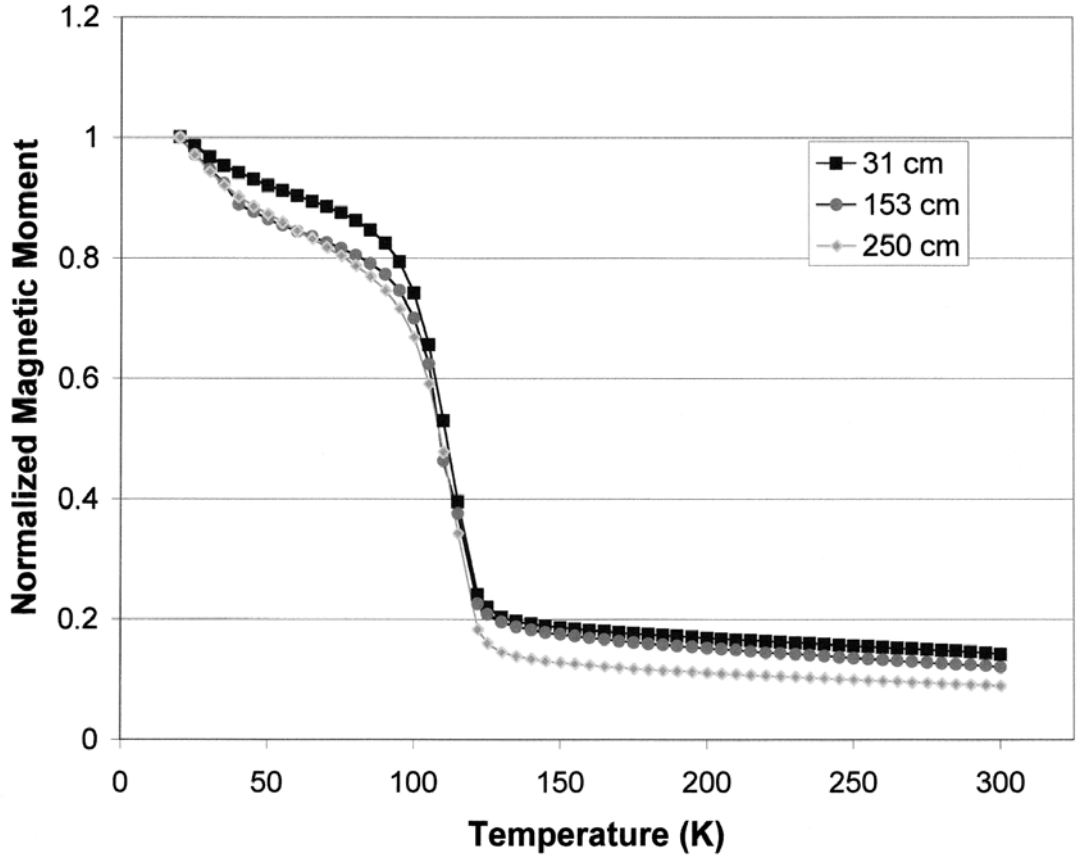

Figure 3. Low temperature measurements on three samples from core KC18C. All depths indicate a magnetite Verwey transition of 120 K.

The concentration, grain size, and composition of magnetic minerals in Andvord Bay sediments yield clues to past depositional processes. The dominant mineral appears to be magnetite. The concentration of magnetite in the Andvord Drift decreases with depth, indicating a change in the flux of terrigenous sediment (Domack, et al. 1993). Magnetic susceptibility highs indicate the sample may contain more terrigenous material, supplied by ice-rafting. Magnetic susceptibility lows reflect increased biogenic silica and possibly higher productivity. The magnetic grain size change at approximately 126 cm could reflect a depositional or diagenetic process.

Examination of the major cations and anions present in interstitial water samples is in progress to look for geochemical boundaries that may coincide with this magnetic feature. In addition, x-ray diffraction and electron microprobe analysis may reveal the presence of diagenetic iron sulfides and reveal subtle variations in magnetic mineralogy that will help us distinguish provenance changes from post-depositional diagenetic alteration.

We thank the crew and science staff of the research ship *Nathaniel B. Palmer*. This work was supported by National Science Foundation (NSF) Office of Polar

Programs grant OPP 96-15695 and also by the University of Minnesota Undergraduate Research Opportunities Program (UROP). This is contribution 0006 from the Institute for Rock Magnetism (IRM). The IRM is supported by grants from NSF and the W.M. Keck Foundation.

References

Domack, E.W., A. Leventer, S. Brachfeld, A. Chong, R. Dunbar, P. Manley, P. Reynolds, and F. Taylor. 1999. *NBP9903 Post-Cruise Report: Paleoenvironmental Investigations Using Sediment Cores*.

Domack, E. W., T. A. Mashiotta, and L. A. Burkley. 1993. 300-year cyclicity in organic matter preservation in Antarctic fjord sediments. In: Kennet, J.P. and Warneke, D.A., eds. *The Antarctic Paleoenvironment: A perspective on global change*. American Geophysical Union Antarctic Research Series, 60, 265-272.

Harris, P.T., E.W. Domack, P.L. Manley, R. Gilbert, and A. Leventer. 1999. Andvord Drift: A new type of inner shelf, glacial marine deposystem from the Antarctic Peninsula. *Geology*, 27, 863-868.

Rock-magnetic analysis of sediments from Andvord Bay

Stefanie A. Brachfeld, *Department of Geology and Geophysics and Institute for Rock Magnetism, University of Minnesota*

Sediment cores from the western Antarctic Peninsula show a distinctive magnetic susceptibility "stratigraphy" that appears to be a regional signal. The signal consists of a late Holocene interval in which magnetic susceptibility shows regularly spaced highs and lows, preceded by a middle Holocene interval in which susceptibility values are uniformly low (Domack and Ishman 1992; Leventer et al. 1996; Kirby et al. 1998). Here we report on rock magnetic investigations from core PD88-22 from Andvord Bay (figure 1), in order to understand the magnetic mineral assemblage that carries the susceptibility signal.

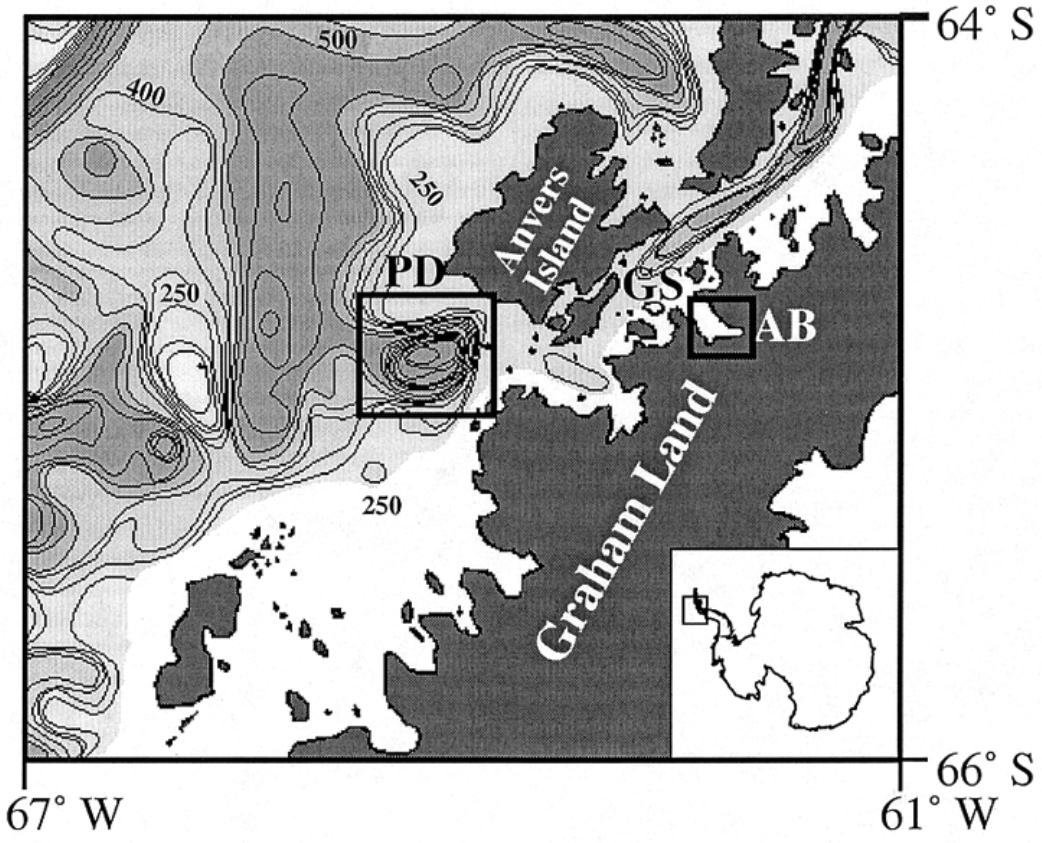

Figure 1. Location of Andvord Bay (AB), the Palmer Deep (PD), and the Gerlache Strait (GS) on the western margin of the Antarctic Peninsula. Bathymetry data are from Rebessco et al., (1998).

Core PD88-22 was collected in 1988 by the *R.V. Polar Duke* from the central basin of Andvord Bay (water depth ~440 m). Domack et al. (1993) observed that magnetic susceptibility is inversely correlated with both biogenic silica and total organic carbon content (TOC) (figure 2), which suggests that magnetic susceptibility is reflecting, in part, the variable dilution of terrigenous material with biogenic material. This same pattern has also been observed in cores from the Gerlache Strait and the Palmer Deep (Domack and Ishman 1992; Leventer et al. 1996; Kirby et al. 1998). However, the magnetic granulometry of PD88-22 is quite different from the patterns observed in the Palmer Deep.

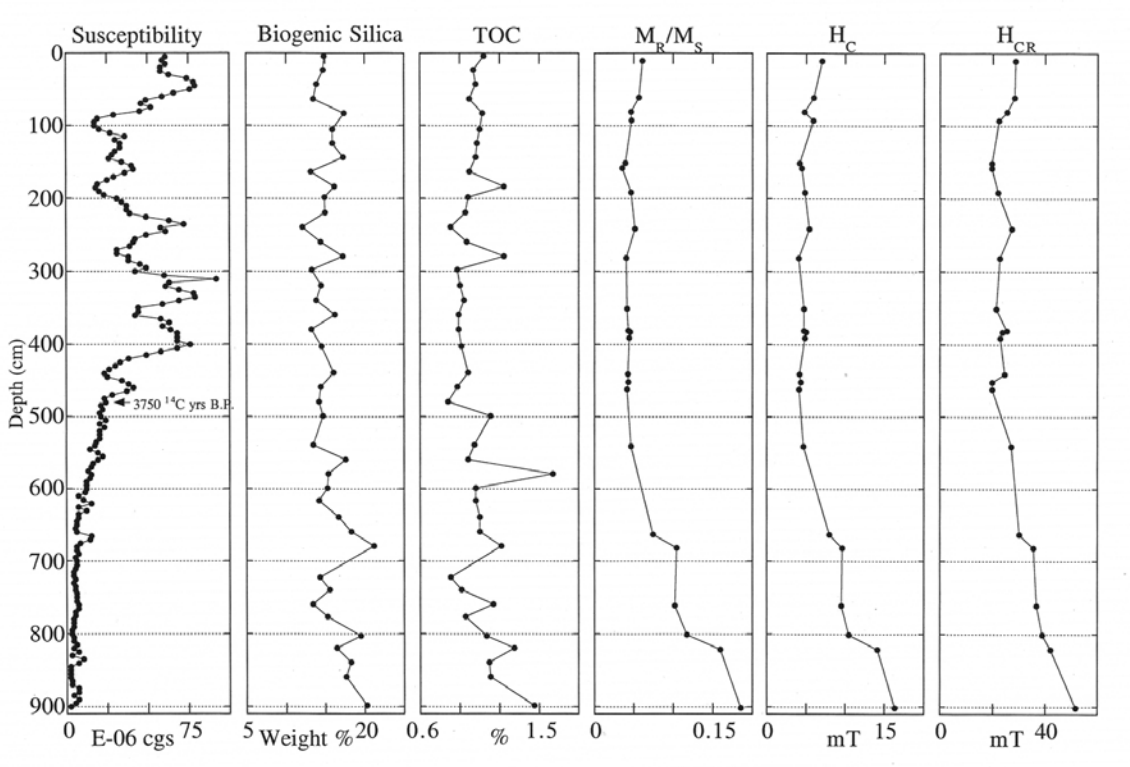

Figure 2. Physical and magnetic properties of core PD88-22, central Andvord Bay.

Magnetic grain size is determined by measuring hysteresis parameters, which vary with magnetic domain state, which is in turn a function of grain volume. For the mineral magnetite the ratio of saturation remanence (M_R) to saturation magnetization (M_S) is less than 0.1 for multi-domain grains (> 10 μm) and in the range of 0.1-0.5 for finer pseudo-single-domain grains (1 to 10 μm). The coercive force (H_C) and coercivity of remanence (H_{CR}) are relatively higher for finer grains and lower for multi-domain grains, with the important exception of ultra-fine < 30 nm superparamagnetic particles, for which H_C and H_{CR} are zero.

In PD88-22 the magnetic grain size is consistently in the multi-domain range for the upper 550 cm, as demonstrated by the relatively constant values of M_R/M_S, H_C, and H_{CR}. In contrast, the magnetic susceptibility fluctuations in the Palmer Deep were accompanied by magnetic grain size changes, with susceptibility peaks containing

coarser magnetic grains than susceptibility lows (Brachfeld and Banerjee 2000). This bimodal distribution is absent in PD88-22. From 550 to 900 cm, the magnetic grain size fines with depth. This is seen in the gradual increases in all three hysteresis parameters. This trend parallels the slight increases in biogenic silica and TOC from 550 to 900 cm.

Magnetic mineralogy was determined by examining the temperature-dependence of magnetic properties over the range 20 to 300 K. In PD88-22 the magnetite Verwey transition is seen at ~110-115 K in all samples examined (figure 3). There is no evidence of the pyrrhotite transition at 35 K. However, other magnetic iron sulfides such as greigite and paramagnetic pyrite have no diagnostic low-temperature behavior. Therefore, the possibility of diagenetic iron sulfides in these sediments cannot be ruled out at the present time.

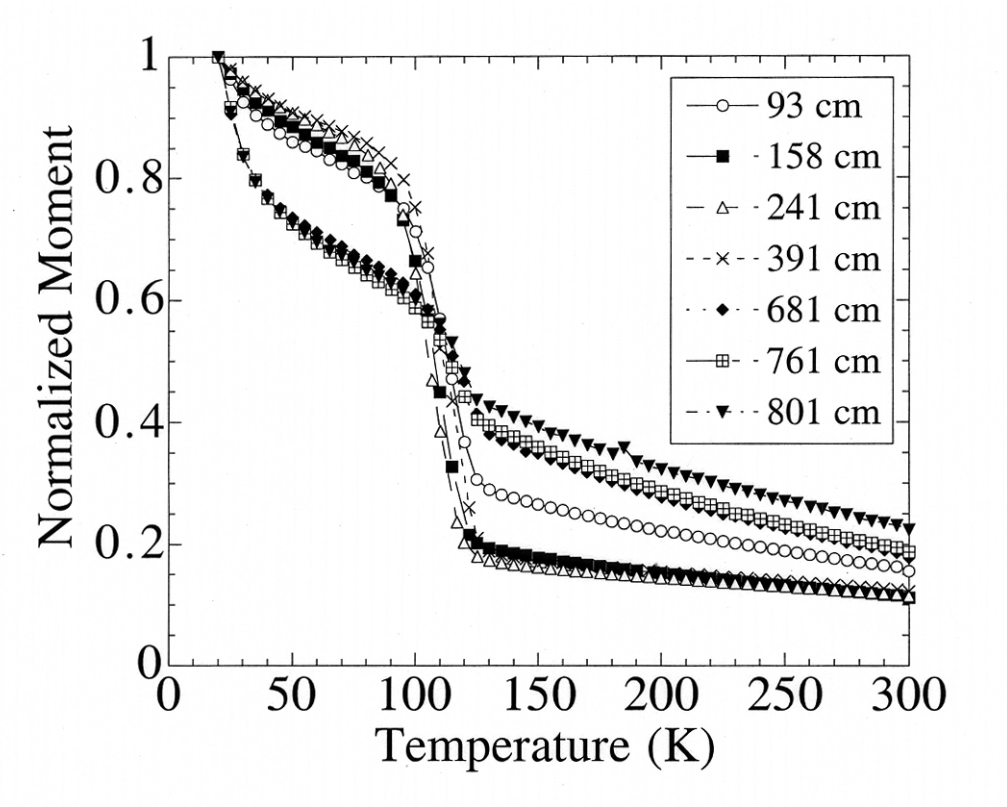

Figure 3. Thermal decay of a low-temperature 2.5 Tesla saturation remanence imparted at 20 K. The abrupt drop in the magnetic moment at ~110-115K is the magnetite Verwey transition.

The continued presence of pure magnetite below 550 cm in PD88-22 is in marked contrast to the Palmer Deep's mid-Holocene low susceptibility interval, which contains only titanium-rich titanomagnetite. In addition, the rapid loss of remanence between 20-50 K in these deeper samples from PD88-22 is consistent with the presence of ultra-fine superparamagnetic (SP) particles. The presence of SP particles has been linked with enhanced productivity in deep-sea sediments (Tarduno 1995). A similar link may exist in Andvord Bay, as evidence for SP particles is seen in intervals of elevated TOC and biogenic silica.

The late Holocene magnetic susceptibility cycles observed in cores from Andvord Bay and the Palmer Deep likely reflect variable productivity, combined with changes in the terrigenous sediment supply. Changes in magnetic grain size and mineralogy may be reflecting variable ice rafted debris content and/or meltwater input. Differing trends in magnetic granulometry between Andvord Bay and the Palmer Deep indicates a sensitivity to very local depositional processes at each site. Characterization of the magnetic granulometry of major rock types on the Antarctic Peninsula could enable the use of magnetic provenance tracers in these sediments.

We thank E. Domack and colleagues for providing samples and data from PD88-22. This work was supported by National Science Foundation Grant OPP 96-15695. This is IRM contribution 0004. The IRM is funded by grants from the National Science Foundation and the Keck Foundation.

References

Brachfeld, S., and S.K. Banerjee. 2000. Rock-magnetic carriers of century-scale susceptibility cycles in glacial-marine sediments from the Palmer Deep, Antarctic Peninsula. *Earth and Planetary Science Letters*, 176, 3-4.

Domack, E.W., and S.E. Ishman. 1992. Magnetic susceptibility of Antarctic glacial marine sediments. *Antarctic Journal of the United States*, 27, 64-65.

Domack, E.W., T.A. Mashiotta, L.A. Burkely, and S.E. Ishman. 1993. 300-year cyclicity in organic matter preservation in Antarctic fjord sediments. In: Kennett, J. and Warnke, D. (eds.), *The Antarctic Paleoenvironment: A perspective on global change, American Geophysical Union, Antarctic Research Series*, 60, 265-272.

Kirby, M.E., E.W. Domack, and C.E. McClennen. 1998. Magnetic stratigraphy and sedimentology of Holocene glacial marine deposits in the Palmer Deep, Bellingshausen Sea, Antarctica: implications for climate change? *Marine Geology,* 152, 247-259.

Leventer, A., E.W. Domack, S.E. Ishman, S. Brachfeld, C.E. McClennen, and P. Manley. 1996. Productivity cycles of 200-300 years in the Antarctic Peninsula region: understanding linkages between the Sun, atmosphere, sea ice and biota. *Geological Society of America Bulletin,* 108, 1626-1644.

Rebessco, M., A. Camerlenghi, and C. Zanolla. 1998. Bathymetry and Morphogenesis of the Continental Margin west of the Antarctic Peninsula. *Terra Antarctica*, 5, 715-725.

Tarduno, J.A. 1995. Superparamagnetism and reduction diagenesis in pelagic sediments: enhancement or depletion? *Geophysical Research Letters,* 22, 1337-1340.

Magnetic granulometry of igneous and meta-sedimentary rocks from northern Graham Land, Antarctic Peninsula

Stefanie Brachfeld, *Institute for Rock Magnetism, University of Minnesota, Minneapolis*

Anne Grunow, *Bryd Polar Research Center, Ohio State University*

Emily Youcha, *Water and Environmental Research Center, University of Alaska, Fairbanks*

The application of magnetic methods to plate tectonic reconstructions, interpretation of aeromagnetic data, and the construction of sedimentary paleoclimate records requires an understanding of the magnetic mineral assemblage that carries the paleomagnetic or rock-magnetic signal. To that end, there has been interest in establishing a rock magnetic database for antarctic rocks to make magnetic data accessible by region and rock type. Here we present preliminary rock magnetic analyses of Cretaceous igneous rocks from Northern Graham Land and suite of rocks obtained from a dredge of Flandres Bay. We discuss the potential for development of magnetic provenance tracers in glacial-marine sediments from the western Antarctic Peninsula.

Sample localities, lithology, and rock magnetic data are summarized in tables 1 and 2. Koenisberger ratios (Q) have been calculated for an ambient field of 50 μT. Magnetic susceptibilities are consistent with values previously reported for this region and these rock-types (e.g., Vaughan et al. 1998). The coarse-grained intrusives (granites, granodiorites, gabbros, and tonalites) have multi-domain hysteresis parameters, while volcanic rocks and meta-sediments have pseudo-single domain hysteresis parameters.

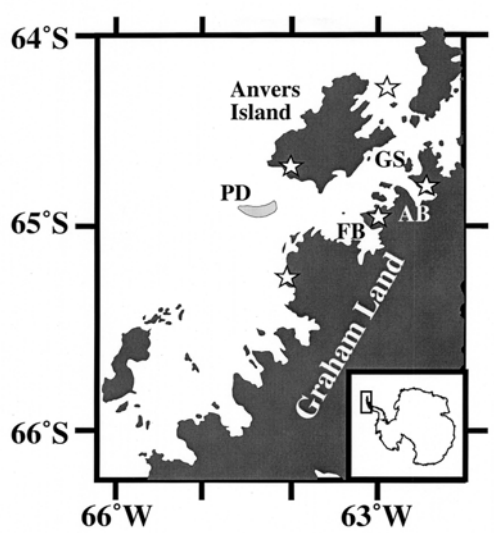

Northern Graham Land with sample locations (stars). PD = Palmer Deep, AB = Andvord Bay, GS = Gerlache Strait, FB = Flandres Bay.

Table 1. Sample Descriptions

Locality	Sample ID	Long (E)	Lat (S)	Lithology	Age (Ma)
Graham Land Intrusives					
Forbes Point, Andvord Bay	AV5A3	297.45	64.88	granite	98
Birdsend Bluff	BB1A6	297.45	64.75	diorite	98
Coughtrey Peninsula	CP1D1	297.12	64.90	volcanic	128 ± 3
Duthiers Point	DP1B1	297.18	64.80	diorite	98
Ferguson Channel	FC2A3A	297.00	64.92	volcanic	98
Rassmussen Island	LM5B3	295.92	65.25	granite	128±3
Cape Tuxen	LM6B4	295.87	65.27	gabbro	85
Lambda Island, Melchoirs	ML1A4	297.02	64.30	granodiorite	98
Gamma Island Melchoirs	ML1E2	297.02	64.33	tonalite	98
South Neko Harbor	NH1B2B	297.45	64.83	pink granite	114±11
Pitt Island	PT1B3	294.52	65.43	gabbro	
Flandres Bay Series					
Flandres Bay	FB1	296.497	64.991	porphyritic andesite	
Flandres Bay	FB2	296.497	64.991	altered mafic intrusive	
Flandres Bay	FB3	296.497	64.991	syenite	
Flandres Bay	FB4	296.497	64.991	aplite	
Flandres Bay	FB5	296.497	64.991	phyllite	
Flandres Bay	FB6	296.497	64.991	granite	
Flandres Bay	FB7	296.497	64.991	schist	
Flandres Bay	FB8	296.497	64.991	calc-arenite	
Flandres Bay	FB9	296.497	64.991	syenite	

Table 2. Rock magnetic Properties

Sample ID	κ (SI)	χ (m^3/kg)	χ_{HF} (m^3/kg)	NRM (A/m)	Q	M_S (Am^2/Kg)	M_R (Am^2/Kg)	H_C (mT)	H_{CR} (mT)	M_R/M_S	H_{CR}/H_C	T_T K	T_C (˚C)
Graham Land Igneous series													
AV5A3	1.148E-02	4.08E-06	9.63E-08	6.96E-02	0.152	4.84E-01	6.85E-03	1.4	10.9	0.014	7.79	113.4	583
BB1A6	4.013E-02	1.41E-05	1.15E-07	7.52E-02	0.047	1.66E+00	5.09E-02	3.83	19.9	0.031	5.20	108.6	584
CP1D1	2.689E-02	9.38E-06	1.95E-07	0.63 - 16.78	0.589 - 15.68	1.17E+00	1.21E-01	12.1	51.1	0.103	4.22	102.7	588
DP1B1	7.465E-02	2.89E-05	2.44E-07	1.79E-01	0.060	4.74E+00	1.09E-01	2.55	13.6	0.023	5.33	113.5	583
FC2A3A	3.307E-04	1.23E-07	7.72E-08	5.37E-01	40.817	5.80E-03	1.34E-03	22.8	60.4	0.231	2.65	117.5	-
LM5B3	1.308E-02	5.23E-06	1.19E-08	1.58E-01	0.303	2.39E-01	8.07E-03	3.87	24.8	0.034	6.41	112.6	585
LM6B4	5.411E-02	1.85E-05	1.29E-07	1.06E+00	0.492	1.88E+00	6.90E-02	4.74	24.5	0.037	5.17	103.5	587
ML1A4	3.187E-02	1.25E-05	1.13E-07	1.03E-01	0.081	6.07E-01	6.33E-03	1.29	14.6	0.01	11.32	102.5	587
ML1E2	9.255E-02	3.43E-05	1.34E-08	4.89E-01	0.133	3.90E+00	5.34E-02	1.35	10.2	0.014	7.56	102.5	588
NH1B2B	7.501E-03	3.00E-06	5.55E-09	9.90E-03	0.033	4.48E-01	9.85E-03	3.03	27.9	0.022	9.21	102.5	593
PT1B3	8.955E-02	2.22E-05	1.03E-07	9.57E-01	0.269	2.72E+00	6.87E-02	3.34	20.5	0.025	6.14	102.6	586

Table 2. Rock magnetic Properties (continued)

Sample ID	κ (SI)	χ (m^3/kg)	χ_{HF} (m^3/kg)	NRM (A/m)	Q	M_S (Am^2/Kg)	M_R (Am^2/Kg)	H_C (mT)	H_{CR} (mT)	M_R/M_S	H_{CR}/H_C	T_T K	T_C (˚C)
Flandres Bay Series													
FB1	6.53E-03	2.12E-06	1.04E-07	9.91E-02	0.381	5.64E-01	4.88E-02	7.61	47.6	0.087	6.25	93.5	573
FB2	3.72E-02	1.32E-05	5.07E-08	6.91E-01	0.466	1.29E+00	5.58E-02	3.04	14.6	0.043	4.8	-	520, 588
FB3	7.41E-02	2.38E-05	4.95E-08	3.16E+00	1.073	2.09E+00	7.94E-02	3.98	16.8	0.038	4.22	113.6	585
FB4	1.63E-03	4.67E-07	4.33E-08	5.34E-02	0.825	1.71E-01	8.46E-03	4.8	15.8	0.049	3.29	112.6	587
FB5	1.98E-04	6.74E-08	5.99E-08	8.45E-04	0.107	1.01E-03	9.12E-05	6.81	22.5	0.09	3.31	-	-
FB6	2.41E-03	8.79E-07	7.57E-08	3.70E-03	0.039	4.37E-01	2.51E-02	8.31	70.6	0.057	8.5	113.5	600
FB7	3.84E-04	1.10E-07	1.53E-07	1.20E-03	0.078	1.66E-03	1.00E-04	6.74	35.9	0.06	5.33	115	-
FB8	9.44E-04	3.12E-07	1.91E-07	1.17E-01	3.112	7.44E-03	1.30E-03	15	38.1	0.174	2.54	122.7	587
FB9	2.86E-04	9.63E-08	4.23E-08	1.68E-03	0.147	7.73E-03	2.33E-03	40.2	187	0.301	4.65	117.6, 250	588

Diagnostic temperature-dependent magnetic behavior, such as Curie temperatures and low-temperature transitions [see Dunlop and Özdemir 1997 for full discussion], were measured to assess each sample's magnetic mineralogy. The granites and diorites have typical magnetite Curie temperatures (~580 to 584 ˚C). The gabbros, tonalites, and granodiorites have elevated Curie temperatures (585 to 590 ˚C). Readman and O'Reilly (1972) observed that titanomagnetite Curie temperatures increased with the degree of oxidation, possibly resulting from strong interactions between the increasing number of Fe^{3+} ions. Further, the gabbros, granodiorites and tonalites have low Verwey transitions at 102 to 104 K, which also suggests some degree of oxidation or non-stoichiometry (Özdemir et al. 1993). In contrast, the granites and diorites have higher Verwey transitions at 108 to 118 K.

The rock magnetic analyses of the Cretaceous igneous rocks from Graham Land suggest that granites, diorites, tonalites, and gabbros have distinctive combinations of Curie temperatures and low-temperature transitions that may be useful as provenance tracers in sediments. These two parameters were compared with similar measurements made on magnetic extracts from the Palmer Deep and Andvord Bay. Intervals from the Palmer Deep and Andvord Bay have magnetic characteristics that are more consistent with a diorite or granite source (Brachfeld and Banerjee 2000). The low-temperature magnetic properties of the sediments do not correlate well with the granodiorites, tonalites, or gabbros, suggesting that these rock types can be excluded as source rocks. Establishing magnetic fingerprints of source rocks that can be detected in sediments can potentially yield information on sediment transport paths and processes such as IRD dispersal patterns, paleowind strength and paleocurrent directions.

This research was supported by National Science Foundation Grant OPP 96-15695 and an Undergraduate Research Opportunities Award (to E.Youcha) from the University of Minnesota.

References

Brachfeld, S., and S.K. Banerjee. 2000. Rock-magnetic carriers of century-scale susceptibility cycles in glacial-marine sediments from the Palmer Deep, Antarctic Peninsula, *Earth and Planetary Science Letters*, 176, 443-455.

Dunlop, D.J. and Ö. Özdemir. 1997. *Rock Magnetism: Fundamentals and Frontiers*, New York: Cambridge University Press.

Özdemir, Ö., D.J. Dunlop, and B.M. Moskowitz. 1993. The effect of oxidation on the Verwey transition in magnetite. *Geophysical Research Letters*, 20, 1671-1674.

Readman, P.W. and O'Reilly, W. 1972. Magnetic properties of oxidized (cation-deficient) titanomagnetites, (Fe, Ti, [])O_4, Journal of Geomagnetism and Geoelectricity, 24, 69-90.

Vaughan, A.P.M., C.D. Wareham, A.C. Johnson, and S.P. Kelly. 1998. A lower Cretaceous, syn-extensional magmatic source for a linear belt of positive magnetic anomalies: the Pacific Margin Anomaly (PMA), western Palmer Land, Antarctica, *Earth and Planetary Science Letters*, 158, 143-155.

Laminations from the Palmer Deep, Antarctica

Athan Barkoukis *and* Amy Leventer, *Department of Geology, Colgate University*

Marine sediment cores with decadal- to century-scale resolution were recovered from the Palmer Deep, Antarctic Peninsula, by the Ocean Drilling Program Leg 178, Site 1098 (64º 51.72'S, 64º 12.48'W; 1012 meters water depth). The high-resolution paleoclimatic record extends back 14,000 years to the last glacial period (Domack et al. submitted). In sections, these biosiliceous cores are strongly laminated, prompting questions of the floral composition of the laminations, and the environmental conditions that lead to laminae formation.

Our primary objective was to determine the distribution of diatom species in the laminated sequences and to evaluate whether distinct patterns in diatom distribution occur. A total of 354 smear slides were made from individual laminations from Core 1098B. The laminations were subsampled with toothpicks to minimize mixing of diatoms between laminated and non-laminated portions of the core (figure 1). The non-uniform distribution of data points reflects the occurrence of laminations, which are coincident with lows in magnetic susceptibility. In particular, note the presence of two turbidites (T I and T2) that were not sampled. In addition, laminations that are likely varves are found below 42 meters; the composition of these laminations have been analyzed quantitatively and described previously (McAndrews et al. *Antarctic Journal,* this issue).

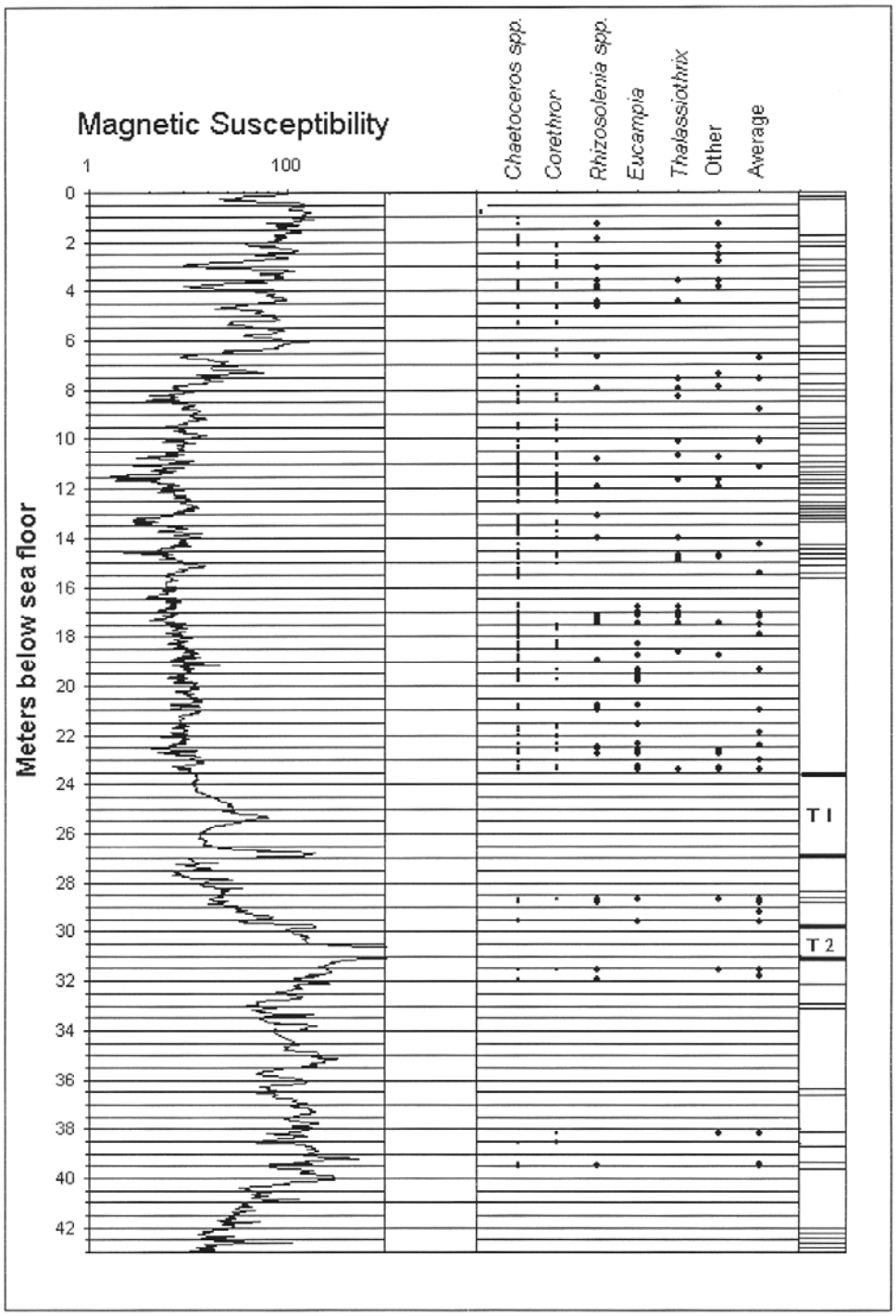

Figure 1. Magnetic susceptibility record (in units of 10^{-5} SI) for Core 1098B (ODP Leg 178) plotted with diatom assemblage composition of 354 laminations. These qualitative diatom data are based on smear slide analysis and reflect the distribution of the most common species in the laminations. Other refers to species that are common in only a few of the laminations. They are grouped together to simplify the graph. Average refers to laminations that were not dominated by any species in particular and appeared more similar to the non-laminated sections of core.

The dominant component of most of the laminations is resting spores of the genus *Chaetoceros* (61 percent of all laminations sampled) (figure 2A). At depths greater than 42 meters below sea floor (mbsf), the laminations are composed entirely of *Chaetoceros* resting spores (McAndrews et al. submitted). *Corethron criophilum,* though not as common, was found in high concentrations in many of the laminations (25 %). Preservation of valves, girdle bands and spines was exceptional in most cases, though some laminations were unusual in having high concentrations of spines only. The average diameter of the *Corethron* was about 30-35 microns, similar to that noted by Crawford (1995) in a *Corethron* layer from the Weddell Sea. However, several of the laminations contained uniformly small valves (17-20 microns diameter).

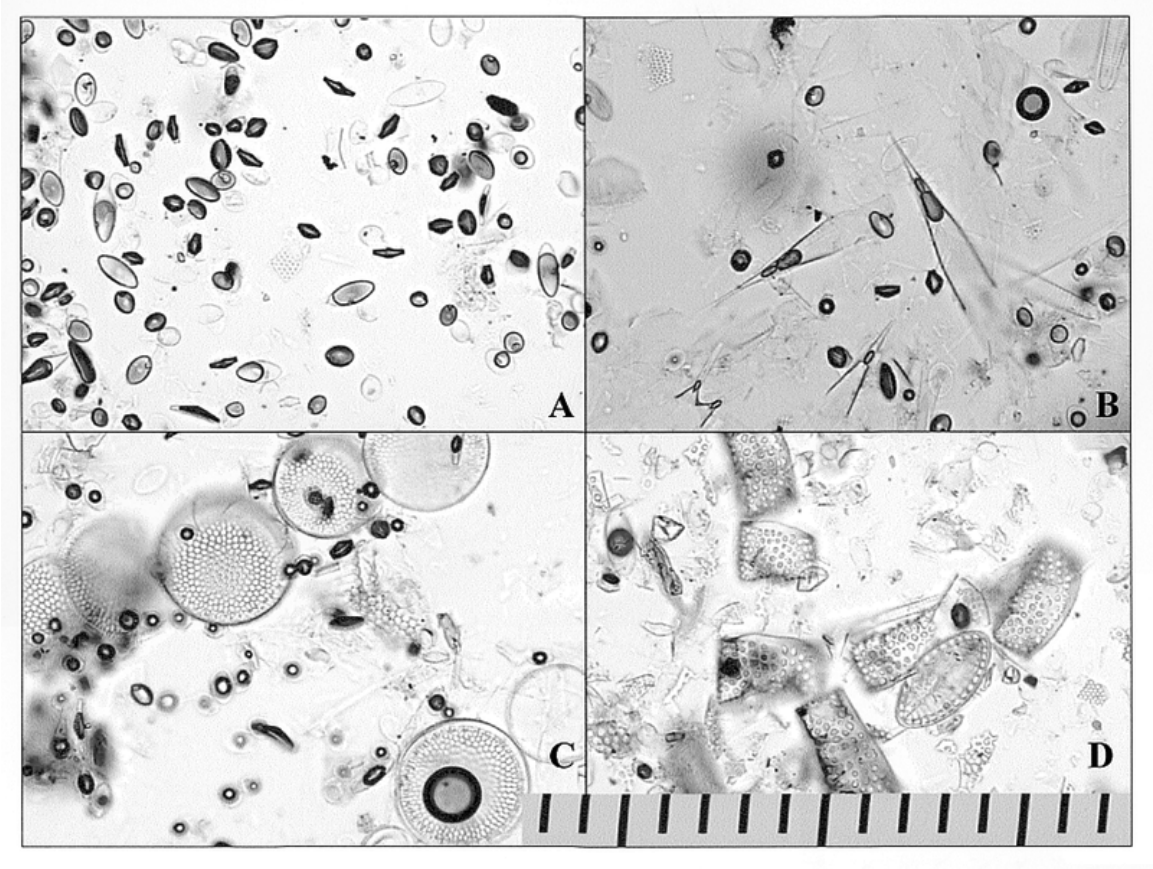

Figure 2. Photographs of common lamination-forming diatoms from ODP Leg 178 Core 1098B. A. **Chaetoceros** ***resting spores from Section IH4, 19.5 cm. B.*** **Rhizosolenia sp.** ***from Section 3W, 106 cm.*** **C. Thalassiosira antarctica** ***from Section 3145, 121 cm. D.*** **Eucampia antarctica** ***from Section 3H5, 8.3 cm. Units on the scale bar are 10 microns.***

Rhizosolenia spp./Proboscia spp. (figure 2B) were observed in low abundances in almost all of the laminations but were very abundant in only 38 of the 354 laminations analyzed (11%). Several different species from these two genera were recognized, but all were grouped together at this time, pending more detailed taxonomic analysis. We noted that within a lamination, the average diameter of the dominant species was fairly uniform, but that the diameter varied between laminations. Other groups that are common

in fewer laminations include *Thalassiothrix longissima* and *Thalassiothrix antarctica, Trichotoxon reinboldiii,* large vegetative cells of *Chaetoceros criophilum, Thalassiosira tumida,* and *Thalassiosira antarctica* (Figure *2C), Eucampia antarctica* (Figure 2D*)* and the silicoflagellate *Distephanus speculum.*

With two important exceptions, the distribution of these different assemblages within laminated intervals appears random, with all occurring throughout the length of the core with no distinctive pattern or grouping. Each species may be responding to slightly different environmental parameters. However, in the larger scheme, these conditions appear to occur with equal frequency throughout episodes of high productivity during the Holocene. As suggested by Leventer et al. (1996), the overall pattern of distribution of the groups together may be more significant than the distribution of individual species. In particular, the occurrence of nearly monospecific laminations indicates conditions of high primary productivity coupled to mass sedimentation. In part, this may be driven by the morphologies of many of the groups, with high surface area to volume ratios promoting easier flotation and long slender valves and /or valve protuberances (as spines and setae) resulting in entanglement. The genera *Thalassiosira* and *Eucampia* (figures 2C and 2D), however, do not meet this description. Their association with sedimentary laminations needs to be examined more closely.

The exceptions to the generalization concerning the seemingly random distribution of species within laminations may be important. First is the presence of laminations containing only *Chaetoceros* resting spores (figure 2A), and none of the other species listed above, below 42 mbsf. This approximately 3-meter section of the core occurs shortly above the glacial diamict, suggesting unique oceanographic conditions that lead to varve formation during initial stages of deglaciation (McAndrews et al. submitted; Katz in preparation). Proximity to retreating glacial ice can explain the more terrigenous "half" of each varve couplet, with higher input of glacially-derived material year-round responsible for the sediment that alternates with the more biogenic spring bloom of diatoms (Domack personal communication). The question of why this post-glacial bloom interval is consistently dominated by *Chaetoceros* only, as contrasted to subsequent blooms in the Holocene, is more difficult to answer,

Second, surprisingly high concentrations of *Eucampia antarctica* (figure 2D) were observed in laminations occurring between 16.5 - 23.0 mbsf. All were heavily silicified and most were asymmetric in broad girdle view, suggesting these are winter forms of the "more northern" variety of this species (Fryxell 1989). Note that, although this section of core was initially described as mostly bioturbated, faint to well-defined laminations were observed upon later detailed sampling. Although magnetic susceptibility, a proxy for paleoproductivity (Leventer et al. 1996), is uniformly low between approximately 8 - 23.5 mbsf, the variable diatom data indicate that oceanographic conditions were not uniform over this interval. Thus, the mid-Holocene is divided into two distinct intervals, from about 8 - 16.5 mbsf and 16.5-23.5 mbsf. Based on the radiocarbon chronology, this is equivalent to time periods from about 6,500 to 3,500 calendar years before present and about 9,000 to 6,500 calendar years before present (Domack et al. submitted). The increased occurrence of the northerly form of *Eucampia antarctica* from 9,000 –to 6,500 calendar years before present suggests that the earlier part of the mid-Holocene was characterized by southward incursion of more

sub-polar waters.

We thank the ODP Leg 178 shipboard and shore-based participants for collecting and sampling the core. National Science Foundation Grant OPP 97-14371 supported this research.

References

Crawford, R.M. 1995. The role of sex in the sedimentation of a marine diatom bloom. *Limnology and Oceanography,* 40, 1, 200-204.

Domack, E., A. Leventer, R. Dunbar, F. Taylor, S. Brachfeld, and ODP Leg 178 Scientific Party. 2001. Holocene climate variability in the Antarctic Peninsula. *The Holocene,* 11, 11-19.

Fryxell, G.A. 1989. Marine phytoplankton at the Weddell Sea ice edge: Seasonal changes at the specific level. *Polar Biology,* 10, 1- 18.

Katz. In preparation. Size and abundance of *Chaetoceros* resting spores from laser diffraction: A rapid method for diatom analysis.

Leventer, A., E.W. Domack, S. Ishman, S. Brachfeld, C. McClennen, and P. Manley. 1996. 200-300 year productivity cycles in the Antarctic Peninsula region: Understanding linkages among the sun, atmosphere, oceans, sea ice and biota. *Geological Society of America Bulletin,* 108, 1626-1644.

McAndrews, E., A. Leventer, and E. Domack. 2004. Annual cycles in Palmer Deep Sediments, *Antarctic Journal of the United States,* this issue.

Annual cycles in Palmer Deep sediments, Antarctica

Beth McAndrews and Amy Leventer, *Department of Geology, Colgate University*

Eugene Domack, *Department of Geology, Hamilton College*

Analysis of laminated sediments retrieved from the Palmer Deep during ODP Leg 178 (Site 1098) is contributing to the development of an ultra-high resolution record of the early Holocene. The Palmer Deep is an enclosed bathymetric depression on the Antarctic Peninsula continental shelf approximately 30 kilometers (km) south of Anvers Island. The systematically laminated makeup of the bottom section of core 1098 hole A (located at 64° 52' S, 64° 14' W in a water depth of 1012 meters), presents great potential for annual assessment of productivity in the Southern Ocean. The primary goal of this project was to examine the section of the 45.9-m core from hole 1098A from approximately 39.9 - 43.3 mbsf to evaluate the working hypothesis that the laminations represent true varves, or annual couplets.

Within the well-laminated section of the core, six 10-14 centimeters (cm) sequences of 3-7 pairs of laminations were subsampled for quantitative diatom counts, grain size, and carbon and nitrogen isotopic analysis. Quantitative diatom slides were made using a settling technique described by Scherer (1995) and permanent slides were made using Norland Optical Adhesive. Due to the overwhelming dominance of *Chaetoceros*, each slide was counted twice. First, the total assemblage was counted and second, a *Chaetoceros* free count was completed. Evaluation of the complete assemblage was based on five fields of view. For the *Chaetoceros* free counts, approximately 400 valves were counted along transects.

The well-laminated sequence from approximately 39.9 - 43.3 mbsf occurs immediately above a diamicton deposited during the last glacial. A total of 146 couplets of mm to cm scale thickness with alternating biogenic and terrigenous layers make up the section. Each couplet contains a biogenic and a terrigenous layer. The biogenic laminations contain a nearly monospecific assemblage of *Chaetoceros* resting spores, an average abundance of approximately 109 diatom valves per gram of sediment, very few sand and gravel grains, and a well-sorted (unimodal) grain size distribution (figures 1a, 2, and 3b).

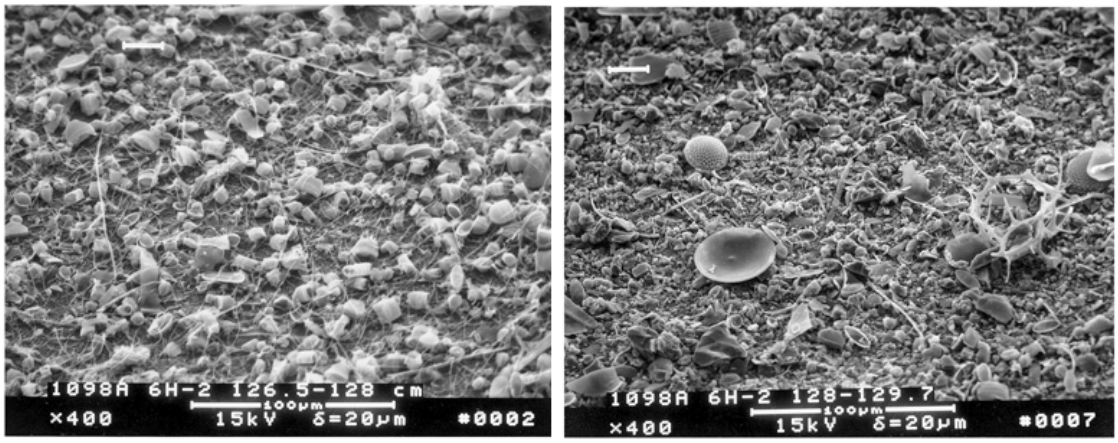

Figure 1. Diatom assemblages from core 1098A. a) Note the monospecific assemblage of* Chaetoceros *in the biogenic layer. b) Note the diverse diatom assemblage of the terrigenous layer.

In contrast, the "terrigenous" layers contain a more diverse diatom assemblage. Though still dominated by *Chaetoceros* resting spores, also present are *Thalassiosira antarctica*, *Fragilariopsis curta*, and *Fragilariopsis cylindrus*. (figure 1b). In addition, the total diatom abundance within the terrigenous layers is an order of magnitude lower than in the biogenic layers, and the grain-size distribution is more poorly sorted with coarse sand and gravel grains visible in x-radiograph (figures 2 and 3a).

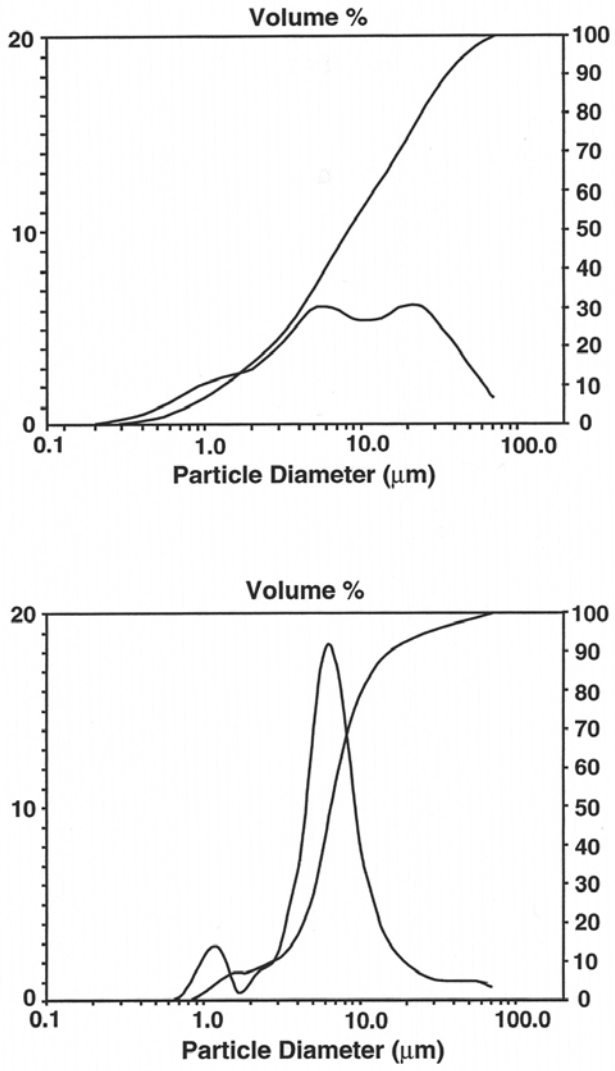

Figure 2. Average abundance of diatom valves vs. depth.

We suggest the biogenic laminae represent seasonal blooms, which were rapidly deposited during annual intense summer blooms. The almost monospecific composition of *Chaetoceros* resting spores within the laminae must be indicative of the high primary productivity that occurs during the bloom. The biogenic laminae are similar to those found in other parts of the world's oceans, including the Mediterranean, Santa Barbara Basin, Gulf of California, and Japan Sea (Sancetta 1994).

"Terrigenous" laminations were probably deposited during the remainder of the year and represent the relatively constant input of ice rafted material. The terrigenous component may be contributed by melting glacial ice retreating shoreward over the Palmer Deep during the transition from glacial to interglacial conditions. The lower abundance of diatoms may be due to a lower overall productivity by a mixed diatom assemblage under non-bloom conditions. These terrigenous laminae occur only

immediately following the glacial and are not seen in the upper section of the core, which is an environment that is more distant to the glacial margin (similar to today). This is most likely because the terrigenous material is less abundant once the melting glacial ice is removed spatially from the system. Once the glacial ice retreats to a point distant from the Palmer Deep, the terrigenous layers disappear and only biogenic laminae are found.

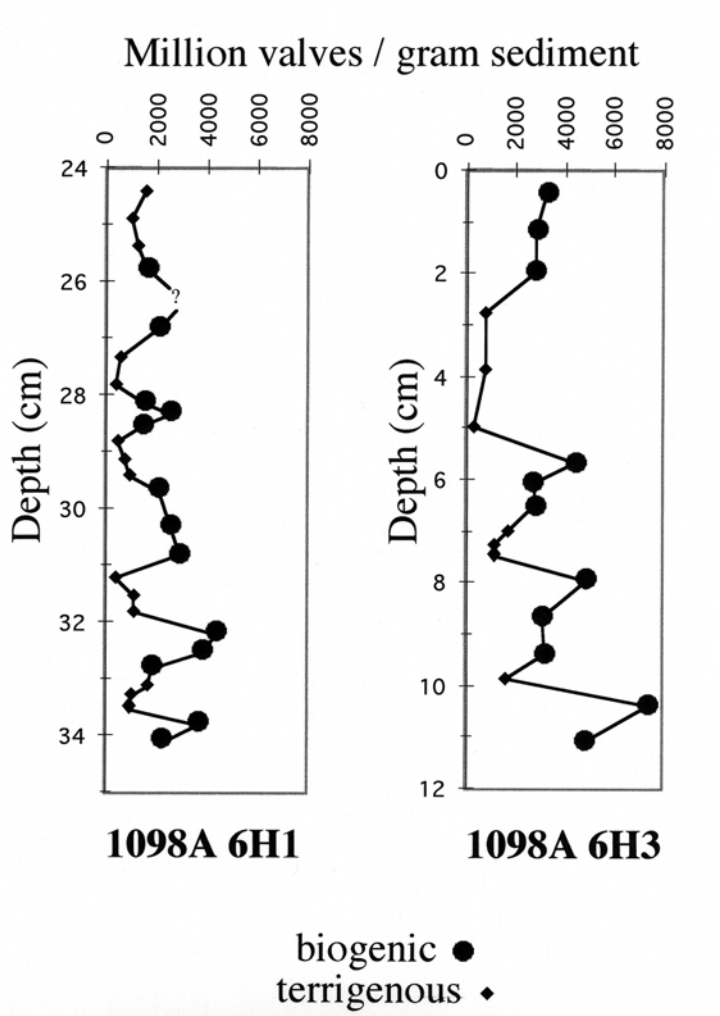

Figure 3. Grain-size distribution of terrigenous and biogenic laminae from core 1098A section 6H2. a) Grain size from a terrigenous layer at a depth of 128-129.7 cm. Note the poorly sorted distribution. b) Grain size from a biogenic layer at a depth of 123.2-124 cm. Note the well-sorted distribution.

The section of the core above approximately 23 mbsf contains laminations that are entirely biogenic. The age of the bottom of this section of the core is approximately 8,000 years before present, indicating an interglacial environment and the probable removal of the terrigenous source, as glacial ice has retreated shoreward. Several different species of diatoms, including *Chaetoceros* resting spores and species with long, slender morphologies such as *Rhizosolenia spp.* and *Corethron criophilum*, dominate these laminations. The biogenic nature of all of the laminae in the upper 23 meters of the core can be attributed to the greater distance of glacial ice and, as a result, a removal of a

nearby source of terrigenous material and ice-rafted debris found in the terrigenous laminae of the lower section of the core.

This study documents the presence of the first annual layers recovered from Antarctica. They serve as a source for high-resolution paleoclimatic data and provide evidence concerning deglacial processes in the Southern Ocean. The makeup of the laminae and stratigraphic position in the lower section of core 1098 provide unparalleled documentation of the transition from glacial to interglacial Holocene conditions. The laminae in the lower section of the core contain couplets composed of a biogenic and terrigenous layer. The presence of *Chaetoceros* resting spores in the biogenic laminae serve as evidence for an annual bloom interrupting the constant terrigenous input as ice-rafted debris. In contrast, the "terrigenous layers" contain a more diverse diatom assemblage, coupled with large terrigenous grains derived from the melting of abundant icebergs. We propose the potential of these sediments for further development of annual records of Holocene climate in the Southern Ocean.

This research was supported by National Science Foundation grants OPP 97-14371 (to Leventer) and OPP 96-15053 (to Domack).

References

Sancetta, C., 1994. Mediterranean sapropels: Seasonal stratification yields high production and carbon flux. *Paleoceanography*, 9, 195-196.

Scherer, R. P., 1995. A new method for the determination of absolute abundance of Diatoms and other silt-sized sedimentary particles, *Journal of Paleolimnology*, 12, 171-179.

The riddle of subglacial lithologies in the West Antarctic Rift System

Wesley E. LeMasurier, *University of Colorado, Denver*

The West Antarctic rift system occupies a 3,000 km x 1,000 km area that is almost entirely buried beneath the West Antarctic Ice Sheet (WAIS). Even a rudimentary knowledge of the major rock types beneath the ice sheet would provide new insights into problems of broad interest to the antarctic community, such as the timing and areal extent of mantle plume activity in West Antarctica, the extent of Cenozoic tectonic activity in the rift system, and the influence of bedrock geology on the dynamics of the ice sheet. At this time, however, there is a perplexing discrepancy between the interpretations of airborne geophysical data over the rift system and the results of sedimentological analyses of basal core samples from the ice sheet.

Aeromagnetic surveys over most of the rift system have revealed large areas of short-wavelength, high-amplitude anomalies (figure 1) that are characteristic of igneous sources (Behrendt et al., 1991). Potential candidates for the source rock are late Cenozoic volcanic rocks, thick piles of Jurassic Kirkpatrick basalts, thick Jurassic mafic intrusions, or late Cretaceous magnetic granitoids (Behrendt et al., 1996). Some of these anomalies are subcircular in plane view, some are associated with seismically defined structures that penetrate late Cenozoic sediments in the Ross Sea, and still others coincide with conical peaks beneath the ice sheet, all of which strongly suggest volcanic or shallow subvolcanic sources of late Cenozoic age (Behrendt et al. 1991; Blankenship et al. 1993). However, many anomalies do not correlate with topographic features. These could represent unconsolidated hydrovolcanic debris (i.e., hyaloclastites and pillow lavas) that was eroded from its source soon after eruption (Behrendt et al. 1995). The estimated volume of volcanic rock that could account for all of the magnetic anomalies is $>10^6$ km^3 (Behrendt et al. 1996), about twice the volume of the Columbia River flood basalt field. Cenozoic volcanic rocks, rather than Jurassic mafic rocks or Cretaceous granitoids, are the source preferred by geophysicists, based on magnetic intensity arguments.

Recently, Tulaczyk and Krukowski (1999) presented preliminary results of a study of more than 100 core samples from ice streams B, C, and D; Crary Ice Rise; Byrd Station; and Unicorn and Siple Dome. The sand-sized fraction of these samples is dominated by quartz and feldspars and the clay fraction by hydrous mica and chlorite, with about 30 percent of the latter composed of kaolinite and montmorillonite. The only location with clear and abundant mafic material is Byrd Station (S. Tulaczyk personal communication 1999).

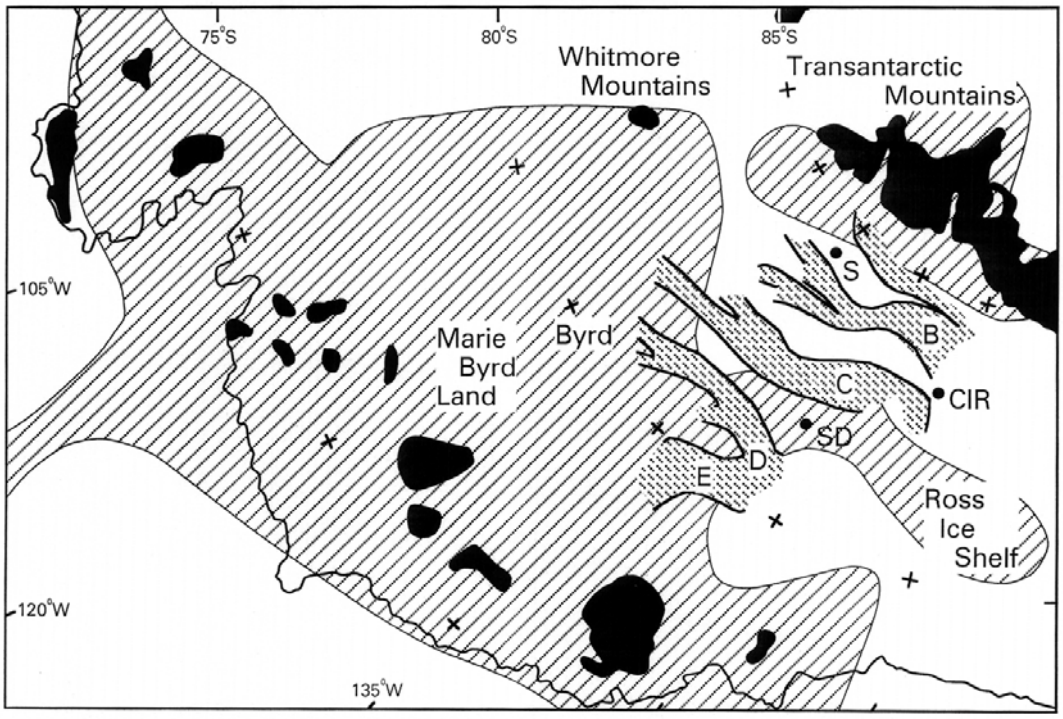

Figure. Location map of the central West Antarctic rift system, which is bounded on the south by the Transantarctic and Whitmore Mountains. Rock exposures are solid black. Ice streams are shaded, and labeled B, C, D, and E. Other basal sediment sample sites are CIR (Crary Ice Rise), SD (Siple Dome), and U (Unicorn) and Byrd. Light shading shows the area of conspicuous high amplitude, short wavelength aeromagnetic anomalies (from Behrendt et al. 1991). The MBL dome is centered between 120°W and 135°W beneath the MBL coastal exposures. Base map modified from Bankenship et al. (1993).

The most obvious source rocks for these samples are quartzo-feldspathic granitoids, which are abundant in coastal Marie Byrd Land (MBL) and the Transantarctic Mountains (figure). Cenozoic volcanic rocks, the preferred source for the aeromagnetic anomalies, are likely to have been erupted subglacially and should be represented by a large proportion of pillow lava and hyaloclastite. These rocks are abundant in coastal MBL, but not the southern Transantarctic Mountains. The constituents of hyaloclastite are volcanic glass fragments that may contain microlites (<0.5 mm) of olivine, plagioclase, and clinopyroxene, and occasional phenocrysts of these same minerals. Large (>10 cm) interbedded pillow fragments and other lithic clasts are common. The glass is invariably altered to palagonite and variable proportions of smectite (e.g., montmorillonite), zeolite (e.g,. phillipsite), and calcite (Ellerman 1989). These volcanic rocks should be recognizable in core samples by finding smectite, zeolite, and calcite(?) in the clay fraction, together with lithic clasts and occasional olivine, plagioclase, and pyroxene in the sand fraction. Preliminary results from the study of core samples do not yet provide support for a large volume of subglacial Cenozoic rock.

The question of how much volcanic rock is buried beneath the WAIS; whether it

is late Cenozoic or Jurassic; and whether it occurs as hyaloclastite, or lava, or subvolcanic plutons has significant petrologic, tectonic and glaciological implications. Verifying that there is indeed a large volume of Cenozoic rock there would lend support to the idea of a large mantle plume beneath most of the rift system (e.g., Hole and LeMasurier 1990; Behrendt et al. 1991). Furthermore, since large volumes of volcanic rock imply high rates of extension, it would imply more late Cenozoic extension than has yet been demonstrated for the rift system. On the other hand, if the aeromagnetic anomalies are produced mainly by Kirkpatrick basalts or magnetic granitoids, this finding would be compatible with the idea that plume activity is more limited—for example, to the MBL dome (LeMasurier and Landis 1996—and that most extension was pre-Cenozoic. Finally, if there is a large volume of Cenozoic rock beneath the ice sheet and it occurs mainly as hyaloclastite and pillow lava, these deposits could be significantly influencing ice sheet dynamics. Hydrovolcanic rocks deform easily, even under their own weight (LeMasurier and Behrendt 1999). Glaciologists believe that deformable beds have an important (though still controversial) role in determining the positions of ice streams and the stability of the ice sheet (Bentley 1998, and references therein). The still unresolved question about instability of the WAIS has direct relevance to society, because sea level would rise 5 meters if it were to collapse. For these reasons, it is important to resolve the discrepancies between interpretations of aeromagnetic data and the message a mere 100 core samples tell us about an area the size of the entire Basin and Range province.

Research on volcanic rocks of MBL was supported by NSF grant OPP 97-20411.

References

Behrendt, J.C., D.D. Blankenship, D. Damaske, and A.K. Cooper. 1995. Glacial removal of late Cenozoic subglacially emplaced volcanic edifices by the West Antarctic ice sheet. *Geology,* 23, 1111-1114.

Behrendt, J.C., W.E. LeMasurier, A.K. Cooper, F. Tessensohn, A. Tréhu, and D. Damaske. 1991. Geophysical studies of the West Antarctic rift system. *Tectonics,* 10, 1257-1273.

Behrendt, J.C., R. Saltus, D. Damaske, A. McCafferty, C.A. Finn, D. Blankenship, and R.E. Bell. 1996. Patterns of late Cenozoic volcanic and tectonic activity in the West Antarctic rift system revealed by aeromagnetic surveys. *Tectonics,* 15, 660-676.

Blankenship, D.D., R.E. Bell, S.M. Hodge, J.M. Brozena, J.C. Behrendt, and C.A. Finn. 1993. Active volcanism beneath the West Antarctic ice sheet and implications for ice-sheet stability. *Nature,* 361, 526-529.

Bentley, C.R. 1998. Ice on the fast track. *Nature,* 394, 21-22.

Ellerman, P.J. 1989. Depositional environments and post-depositional alteration of Cenozoic hyaloclastites in Antarctica. Ph.D. dissertation, University of Colorado, Boulder.

Hole, M.J. and W.E. LeMasurier. 1990. Geochemical variations and tectonic affinities of Cenozoic alkali basaltic rocks from the Pacific margin of West Antarctica (abstract). *EOS Transactions American Geophysical Union,* 71, 1699.

LeMasurier, W.E. and J.C. Behrendt. 1999. Deformation characteristics of hyaloclastites and pillow lavas, West Antarctic rift system (abstract). *Abstracts with Programs, Geological Society of America,* 31, A-203.

LeMasurier, W.E. and C.A. Landis. 1996. Mantle-plume activity recorded by low-relief erosion surfaces in West Antarctica and New Zealand. *Geological Society of America Bulletin,* 108, 1450-1466.

Tulaczyk, S.M. and J. Krukowski. 1999. Geologic setting of the West Antarctic ice sheet and its influence on ice-sheet dynamics. *Abstracts with Programs, Geological Society of America,* 31, A-203.

Crustal structure and Cenozoic tectonics on the eastern margin of the Ross Sea, Marie Byrd Land

Christine Smith Siddoway, *Department of Geology, Colorado College*

Bruce P. Luyendyk, *Department of Geological Sciences, University of California at Santa Barbara*

Recent reconstructions of the Southern Ocean between New Zealand and West Antarctica suggest that significant continental extension in West Antarctica occurred almost entirely during Cretaceous rifting events between the two landmasses (Lawver and Gahagan 1994; McAdoo and Laxon 1997), with little extension accomplished by the Cenozoic and active West Antarctic Rift (e.g., Behrendt et al. 1994). Faulting and volcanism, mountain uplift, and glacier downcutting, however, appear to be active now in western Marie Byrd Land, where generally east-to-west-flowing outlet glaciers incise Paleozoic and Mesozoic bedrock exposed in basin-and-range-style mountains (figure 1*A*). Deglaciated summits indicate a previous north-south glacial flow direction (Richard and Luyendyk 1991); thus, it appears that differential movement has occurred between range blocks since initiation of west antarctic glaciation in Miocene time (Hambrey and Barrett 1993). It is important to gain understanding of Neogene structural activity because faults potentially influence locations and orientations of outlet glaciers and ice streams initiating in the west antarctic ice sheet.

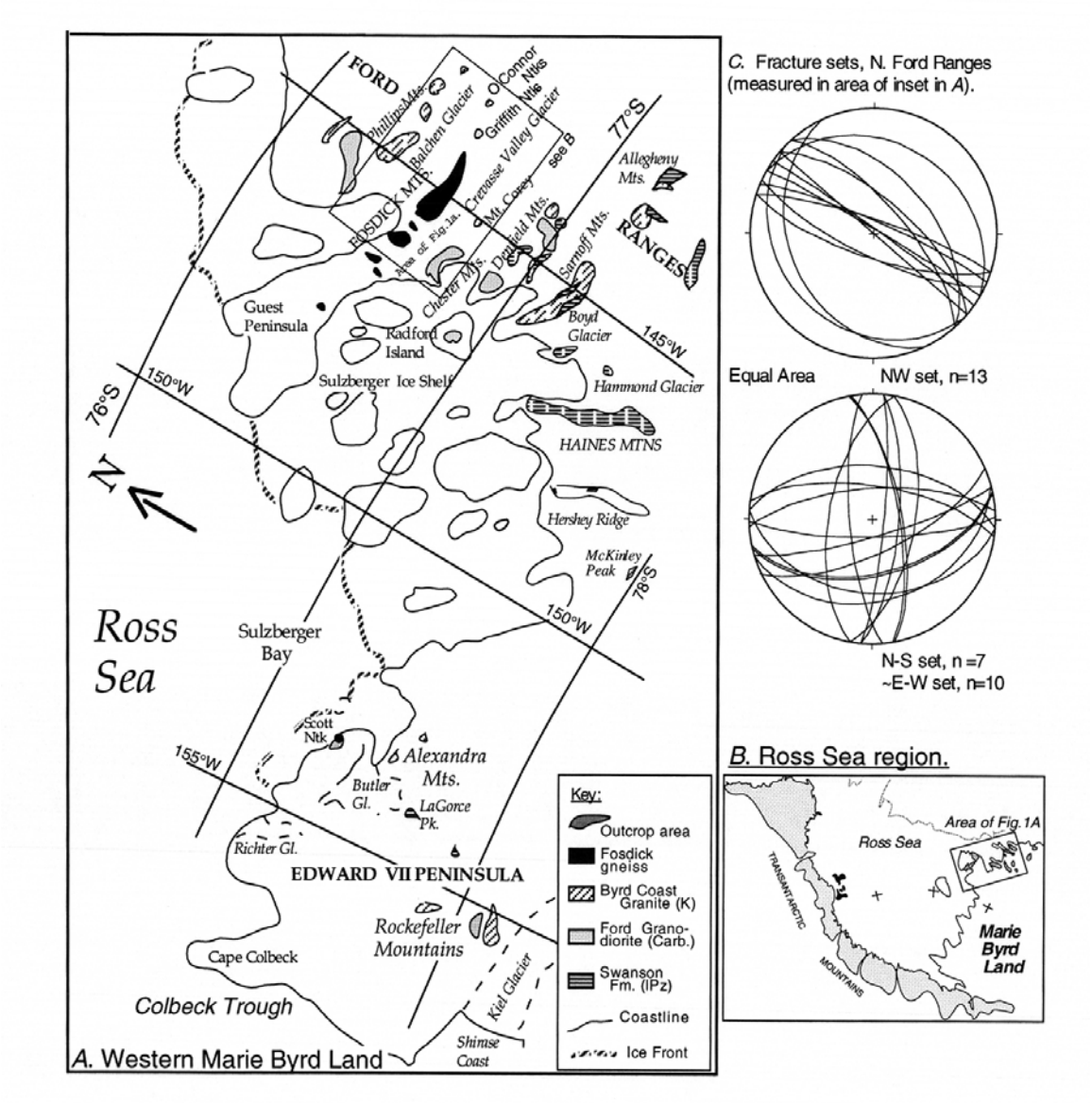

Figure 1.* A. *Generalized geological map for the Ford Ranges and Edward VII Peninsula, western Marie Byrd Land. The box outlines the area in which the structural measurements shown in* B *were collected.* B. *Location map for western Marie Byrd Land in the Ross Sea region, with boundary of* A *shown.* C. *Equal area stereonets for three brittle fracture sets developed in the northern Ford Ranges; data are for shear joints, joints, and minor faults.

Although major fault zones are concealed by glacier ice, minor structures promise to reveal the style and geometry of regional deformation in West Antarctica (e.g., Wilson 1995), once age relations are established. Joints, striated surfaces, and small-scale chloritic shear zones cut granitoids in the region, and minor faults cut basalts as young as 1.4 million years. Preliminary structural measurements recorded during prior field seasons (Luyendyk et al. 1992) show that brittle features strike predominantly northwest, with steep or moderate northeasterly dips. Lesser fault and fracture sets strike approximately east to west and north to south (figure 1*C*). Preliminary interpretations are that the lesser east-west and north-south sets coincide in orientation with fractures along

which volcanic centers have propagated in the central parts of the Marie Byrd Land "dome" (LeMasurier and Rex 1989; LeMasurier and Landis 1996). The northwest set coincides in orientation with the Colbeck Trough fault, recognized during 1996 marine work as the major structure on the east side of the Ross Sea rift (Luyendyk, Sorlien, and Bartek 1996).

Recently, fabrics indicative of a brittle-ductile shear zone (mylonitic fault zone) have been discovered in dredge samples retrieved from bedrock flanking Colbeck Trough (figure 1). Eighty-three of the 120 rock samples are coarse-grained granitic gneiss with well-developed mineral lineation and S-C fabric (figure 2). Consistent fabric asymmetry throughout individual clasts indicates development through plane strain simple shear in a potentially substantial shear zone. Were the samples oriented, an interpretation of kinematic shear sense would be possible. Fission track ages on Edward VII Peninsula suggest cooling in early Tertiary time (Lisker and Olesch 1997), a possible indication of timing of activity on this fault zone.

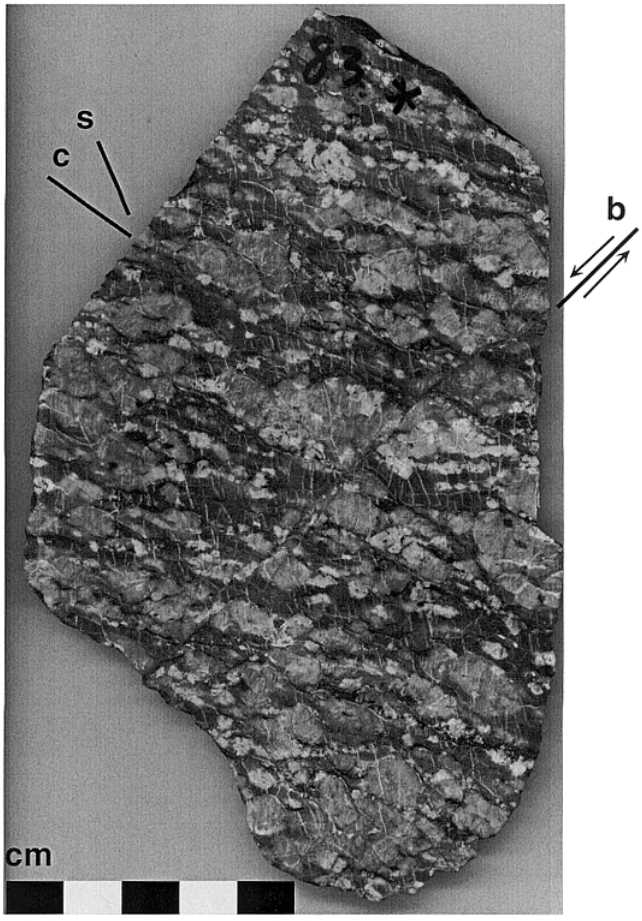

Figure 2. Hand sample (NBP-9601-D2-83) exhibiting mylonitic fabrics (labeled S, C), cut by a brittle fracture (indicated with "b"). Slab was cut parallel to the tectonic mineral lineation. Scale bar is 5 centimeters in length

The uniformity in rock type and deformational fabric among the 123 dredge samples suggests that the samples

- were recovered from their bedrock source and do not represent a random collection of glacial dropstones and
- are materials from a shear zone exposed on the margin of Colbeck Trough.

Samples of black, flinty cataclasite and chloritic breccia attest to a brittle deformational overprint, probably developed during exhumation of the mylonites to shallow crustal levels. A planar brittle offset is evident in figure 2. Nearby on land, a meter-thick cataclasite zone strikes approximately east to west, with a shallow northerly dip, and potentially provides an indication of the regional orientation of brittle structures.

These compelling findings have led us to undertake combined aerogeophysical and ground-based geological-geophysical research, focusing on the Cenozoic tectonic evolution of the Ford Ranges of Marie Byrd Land, at the boundary between the Ross Sea Rift and the Marie Byrd Land volcanic province. Our study will include aerogeophysics in a 123,000-square-kilometer area over the Ford Ranges, using the SOAR facility aircraft (Support Office for Aerogeophysical Research). The aerial surveys will target several key features in the region including the eastern edge of the Ross Sea rift, ice stream E, the transition from plateau topography on Edward VII Peninsula to the Ford Ranges, a gravity high mapped over the Fosdick Mountains (Luyendyk, Siddoway, and Druivenga in preparation), and the high-amplitude magnetic anomalies (volcanic centers?) detected southeast of the northern Ford Ranges, among others. Investigations during 1998–1999 and 1999–2000 seek to reveal the crustal structure in both outcrop and ice-covered areas. They will allow us to determine whether structure at the boundary is a result of

- Cenozoic extension on the eastern margin of the Ross Sea rift (Behrendt and Cooper 1991),
- uplift and crustal extension related to Neogene mantle plume activity (LeMasurier and Rex 1989) in western Marie Byrd Land, or
- a combination of the two.

The work is important for determining the influence of Neogene tectonics on the ice streams and west antarctic ice sheet.

The current research is supported by National Science Foundation grant OPP 96-15281. Previous work in the Ford Ranges was supported by National Science Foundation grant DPP 88-17615 (1989–1993) and by the German National Antarctic Program (1992–1993).

References

Behrendt, J.C., D.D. Blankenship, C.A. Finn, R.E. Bell, R.E. Sweeney, S.M. Hodge, and J.M. Brozena. 1994. CASERTZ aeromagnetic data reveal late Cenozoic flood basalts(?) in the west antarctic rift system. *Geology*, 22, 527–530.

Behrendt, J.C., and A. Cooper. 1991. Evidence of rapid Cenozoic uplift of the shoulder escarpment of the Cenozoic west antarctic rift system and a speculation on possible climate forcing. *Geology*, 19, 315–319.

Hambrey, M.J., and P.J. Barrett. 1993. Cenozoic sedimentary and climatic record, Ross Sea region, Antarctica. In J.P. Kennett and D.A. Warnke (Eds.), *The antarctic paleoenvironment: A perspective on global change, part two* (Antarctic Research Series, Vol. 60). Washington, D.C.: American Geophysical Union.

Lawver, L.A., and L.M. Gahagan. 1994. Constraints on timing of extension in the Ross Sea Region. *Terra Antarctica*, 1(3), 545–552.

LeMasurier, W.E., and C.A. Landis. 1996. Mantle plume activity recorded by low relief erosion surfaces in West Antarctica and New Zealand. *Geological Society of America Bulletin*, 108(11), 1450–1466.

LeMasurier, W., and D. Rex. 1989. Evolution of linear volcanic ranges in Marie Byrd Land, West Antarctica. *Journal of Geophysical Research*, 94, 7223–7236.

Lisker, F., and M. Olesch. 1997. Cooling and denudation history of Edward VII Peninsula, Marie Byrd Land, based on apatite fission track analysis. In C.A. Ricci (Ed.), *The antarctic region: Geological evolution and processes*. Siena, Italy: TerraAntarctica Publications.

Luyendyk, B.P., S.M. Richard, C.H. Smith, and D.L. Kimbrough. 1992. Geological and geophysical investigations in the northern Ford Ranges, Marie Byrd Land, West Antarctica. *Antarctic Journal of the U.S.*, 27(5), 37–40.

Luyendyk, B.P., C.S. Siddoway, and G. Druivenga. In preparation. Gravity measurements on King Edward VII Peninsula, Marie Byrd Land, West Antarctica, during GANOVEX VII. *Geologisches Jahrbuch*.

Luyendyk, B.P., C.C. Sorlien, and L.R. Bartek. 1996. Early Tertiary rifting in the eastern Ross Sea and offshore western Marie Byrd Land, Antarctica. *EOS, Transactions of the American Geophysical Union*, 77(46), F312.

McAdoo, D., and S. Laxon. 1997. Antarctic tectonics: Constraints from an ERS-1 satellite marine gravity field. *Science*, 276, 556–560.

Richard, S.M., and B.P. Luyendyk. 1991. Glacial flow reorientation in the southwest Fordick Mountains, Ford Ranges, Marie Byrd Land. *Antarctic Journal of the U.S.*, 26(5), 67–68.

Wilson, T. 1995. Cenozoic transtension along the Transantarctic Mountains–west antarctic rift boundary, southern Victoria Land, Antarctica. *Tectonics*, 14, 531–545.

Open-system degassing of fractionating magma, Mount Erebus, Ross Island

A.J. Eschenbacher and P.R. Kyle, *Department of Earth and Environmental Science, New Mexico Institute of Mining and Technology*

J.B. Lowenstern, *U.S. Geological Survey, Menlo Park, California*

Current volcanic activity at Mount Erebus takes the form of a convecting anorthoclase phonolite lava lake with frequent small explosive eruptions and a continuous gas plume. The continuous nature of the activity is thought to be related to the volatile budget of the magma feeding the system. The volcano is comprised predominantly of anorthoclase phonolite lavas with lesser amounts of basanite, phonotephrite and tephriphonolite. These lava compositions define a nearly continuous differentiation lineage. The basanite lava is presumed to represent the parental magma composition of the more evolved lava compositions.

Melt inclusions (MI) trapped in phenocrysts from the range of lava compositions were used to investigate the behavior of volatiles during fractional crystallization. Melt inclusions preserve the pre-eruptive magma composition, so the volatile concentrations are indicative of the undegassed magma (Lowenstern 1995). Water (H_2O) and carbon dioxide (CO_2) concentrations of melt inclusions were determined using Fourier Transform Infrared Spectroscopy and fluorine (F), chlorine (Cl), and sulfur (S) concentrations were determined by electron microprobe.

Electron microprobe and ion probe analyses of MI from the compositional range of lavas closely follow the trend of the bulk rock composition and mimic fractional crystallization models (Kyle, Moore, and Thirlwall 1992). Incompatible trace elements [lithium (Li), boron (B), rubidium (Rb), zirconium (Zr), and thorium (Th)] within the MI exhibit a fourfold increase in concentration; this is consistent with the phonolite being a residual liquid after 75 percent crystallization of the basanite parent. Volatiles dissolved in the magma also act as incompatible elements. Therefore, if the volatiles are completely conserved in the fractionating magma, their concentrations should exhibit a factor of four increase with fractional crystallization. Any deviation from such a trend indicates the stage at which volatiles degas.

Water concentrations in basanite MI range from 1.15 to 1.75 percent weight. Then the water contents drop to 0.1 percent weight in phonolite. Carbon dioxide contents of basanite MI range from 4000 to 7300 parts-per-million (ppm). The CO_2 contents decrease to values around 700 ppm in phonolite. Sulfur contents of melt inclusions exhibit a decreasing trend from basanite (~2,500 ppm) to phonolite (~400 ppm). Fluorine concentrations in MI remain somewhat constant through the range of melt compositions. Average fluorine contents range from ~1,600 to 2,600 ppm. Chlorine concentrations of MI show a trend of increasing trend from 740 ppm in basanite to 1500 ppm in phonolite.

None of the volatiles exhibit concentration increases on the order predicted by the

incompatible nature of volatiles. The pre-eruptive volatile contents indicate that the volatiles are not completely conserved in the fractionating magma. This suggests that degassing is continuous through fractionation of basanite to phonolite. The degassing of CO_2, H_2O, and S is likely due to solubility of the volatiles, decreasing with magma evolution (Dixon 1997; Moore, Vennemann, and Carmichael 1998; Carroll and Webster 1994). The solubility decrease is caused by the changing magma composition, as well as the decreasing pressure as the magma rises to shallower levels in the crust. The relatively small fraction of F and Cl lost is probably due to limited partitioning of these elements into the H_2O-bearing fluid phase (Carroll and Webster, 1994).

The CO_2 and H_2O contents of the basanite MI equate to vapor saturation pressures of 3 to 4.5 kilobars (figure). The saturation pressure also provides a minimum estimate of the melt inclusion entrapment depths of 8 to 13 kilometers. At these pressures, the magma will be saturated with respect to H_2O and CO_2 and will begin to degas. The dashed contours on Figure 1 indicate the composition of the fluid phase that will exsolve from the magma at a given melt composition. The MI in the basanite reflect crystallization at depths of 8 to 13 kilometers in equilibrium with a CO_2-rich fluid (~90 mole percentage CO_2). The data require that degassing initiates deep within the Mount Erebus magmatic system.

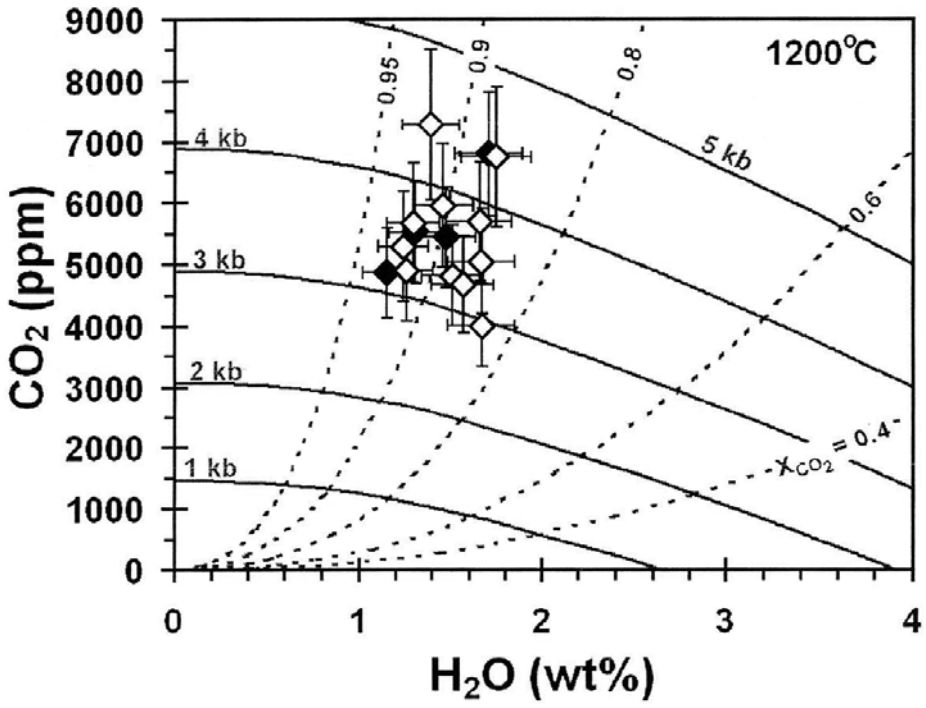

Vapor saturation diagram modeled for basanite at 1200°C. Solid contours represent the isobaric range of melt compositions in equilibrium with an H_2O-CO_2 vapor. Intersection of the isobar with the X-axis is equal to the end-member solubility of H_2O, and intersection of the isobar with the Y-axis equals the CO_2 solubility. Dashed contours are isopleths for the composition of exsolved fluid in equilibrium with the silicate melt. Interpolation of the MI compositions yields the minimum pressure at which the inclusion could have been trapped, and the composition of fluid exsolved from the melt at that pressure. Error bars represent 2σ uncertainty of the basanite melt inclusion H_2O and CO_2 analyses.

The volatile contents of melt inclusions from the series of lava compositions have been determined in order to assess where degassing initiates in the Mount Erebus magma system. The MI data suggest that the magma is degassing under open system conditions, as well as continuously throughout the fractionation process. The MI data also indicates the degassing process commences at a depth of at least 13 km. The open-system degassing helps to explain the large flux of gases from the volcano in comparison to the relatively small flux of lava erupted out of the volcano. We believe the style of degassing may also contribute to the inherent stability and continuity of the volcanic activity of Mount Erebus. Volatile-rich magma buoyantly rises through degassed magma and drives convection. The volatiles, especially CO_2, heat upon irreversible decompression (degassing) because of the Joule-Thomson effect. Thus, volatile degassing maintains the near-surface phonolite magma reservoir by driving convection and providing a rapidly transferable heat source.

This study was funded by NSF OPP 94-19267. Thanks to Nelia Dunbar for help with the electron microprobe analyses and Richard Hervig for help with the ion probe analyses.

References

Carroll, M.R., Webster, J.D., 1994. Solubilities of sulfur, noble gases, nitrogen, chlorine, and fluorine in magmas. In: Carroll, M.R., Holloway, J.R., (eds.) *Volatiles in Magmas.* Washington, D.C.: Mineralogical Society of America*, Reviews in Mineralogy* (30), pp. 231-279.

Dixon, J.E., 1997. Degassing of alkalic basalts. *American Mineralogist*, 82(7-8)**,** pp. 368-378.

Lowenstern, J.B., 1995. Applications of silicate-melt inclusions to the study of magmatic volatiles. In: Thompson, J.F.H. (ed.), *Magmas, Fluids, and Ore Deposits.* Nepean, Ontario: Mineralogical Association of Canada Short Course Series (23)**,** pp.71-99.

Kyle, P.R., Moore, J.A., Thirlwall, M.F., 1992. Petrologic evolution of anorthoclase phonolite lavas at Mount Erebus, Ross Island, Antarctica. *Journal of Petrology,* 33 (4)**,** pp. 849-875.

Moore, G., Vennemann, T., Carmichael, I.S.E., 1998. An empirical model for the solubility of H_2O in magmas to 3 kilobars. *American Mineralogist,* 83 (1), pp. 36-42.

New Holocene $^{40}Ar/^{39}Ar$ dates for Mount Erebus summit plateau lava flows

Christopher J. Harpel, Philip R. Kyle *and*, W.C. McIntosh, *Department of Earth and Environmental Science, New Mexico Institute of Mining and Technology*

Mount Erebus is an active anorthoclase phonolite volcano and is the dominant feature of Ross Island. Many aspects of Mount Erebus have been studied and are summarized in Kyle (1994). Initial age constraints on Mount Erebus were limited to a handful of conventional potassium/argon (K/Ar) dates (Treves 1968; Armstrong 1978; Moore and Kyle 1987). Esser (1996) used the $^{40}Ar/^{39}Ar$ dating method to develop the beginnings of an eruptive history for Mount Erebus with ages ranging from 1131±16 to 11±8 thousand years ago. The current study was undertaken to investigate the young eruptive activity in the summit plateau area of Mount Erebus, in the hopes of documenting Holocene activity before the first historic records that begin in 1841 (Kyle et al. 1982).

The current activity of Mount Erebus includes a convecting lava lake in the main crater of the summit cone, and frequent small strombolian eruptions (Kyle et al. 1982). Surrounding the summit cone is a broad plateau interpreted as a caldera that has been filled by post-collapse lava flows. These lava flows have abundant fresh flow features (ropy pahoehoe) and are some of the youngest features on Mount Erebus (Moore and Kyle 1987). Caldwell (1989) mapped 10 separate flow units, and the associated vents within the summit plateau. Due to a lack of exposed overlapping relationships, he was able to determine only a very tentative stratigraphy. Esser (1996) determined that caldera collapse occurred after 87 thousands of years ago by dating a truncated pre-caldera-collapse flow and the post-collapse Lower Hut Flow (these names are all unofficial, after Caldwell, 1989) at 11±8 thousand years old.

Both Armstrong (1978) and Esser et al. (1997) found excess argon in rocks from Mount Erebus. Abundant large (≤10 centimeters) anorthoclase phenocrysts containing up to 30 percent (by volume) melt inclusions are present in all of the summit plateau lava flows (Dunbar, Cashman, and Dupré 1994). These melt inclusions act as a host for the excess argon. Zero-age anorthoclase can yield $^{40}Ar/^{39}Ar$ ages as high as 670 thousand years old (Esser et al. 1997). To avoid this problem, Esser et al. (1997) developed a process of crushing and acid-leaching to remove the excess argon-bearing glass from the anorthoclase.

Anorthoclase phenocrysts from four post-collapse lava flows on the summit plateau were prepared using the methods of Esser et al (1997). $^{40}Ar/^{39}Ar$ analyses were performed using the methods summarized in table 1 and detailed in Esser (1996). All of the age spectra yielded plateau ages, and are relatively flat at temperatures below 1200° C, suggesting that excess argon was not present (figure). Steps above 1,200°C give anomalously old ages, probably due to excess argon released from melt inclusions during melting of the anorthoclase (Esser et al 1997).

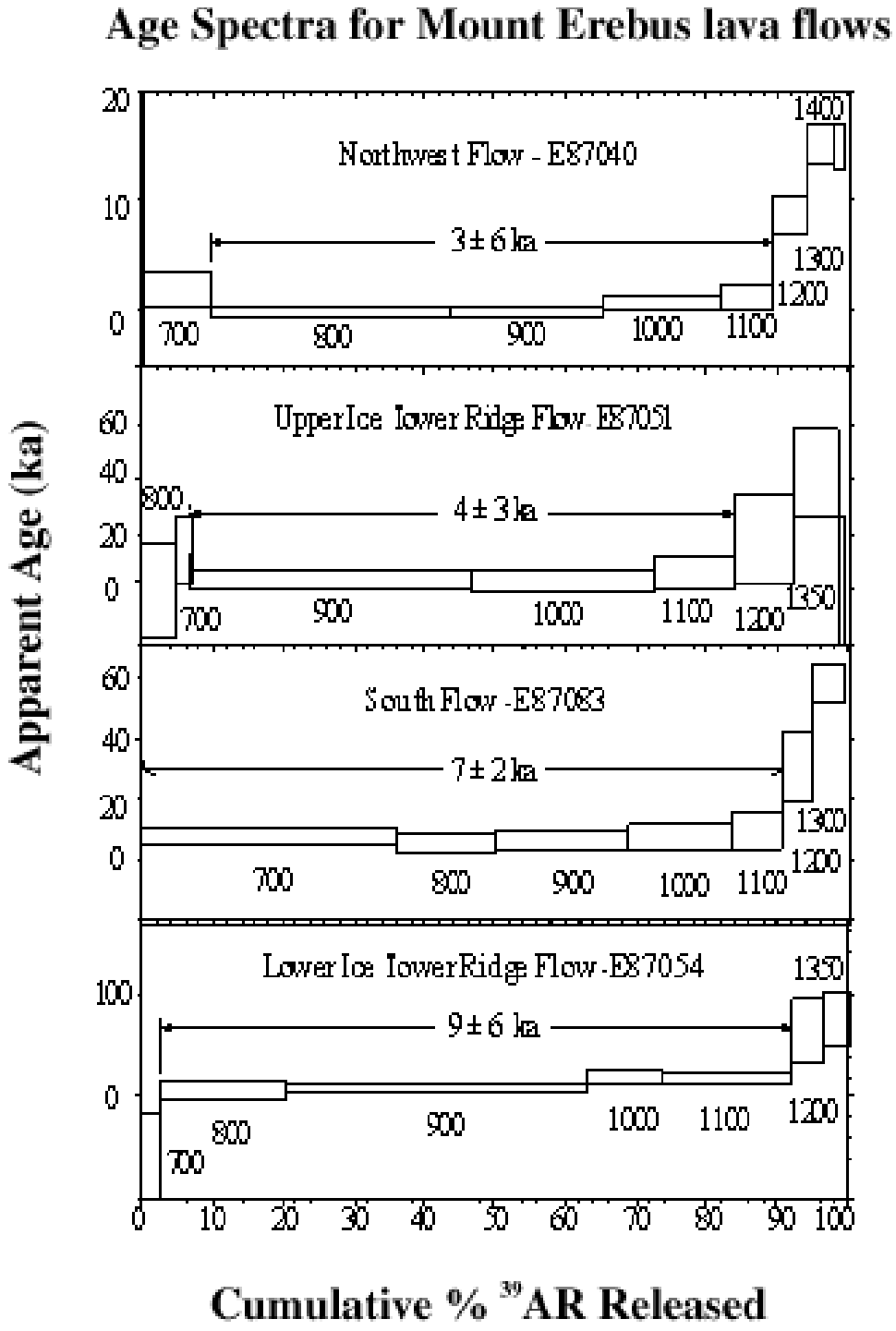

Age spectra for the dated summit plateau lava flows. Argon is extracted from each sample at progressively higher temperatures. For each temperature step an apparent age is calculated from the gas released and is plotted against the cumulative percent ^{39}Ar released. Temperatures are listed in degrees Celsius below or beside the corresponding steps. Final ages are calculated as plateau ages where a plateau is defined as three or more consecutive steps of the same age (within 95 percent confidence) that comprise more than 50 percent of the cumulative ^{39}Ar released. The overall age of the sample is a weighted mean of the apparent ages of the plateau forming steps. The plateau-forming steps and the sample ages in thousands of years are shown.

Summary table of $^{40}Ar/^{39}Ar$ ages for the summit plateau lava flows of Mount Erebus.

Flow Unit	Sample #	Age (±2σ)	Reference
Northwest	E87040	1 ± 5 ka	This study
Upper Ice Tower Ridge	E87051	4 ± 3 ka	This study
South	E87083	6 ± 2 ka	This study
Lower Ice Tower Ridge	E87054	9 ± 7 ka	This study
Lower Hut	E87034	11 ± 4 ka	This study

Notes: Samples were irradiated at the University of Michigan Ford Research Reactor. Fish Canyon Tuff Sanidine (27.84 Ma, after Deino and Potts 1990, based on an age of 520.4 Ma for MMhb-1 after Samson and Alexander 1987) was used as a flux monitor. All analyses were performed at the New Mexico Geochronological Research Laboratory, New Mexico Institute of Mining and Technology using the decay constants of Steiger and Jäger (1977). All ages have been corrected for blank, mass discrimination, and reactor induced interference. Sample locations are given in Caldwell (1989).

The four dated lava flows are shown in table 1. The Lower Ice Tower Ridge Flow (9±7 thousand years old), South Flow (6±2 thousand years old), Upper Ice Tower Ridge Flow (4±3 thousand years old), and Northwest Flow (1±5 thousand years old) (table 1). These new ages demonstrate that Mount Erebus has been active throughout much of the Holocene. The proximal location of the summit plateau lava flows to the current vent and the lack of Holocene eruptive products elsewhere on the volcanic edifice indicate that eruptive activity has been concentrated within the summit plateau since the Late Pleistocene.

Samples used for dating were collected during the 1987 Antarctic field season by D.A. Caldwell and P.R. Kyle. Field work during 1997 was greatly aided by Al Eschenbacher, L. Jean Wardell, and Kurt Panter. Matt Heizler, Lisa Peters, and Rich Esser of the New Mexico Geochronological Research Laboratory provided invaluable assistance in dating of the samples. Also, without the able pilots of Petroleum Helicopters Inc., none of this work could have been accomplished. This work was supported by National Science Foundation grant OPP 94-19267

References

Armstrong, R.L. 1978. K-Ar dating: Late Cenozoic McMurdo Volcanic Group and dry valley glacial history, Victoria Land, Antarctica. *New Zealand Journal of Geology and Geophysics*, 21(6), 685-698.

Caldwell, D.A. 1989. Physical and geochemical properties of summit flows and recent volcanic ejecta from Mount Erebus, Ross Island, Antarctica. (M.S. independent study, New Mexico Institute of Mining and Technology, Socorro, New Mexico.)

Deino, A., and R. Potts. 1990. Single crystal $^{40}Ar/^{39}Ar$ dating of the Olorgesailie Formation, southern Kenya Rift. *Journal of Geophysical Research*, 95(B6), 8453-8470.

Dunbar, N.W., K.V. Cashman, and R. Dupré. 1994. Crystallization processes of anorthoclase phenocrysts in the Mount Erebus magmatic system: Evidence from crystal composition, crystal size distributions, and volatile contents of melt inclusions. In P.R. Kyle (Ed.), *Volcanological and environmental studies of Mount Erebus, Antarctica-* (Antarctic Research Series, Vol. 66). Washington, D.C.: American Geophysical Union.

Esser, R.P. 1996. $^{40}Ar/^{39}Ar$ dating of Mount Erebus volcano, Antarctica. (M.S. thesis, New Mexico Institute of Mining and Technology, Socorro, New Mexico.)

Esser, R.P., W.C. McIntosh, M.T. Heizler, and P.R. Kyle. 1997. Excess argon in melt inclusions in zero-age anorthoclase feldspar from Mt. Erebus, Antarctica, as revealed by the $^{40}Ar/^{39}Ar$ method. *Geochimica et Cosmochimica Acta*, 61(18), 3789-3801.

Kyle, P.R. (Ed.). 1994. *Volcanological and environmental studies of Mount Erebus, Antarctica* (Antarctic Research Series, Vol. 66). Washington, D.C.: American Geophysical Union.

Kyle, P.R., R.R. Dibble, W.F. Giggenbach, and J. Keys. 1982. Volcanic activity associated with the anorthoclase phonolite lava lake, Mount Erebus, Antarctica. In C. Craddock (Ed.), *Antarctic Geoscience-* (International Union of Geological Sciences, Series B, No. 4). Madison, Wisconsin: University of Wisconsin Press.

Moore, J.A., and P.R. Kyle. 1987. Volcanic geology of Mount Erebus, Ross Island, Antarctica. *Proceedings of the NIPR symposium on Antarctic geosciences*, 1, Tokyo, Japan, 48-65.

Samson, S.D., and E.C. Alexander, Jr. 1987. Calibration of the interlaboratory ^{40}Ar-^{39}Ar dating standard MMhb-1. *Chemical Geology*, 66, 27-34.

Steiger, R.H., and E. Jäger. 1977. Subcomission on geochronology: Convention on the use of decay constants in geo- and cosmochronology. *Earth and Planetary Science Letters*, 36, 359-362.

Treves, S.B. 1968. Volcanic rocks of the Ross Island area. *Antarctic Journal of the United States*, 3(4), 108-109.

Broadband seismic recording of Strombolian explosions at Mount Erebus

C.A Rowe, EES-11, *Los Alamos National Laboratory*

R.C. Aster and P.R. Kyle, *Department of Earth and Environmental Science, New Mexico Institute of Mining and Technology*

In December 1996 and January 1997, five Incorporated Research Institutions for Seismology (IRIS) PASSCAL (Program for Array Seismic Studies of the Continental Lithosphere) seismographs were deployed on Mount Erebus to augment the permanent, short-period (SP) Mount Erebus Volcano Observatory (MEVO) network (figure 1). Three, three-component Guralp CMG-3ESP broadband sensors with a low-frequency response corner at 30 seconds and sample rate of 40 Hz were installed on the summit plateau in a radial line at distances of 0.7, 1.4, and 1.9 kilometers from the lava lake (figure lb), providing the first broadband seismic observations of the volcano's frequent lava lake explosions (Rowe et al., 1998; Rowe et al., 2000; Aster et al., 2003; Aster et al., 2004).

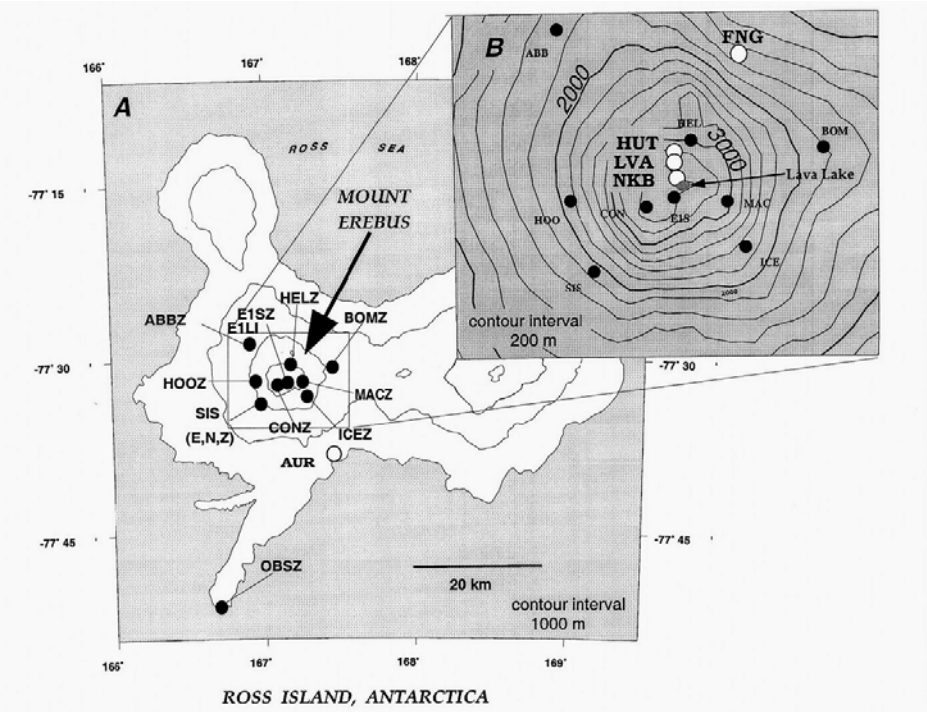

Figure 1. Map of Ross Island, Antarctica, showing stations in the permanent MEVO short-period seismic network (black circles) and IRIS/PASSCAL stations (larger, white circles). Broadband stations NKB, LVA and HUT (inset) were deployed in a near-radial line extending North from the phonolitic lava lake during this pilot deployment.

Figure 2a shows a typical explosion detected by the SP network on 15 December 1996. Explosion onsets on SP records are emergent and usually show small-amplitude, lower frequency (approximately 1 Hz) precursory signals a second or two ahead of the first strong arrival (Dibble, O'Brien and Rowe, 1994). SP spectra show energy largely

confined between frequencies of 1 and 6 Hz (Rowe et al., 1998).

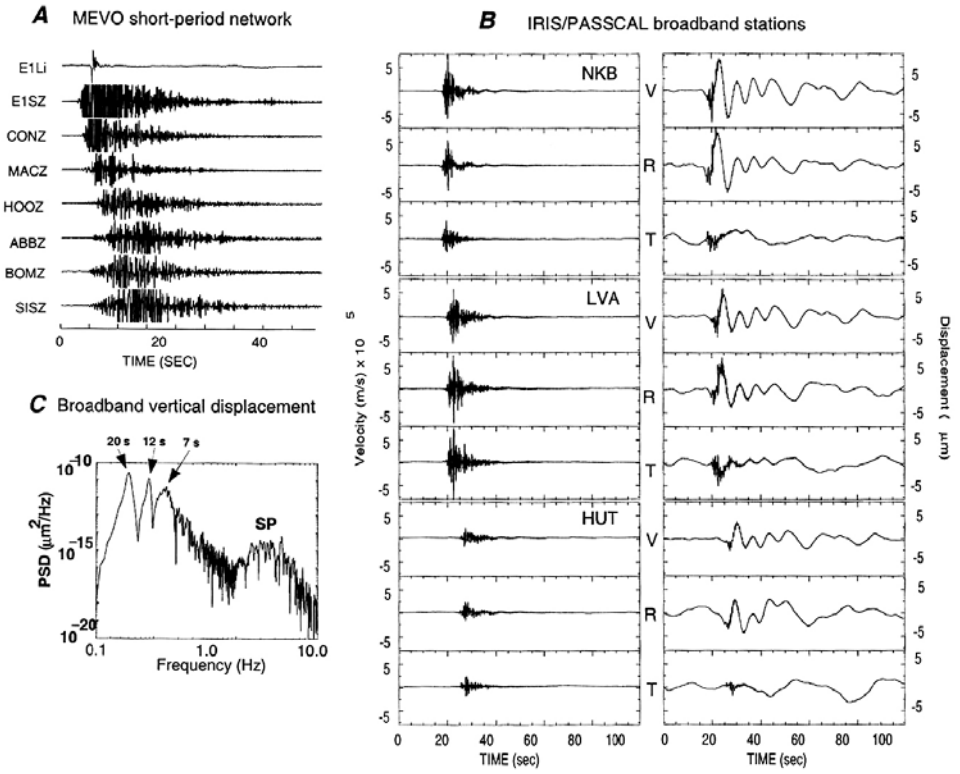

Figure 2.

a) ***15 December 1996 explosion recorded by the short-period MEVO network (vertical component velocity sensors, except for infrasonic sensor EILI)***

b) ***Same explosion recorded by broadband sensors NKB, LVA and HUT, rotated into V (vertical), R (radial) and T (tangential) components, with velocity records at left and corresponding displacement records at right.***

c) ***Displacement-power, spectral-density plot for NKB vertical component. Note prominent VLP spectral peaks near 7, 12, and 20 seconds and short-period (SP) surface explosion energy.***

Figure 2b shows three-component velocity and displacement seismograms for the broadband stations NKB, LVA and HUT for the explosion shown in figure 2a. The longer-period signal visible in the broadband traces is sufficiently outside of the passband of the SP seismometers to be invisible to them (figure 2a). A displacement power spectrum (figure 2c) from station NKB shows large peaks near 7, 12, and 20 seconds, arising from very long period (VLP) signals. Displacement VLP records (figure 2b) are very similar among events and among stations in the broadband network and persist for at least 80 seconds. For the largest events, inter-event similarity is observable for over 150 seconds (e.g., Rowe et al. 2000), indicating a nondestructive or self-reconstructing source process (figure 3a). Displacement seismograms also reveal that the VLP signal arrives at least 1.5 seconds before the initial SP arrival; the first motion indicates an implosive initiation during this time period of observation, and the VLP signal is largely restricted to the vertical-radial (VR) plane (figure 2b).

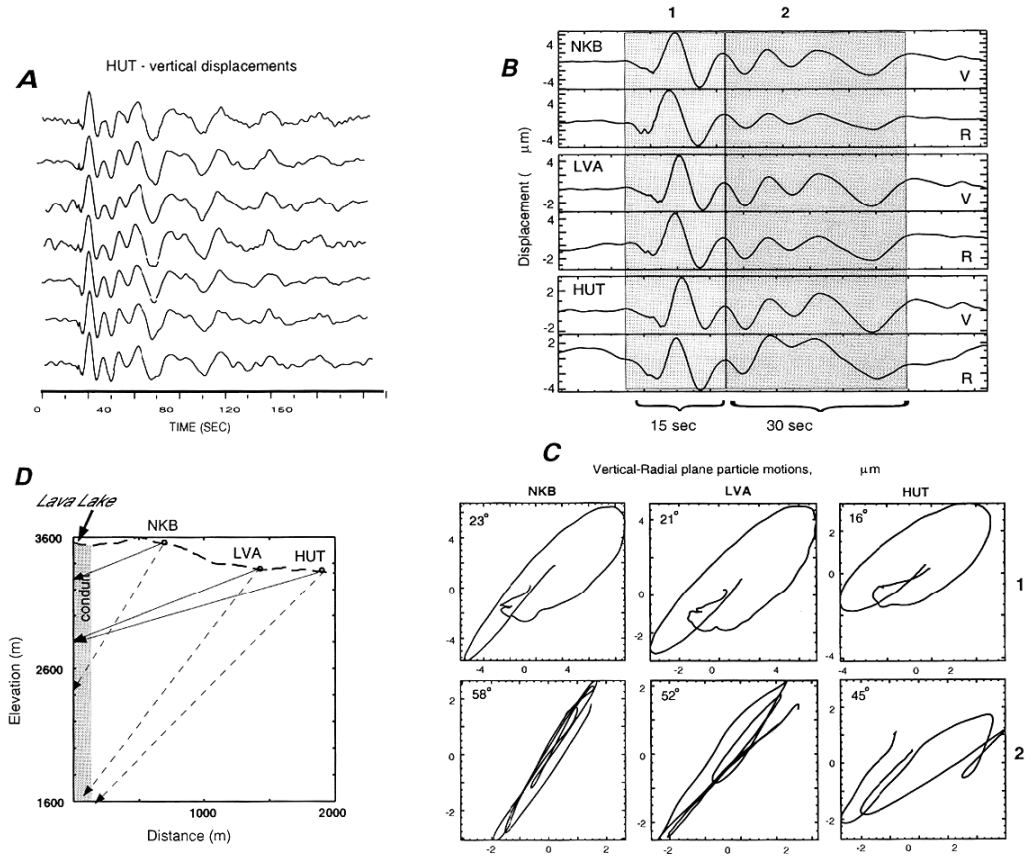

Figure 3.

*a) **Seven 0.5 Hz low-pass, filtered vertical displacement explosion records from HUT illustrating VLP repeatability among explosions.***

*b) **Vertical (V) and radial (R) component displacement records for the 15 December explosion (figure 2). The 15-second time window labeled "1" corresponds to the upper particle motion plots in 3c. The 30-second time window labeled "2" corresponds to the lower particle motion plots in 3c.***

*c) **Particle motions in the vertical-radial plane for the traces shown in 3b, time segments I and 2. Initial and final inclination of the elliptical particle motion major axis is indicated for each trace.***

Projections of initial and final particle motion directions: solid lines correspond to time window (1) and dotted lines correspond to time window (2). Recent moment tensor inversion (McNamara, 2004) indicates that the VLP signal arises from a subhorizontal crack-like source with superimposed single (inertial) forces associated with magma and gas transport.

Vertical (V) and radial (R) component traces (figure 3b) at all three summit plateau stations show that the VLP displacement signal exhibits a retrograde elliptical particle motion during its first 15 seconds, whose major axis dips inwards and downwards, towards the volcano axis (figure 3c, top). The initial, dilatational dip angle ranges from 23 degrees at NKB (0.7 km from the lava lake) to 16 degrees at HUT (1.9 km from the lava lake). In the course of about 15 seconds, the dip axis steepens (Rowe et al. 1998; Rowe et al. 2000, Aster et al., 2003), and the motion becomes more linear

(figure 3c, bottom). Later inclinations range from 58 degrees (NKB) to 45 degrees (HUT). An examination of seven other high-quality explosion recordings from HUT confirms the consistency of this behavior.

Mogi (1958) showed that quasi-static displacements due to a spherical pressure source in an elastic half-space are radial with respect to the source centroid; hence, VLP particle motions suggest that the VLP source resides 300 to 800 meters beneath the lava lake surface. Figure 3d illustrates the projections of both the initial and later particle motions for this explosion. Topography, structural heterogeneity and (especially) radial tilt, however, will all contribute to an exaggerated apparent depth.Subsequent moment tensor analysis (McNamara, 2004) has shown that the VLP waveforms can be well fit with a very shallow (less than 100 m) subhorizontal crack-like source, coupled with a vertical single force.

Our observations are consistent with a model in which explosions initiate with the sudden buoyant rise of a large gas slug accumulating at some constriction at depth (e.g. Chouet et al. 1997; Hagerty et al. 1997. The implosive volumetric source decays with a time constant on the order of 10 seconds (Chouet et al. 1998), producing an implosive VLP signal (Neuberg et al. 1994). VLP signals continuing for up to 200 s result from the interaction of low-rigidity conduit structures during recharge of the explosively eviscerated lava lake, perhaps in association with resonance and/or nonlinear excitation mechanisms (e.g., Julian 1994, Aster et al., 2003). Study of these unusual eruption signals is presently ongoing using a larger network of broadband and other geophysical sensors (Aster et al., 2004).

This research was supported by NSF grant OPP 94-19267. Instrumental support was provided by the NSF IRIS Consortium PASSCAL program. We thank Glen Grant of Antarctic Support Associates for significant field assistance during the experiment.

References

Aster, R., S.Y. Mah, P. Kyle, W. McIntosh, N. Dunbar, J. Johnson, M. Ruiz, S. McNamara, 2003. Very long period oscillations of Mount Erebus volcano, *J. Geophys. Res*. 108(B11), 2522, doi:10.1029/2002JB002101.

Aster, R., W. McIntosh, P. Kyle, R. Esser, B. Bartel, N. Dunbar, B. Johns, J. Johnson, R. Karstens, C. Kurnik, M. McGowan, S. McNamara, C. Meertens, B. Pauly, M. Richmond and M. Ruiz, 2004. Real-time data received from Mount Erebus, Antarctica, *EOS*, Trans. AGU, 85(10), 97, 10.1029/2004EO100001.

Chouet, B., G. Saccorotti, M. Martini, P. Dawson, G. De Luca, G. Milana, and R. Scarpa. 1997. Source and path effects in the wave fields of tremor and explosions at Stromboli Volcano, Italy, *Journal of Geophysical Research, v.* 102, pp. 15,129-15,150.

Chouet, B., P. Dawson, G. DeLuca, M. Martini, G. Milana, G. Saccorotti, and R. Scarpa. 1998. *Array Analyses of Seismic Wavefields Radiated by Eruptive Activity at Stromboli Volcano, Italy*, Gruppo Nazionale per la Vulcanologia, Italia, Litografia Felici, Pisa, Italy, 158 pp.

Dibble, R.R., B. O'Brien, and C.A. Rowe. 1994. The velocity structure of Mount Erebus, Antarctica, and its lava lake. In P.R. Kyle (editor) *Volcanological and Environmental Studies of Mount Erebus, Antarctica,* Antarctic Research Series, Volume 66. Washington D. C.: American Geophysical Union.

Hagerty, M., S.Y. Schwartz, M. Protti, M. Garces, and T. Dixon. 1997. Observations at Costa Rican volcano offer clues to causes of eruptions. *EOS,* American Geophysical Union, v. 78, pp. 565, 570-571.

Julian, B. 1994. Volcanic tremor: nonlinear excitation by fluid *flow. Journal of Geophysical Research, v.* 99, pp. 11,859-11,877.

McNamara, S., 2004. *Source Mechanism Inversion of Very Long Period Signals Associated with Strombolian Eruptions at Mount Erebus, Antarctica*, M.S. Thesis, New Mexico Institute of Mining and Technology, 77 pp.

Mogi, K. 1958. Relations of the eruptions of various volcanoes and the deformations of the ground surfaces around them. *Bulletin of the Earthquake Research Institute of Tokyo University,* v. 36, pp. 99-134.

Neuberg, J., R. Luckett, M. Ripepe, T. Braun. 1994. Highlights from a seismic broadband array on Stromboli volcano. *Geophysical Research Letters,* v.21, pp. 749-752.

Rowe, C.A., R.C. Aster, P.R. Kyle, J.W. Schlue and R.R. Dibble. 1998. Broadband recording of Strombolian explosions and associated very-long-period seismic signals on Mount Erebus volcano, Ross Island, Antarctica. *Geophysical Research Letters,* v.25, pp. 2297-2300.

Rowe, C.A., R.C. Aster, P.R. Kyle, R.R. Dibble and J.W. Schlue, 2000. Seismic and acoustic observations at Mount Erebus volcano, Ross Island, Antarctica, 1994-1998. *Journal of Volcanology and Geothermal Research*, v. 101, pp. 105-128.

Seismic observations at the Mount Erebus Volcano Observatory: 1997-1998

C.A. Rowe, *EES-11, Los Alamos National Laboratory*

R.C. Aster, P.R. Kyle and A. Eschenbacher, *Department of Earth and Environmental Science, New Mexico Institute of Mining and Technology*

The Mount Erebus Volcano Observatory (MEVO) seismic network (figure 1, Rowe, Aster and Kyle *Antarctic Journal*, in this issue) continues to provide new insights into the nature of Mount Erebus seismic events. The addition of continuous digital recording in 1997 has permitted detailed analysis of sustained signals that previously were available only in analog form. Discrete seismic signals are dominated by lava lake explosions and icequakes within or beneath Ross Island glaciers. Sustained signals include lava lake degassing, glacier movement on the volcano's flanks, and volcanic tremor.

Lava lake explosion counts vary from several per day up to swarms of 900 per day. Explosion behavior is likely controlled by the shallow magmatic volatile budget. The gas source is generally considered to be exsolution of magmatic volatiles, although external contributions may also be important. On 19 December 1997, an avalanche of rock, snow, and ice was observed to slump off the crater wall into the lava lake. Within seconds, MEVO personnel on the crater rim observed numerous small bubble bursts. This elevated activity comprised a 3-day swarm of over 630 events. Such occurrences are probably infrequent, however, and the usual mechanism for triggering explosion swarm activity may be a combination of factors perturbing the shallow volatile regime.

Cumulative explosion size at station ABB (figure 1, Rowe, Aster and Kyle, *Antarctic Journal*, in this issue), calculated from triggered seismic records, is shown in figure 1a for 364 events from October 1997 to July 1998. The overall curve is comprised of distinct pulses of activity, corresponding to episodic swarm behavior illustrated in figure lb, wherein explosions and their relative sizes are plotted against time. This behavior may represent cycles of volatile recharge. Explosion sizes follow an approximate power law distribution. Figure lc illustrates the histogram of event numbers as a function of maximum ground velocity. Figure ld shows the corresponding cumulative log(count)/log(size) slope (b-value) is approximately 1.7. This power law distribution indicates self-similarity in the explosion population and thus argues against a preferred size over the range examined; however, Rowe et al. (2000) note that the significant break in slope corresponds to an observed decay in seismic vs. acoustic amplitude for these explosions, and suggests poorer seismic coupling among small events.

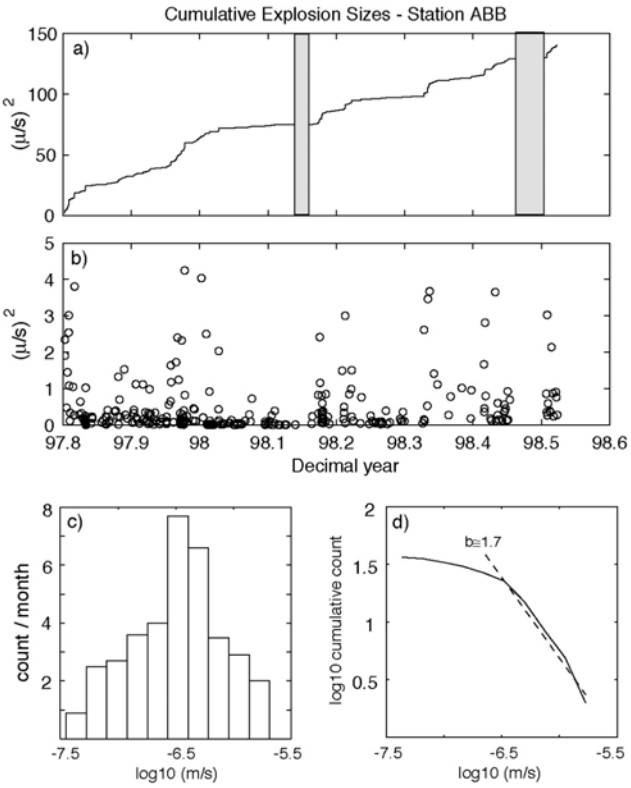

Figure 1. Explosion behavior between October 1997 and July 1998.

d) ***Cumulative curve of explosion size (maximum ground velocity at station ABB); 364 events showing that explosive volatile release proceeds in pulses, corresponding to explosion "swarms" indicated in b). Shaded areas of the cumulative curve represent times of high wind noise (near 98.1) or network outages (during winter months near 98.5) that resulted in a reduction or inability of the event detection algorithm to detect explosive seismicity.***

e) ***Explosion sizes (vertical scale) plotted as a function of time (horizontal axis) illuminating swarm-type behavior.***

d) ***Size distribution plotted as a histogram of counts per month versus size, and d) as log(count) vs. log(size), showing an approximate slope (b-value) of 2 (dashed line) indicating an approximate power law distribution over the range considered.***

An evaluation of discrete non-explosion events suggests that most originate within Ross Island glaciers. The strongly seasonal nature of overall triggered seismicity counts (figure 2), with seismicity peaks during the late summer and early autumn, suggests that many non-explosion events represent glacier activity.

Many extended, chaotic signals appear to originate within the summit crater and may arise from degassing within the lava lake (e.g., Dibble et al 1988). Because no evidence exists for rock avalanches outside of the crater, nor current eruption or fumarolic emissions on the volcano's flanks, we believe most extended flank signals probably arise from glacier activity.

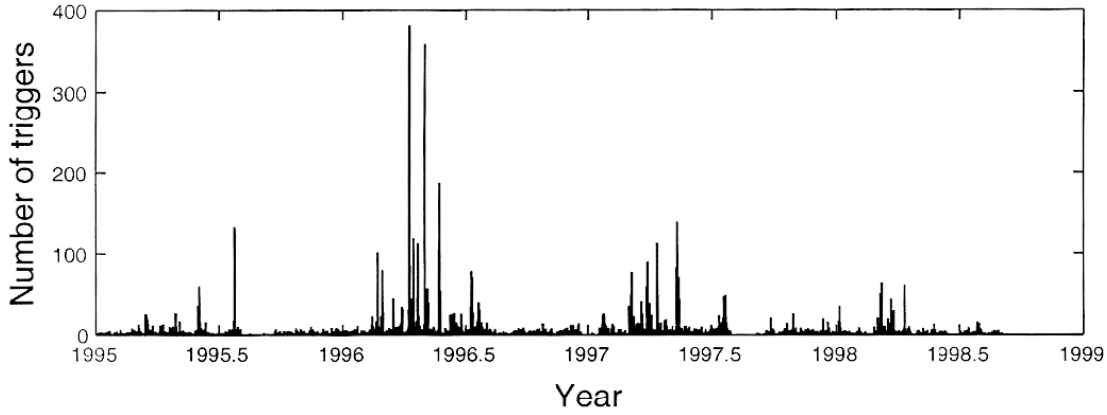

Figure 2. Three-year histogram of triggered event counts for the MEVO network. The annual cycle peaking in late summer/ early autumn shows that the source of most triggered events is seasonally-dependent; this supports the interpretation of much non-explosion seismicity as ice/temperature-related. Variation between annual maxima is partly due to modification of triggering parameters in the data acquisition system. Brief periods of zero triggering near 1995.5, 1996.5 and 1997.5 represent seasonal network outages due to power loss during the austral winter.

Erebus has exhibited surprisingly few instances of harmonic tremor, despite its ongoing eruptive behavior. Tremor was observed on analog records in October 1982 (Kienle et al. 1983). In January 1985, the MEVO triggered digital system captured a 20-minute episode of monochromatic tremor (Knight et al. 1996).

On 11 May 1998, a more complex episode of tremor occurred (Rowe et al. 2000). A 30-second sample of the 50-samples-per-second, continuous digital recording is shown in figure 3a. This instance of tremor exhibits at least 12 strong spectral peaks (figure 3b). Highest amplitudes of -0.6 mm/s occur at station EIS (figure 1, Rowe, Aster and Kyle *Antarctic Journal*, in this issue), nearest the central conduit and lava lake. Gliding—a gradual, proportional frequency shifting of spectral peaks (e.g., Hagerty et al. 1997)—is clearly evident (figure 3b). Gliding may represent alteration of the physical dimensions of a resonating chamber (e.g., Chouet 1996) or a change in acoustic properties of the melt (e.g., Garces et al. 1998). Another episode of complex tremor occurred on 2 September1998. Tremor amplitudes are about five times less attenuated with distance than those of lava lake explosions, implying a comparatively deep tremor source. Since 1998, additional episodes of tremor-like signals have been noted; however, these have been determined to arise from interaction of mega-icebergs, and are not attributable to activity within the volcano (Ruiz, 2003).

This study was funded by NSF grant OPP 94-19267. We thank Jeanne Kelley of Antarctic Support Associates for field assistance and operational support during the year.

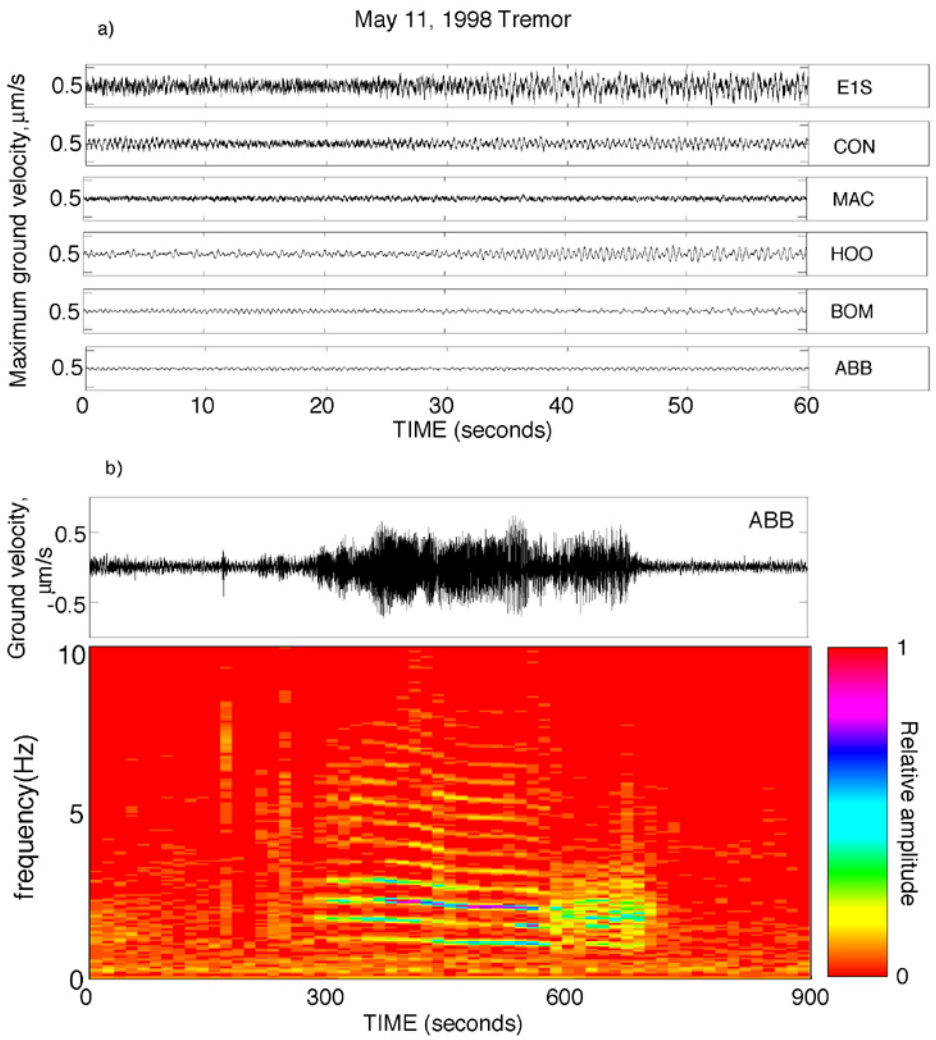

Figure 3. Polychromatic tremor recorded 11 May 1998 (after Rowe et al., 2000). More recently recorded episodes of tremor have been linked to ice-ground and/or ice-ice collisions associated with very large icebergs calved from the Ross Ice Shelf (Ruiz, 2004). Data quality for this 1998 example are inadequate to unambiguously determine the source.

a) Example seismograms showing the complex nature of the signal.

b) Seismogram for station ABB showing 900 seconds of signal and associated spectrogram.

Note at least 12 identifiable spectral peaks during this short (approximately 10-minute) episode of tremor.

Gliding (proportional shifting of all visible spectral peaks) can be clearly seen as the signal evolves.

References

Chouet, B. 1996. Long-period volcano seismicity: Its source and use in eruption forecasting, *Nature, v.* 380, pp 309-316.

Dibble, R.R., S.I.D. Barrett, K. Kaminuma, S. Miura, J. Kienle, C.A. Rowe, P.R. Kyle, and W.C. McIntosh. 1988. Time comparisons between video and seismic signals from explosions in the lava lake of Erebus Volcano. Antarctica Disaster Research Institute, Kyoto University, Uji, Japan, *Bulletin 38,* pp. 49-63.

Garces, M.A., M.T. Hagerty, and S.Y Schwartz. 1998. Magma acoustics and time-varying melt properties at Arenal volcano, Costa Rica. *Geophysical Research Letters,* 25, pp. 22932296

Hagerty, M., S.Y Schwartz, M. Protti, M. Garces, and T. Dixon. 1997. Observations at Costa Rican volcano offer clues to causes of eruptions. *EOS*, Transactions, American Geophysical Union, v. 78, pp. 565, 570-571.

Kienle, J., D.L. Marshall, P.R. Kyle, K. Kaminuma, K. Shibuya, and R.R. Dibble. 1983. Volcanic activity and seismicity of Mt. Erebus, 1982-1983. *Antarctic Journal of the U.S. v.* 18, no. 5, pp. 41-44.

Knight, R.L., R.R. Dibble, R.C. Aster, P.R. Kyle, and A.K. Ameko. 1996. Digital recording of the seismicity of Mount Erebus Volcano, November 1994 - June 1996. *Antarctic Journal of the U.S., v.* 31, no. 2, pp. 41-43.

Rowe, C.A., R.C. Aster, P.R. Kyle, J.W. Schlue and R.R. Dibble. 1998. Broadband recording of Strombolian explosions and associated very-long-period seismic signals on Mount Erebus volcano, Ross Island, Antarctica. *Geophysical Research Letters,* v.25, pp. 2297-2300.

Rowe, C.A., R.C. Aster, P.R. Kyle, R.R. Dibble and J.W. Schlue, 2000. Seismic and acoustic observations at Mount Erebus volcano, Ross Island, Antarctica, 1994-1998. *Journal of Volcanology and Geothermal Research*, v. 101, pp. 105-128.

Rowe, C.A., R.C. Aster and P.R. Kyle. 2004. Broadband seismic recording of Strombolian explosions at Erebus volcano, *Antarctic Journal of the U.S.,* this issue.

Ruiz, M., 2003. *Analysis of Tremor Activity at Mt. Erebus Volcano, Antarctica*. M.S. Thesis, New Mexico Institute of Mining and Technology, 159 pp.

Volcanic carbon-dioxide emissions from Mt Erebus

L.J. Wardell *and* P.R. Kyle, *Department of Earth & Environmental Science, New Mexico Institute of Mining and Technology*

Estimates of carbon dioxide (CO_2) emissions from volcanoes can provide insight into the role of volcanism in the global carbon cycle and can also be useful for hazard prediction (Gerlach et al. 1997). Only limited data are currently available for CO_2 degassing from volcanoes, due to the difficulty of analyzing fluxes of magmatic CO_2. A variety of estimates exist for approximately 12 volcanoes, but direct measurement of the CO_2 flux using the sensitive LI-COR analyzer had been made at only two volcanoes before the airborne measurement at Mount Erebus [at Oldoinyo Lengai, Tanzania (Koepenick et. al. 1996) and Popocatepetl, Mexico (Gerlach et al. 1997)]. During the 1997-1998 field season, the flux of CO_2 from the Mount Erebus plume was calculated using direct airborne measurements. Numerous CO_2 flux measurements were also made from warm soils and ice fumaroles on the flanks of Mt Erebus.

Airborne carbon dioxide measurement

Carbon dioxide measurements were made with a portable infrared CO_2 analyzer (model LI-COR 6262), using a procedure similar to that described by Gerlach et al. 1997. The inlet hose for the analyzer was mounted on the nose antenna of an A-Star helicopter. The helicopter flew transects at a constant velocity across the plume, perpendicular to the wind direction. The first transect began below the volcano plume, and each sequential transect was collected approximately 30 meters higher than the last. About 10 to 12 of such transects were required to reach the top of the plume. Carbon dioxide concentrations were recorded at one-second intervals during the plume transects. Differential global positional system (GPS) locations were also recorded at one-second interval and coordinated with the CO_2 data. The differential GPS equipment and assistance was provided by UNAVCO (Boulder, CO). With SURFER software (Golden Software, Inc.), we used CO_2 concentrations, combined with the GPS locations, to produce a concentration plot of the plume cross-section.

The plume CO_2 flux is calculated by multiplying wind speed by the sum of the concentration of the cross-section. The calculated CO_2 flux for Mount Erebus is 1,850 $x10^6$ g per day. The major contribution of uncertainty for this value is associated with the wind speed and the background CO_2 levels, which were observed to change with altitude. Koepenick et al. (1996) report the accuracy of this technique to be within 10 percent when evaluated at a coal-burning power plant. The CO_2 flux from Mount Erebus compares in magnitude to estimated emission rates from White Island, New Zealand (Tedesco and Toutain 1991) and Redoubt, Alaska (Casadevall et al. 1990).

Soil gas flux

Diffuse CO_2 emissions from the flanks of volcanoes may approach the levels of

those from the centralized volcanic plume, as shown by a study of Mount Etna volcano (Allard et. al, 1991). In order to estimate the non-plume emissions of CO_2 from Mt Erebus, we measured CO_2 fluxes from a number of active fumaroles and exposed soil sites around the summit plateau of the volcano (figure).

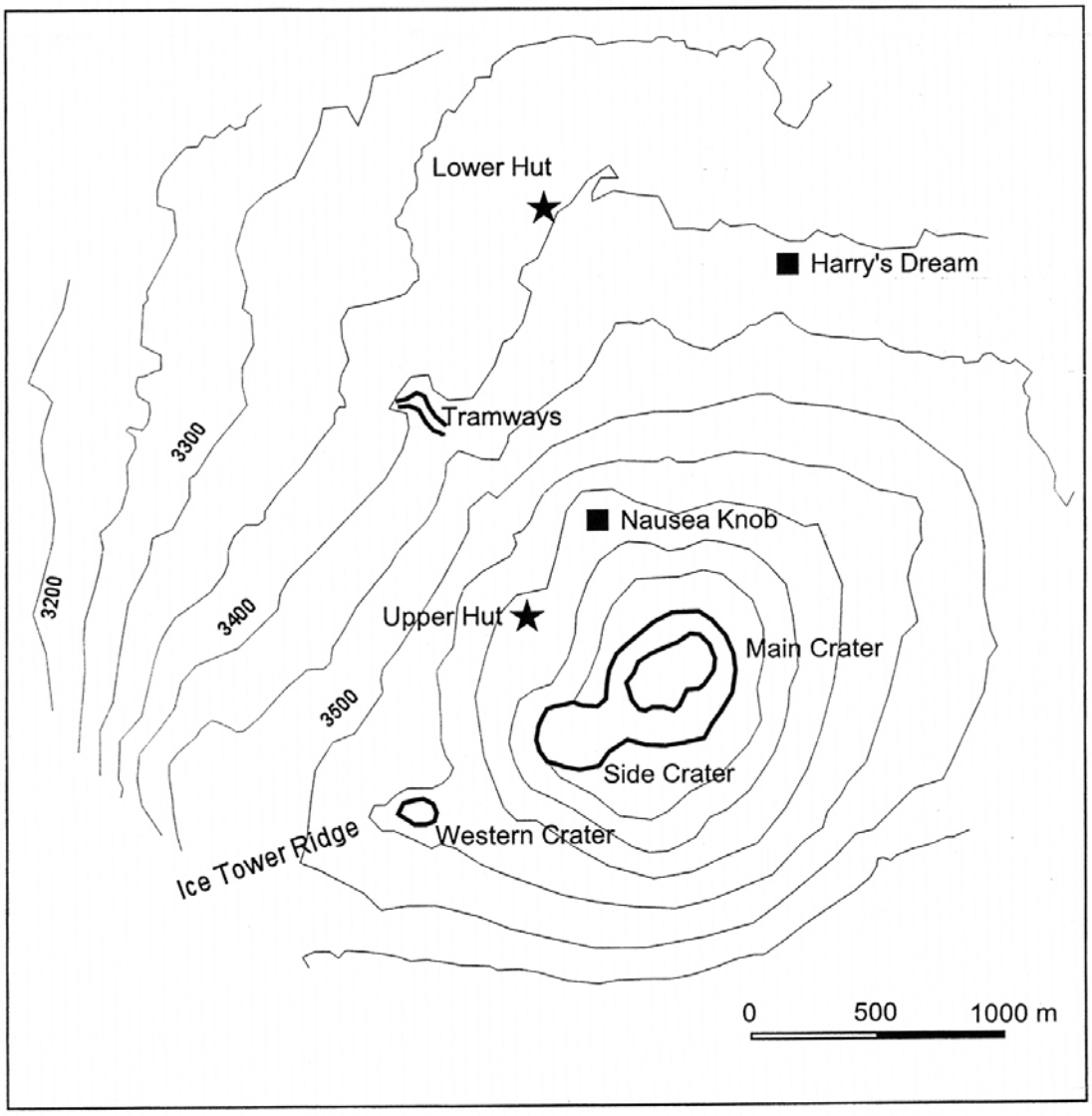

Summit map of Mt Erebus.

The warmest soil areas were in the area of the Tramways site, which is a Special Site of Scientific Interest (SSSI). Approximate locations of studied areas are shown in the figure. At a depth of 20 cm, soil temperatures at Tramways ranged from 39º to 62° C. Carbon dioxide flux values varied widely, ranging from 20 to 4,400 grams per square meter per day ($g/m^2/day$) and did not correlate with temperature. Exposed soil areas at the east edge of the Tramways site exhibited fluxes ranging up to 570 $g/m^2/day$. The highest flux reading at Western Crater was 410 $g/m^2/d$. Very low fluxes were observed at

exposed soil surfaces at Nausea Knob, Ice Tower Ridge, and the north-northwest side of Tramways. The highest CO_2 flux values were from exposed soil areas below the Upper Hut. Measurements there ranged from 4,160 to 5,800 $g/m^2/d$.

Carbon isotopic analysis of soil gases indicates that the CO_2 is magmatic in origin. Gas samples were collected and transported to New Mexico Institute of Mining and Technology for analysis. δC^{13} values from soil gases were relatively consistent and values from Tramways ranged from -3.4 to -3.8 per mil (‰). A soil gas sample from the crater rim had a δC^{13} value of -3.7‰. δC^{13} values of CO_2 collected at geothermal sites are generally found to be between -2 to -6‰ (Faure, 1986).

Fumaroles

Fumaroles are potentially significant sources of CO_2 emissions from Mount Erebus. We were unable to take flux measurements at the floors of the fumaroles because access was difficult and wet conditions threatened to damage the electronic equipment. A long hose could be positioned inside the fumarole, however, and CO_2 concentration measurements could be made by drawing gas through the hose. The CO_2 concentration inside five fumaroles at Ice Tower Ridge were measured. All concentrations were above the ambient outside CO_2 level. The higher values were at two fumaroles with concentrations of 1,030 and 1,380 ppm. These fumaroles were close to each other and may actually be connected. The lower values at the other three towers were at 325, 470 and 600 ppm. Concentrations in the fumarole known as "Harry's Dream" were above the range of the portable CO_2 analyzer. Air velocities as high as 4.8 meters per second were measured coming from the floor of Harry's Dream. Gas samples collected from inside Harry's Dream and from a fumarole directly to the north of Harry's Dream were analyzed by gas chromatography at the Crary Lab in McMurdo Station. The samples from Harry's Dream and the fumarole to the north exhibited CO_2 concentrations of 14,930 and 2,800 ppm, respectively.

Carbon isotope values showed a slight variability for different fumaroles but all indicated a magmatic source for the CO_2. The δC^{13} value from gases collected at Harry's Dream was at -3.5‰. The fumarole north of Harry's Dream exhibited the highest δC^{13} value of -2.1‰. Samples from an ice tower located by Tramways and from an ice cave near Lower Hut showed δC^{13} values of -4.3 and -4.7‰, respectively.

Direct measurements indicate that the plume of Mount Erebus emits CO_2 at a rate of 1,850 1,850 $x10^6$ g per day. Degassing from the flanks of Mount Erebus also occurs through exposed areas of warm soil and active fumaroles. Total non-plume emissions appear to be only a small fraction of that from the plume. Isotopic analyses of these emissions indicate that it is magmatic in origin.

This work was supported by National Science Foundation grant OPP 94-19267. We thank Mark Pomeroy at ASA and Dr. Andy Campbell at NMT for graciously making the laboratory analyses and Bjorn Johns and Oivind Rund for their assistance with the GPS data.

References

Allard P., Carbonnelle J., Dajlevic D., Le Bronec J., Morel P., Robe M., Maurenas J., Paiver-Pierret R., Martin D., Sabroux J., and Zettwoog P. (1991) Eruptive and diffuse emissions of CO2 from Mount Etna. *Letters to Nature,* 351 (6352), 387-391.

Casadevall T., Neal C., McGimsey R., Doukas M., and Gardner C. (1990) Emission rates of sulfur dioxide and carbon dioxide from Redoubt Volcano, Alaska during the 1989-1990 eruptions. *Journal of Volcanology and Geothermal Research*, 62(1-4), 519-530.

Faure, G. (1986). *Principals of Isotope Geology, 2nd ed*. John Wiley & Sons.

Gerlach T., Delgado H., McGee K., Doukas M., Venegas J., and Cardenas L. (1997) Application of the LI-COR CO2 analyzer to volcanic plumes: A case study, volcano Popocatepetl, Mexico, June 7 and 10, 1995. *Journal of Geophysical Research,* 102(B4), 8005-8019.

Koepenick K., Brantley S., Thompson J., Rowe G., Nyblade A., and Moshy c. (1996) Volatile emissions from the crater and flank of Oldoinyo Lengai volcano, Tanzania. *Journal of Geophysical Research* 10(B6), 13,819-13,830.

Tedesco D. and Toutain J. (1991) Chemistry and emission rate of volatiles from White Island volcano (New Zealand). *Geophysical Research Letters,* 18(1), 113-116.

Preliminary investigation of the secondary minerals in the Kirkpatrick Basalt, Prince Albert Mountains

C.H. Conaway, T.H. Fleming, *and* D.H. Elliot, *Byrd Polar Research Center and Department of Geological Sciences, Ohio State University*

Minerals record the chemical and physical conditions at their time of crystallization and, therefore, provide information about the rock in which they form. Secondary minerals, minerals that postdate the formation of rocks in which they occur, offer important clues to the history of a rock. They form as a result of precipitation from aqueous solutions that have interacted with the rocks, frequently at elevated temperatures. Among the minerals so formed, zeolites are common and constitute a group of hydrous silicate minerals of similar composition and occurrence, often found in cavities and veins in basic igneous rocks such as basalt. Investigation of secondary minerals in the Kirkpatrick Basalt, combined with earlier reports from underlying sedimentary units, suggests that there is a zoning of zeolite minerals and that that zoning holds important implications for the postemplacement history of the rocks.

The Kirkpatrick Basalt forms part of the mid-Jurassic continental flood basalt province in Antarctica (Ferrar Group) associated with the break-up of Gondwanaland (Elliot 1992). The Kirkpatrick Basalt is exposed in two widely separated areas in the Transantarctic Mountains (figure 1) and probably represents the remnants of an originally much larger flood basalt field (Hanson and Elliot 1996). The basalt sequences exposed in the Prince Albert Mountains consist of stacks of individual lava flows, ranging in thickness from several meters to over 100 meters. The stratigraphic thickness of the basalts is several hundred meters (more than 450 meters at Brimstone Peak). Samples of secondary minerals in the Kirkpatrick Basalt were collected from three locations in the Prince Albert Mountains: Brimstone Peak, Tent Rock, and Thomas Rock (figure 2).

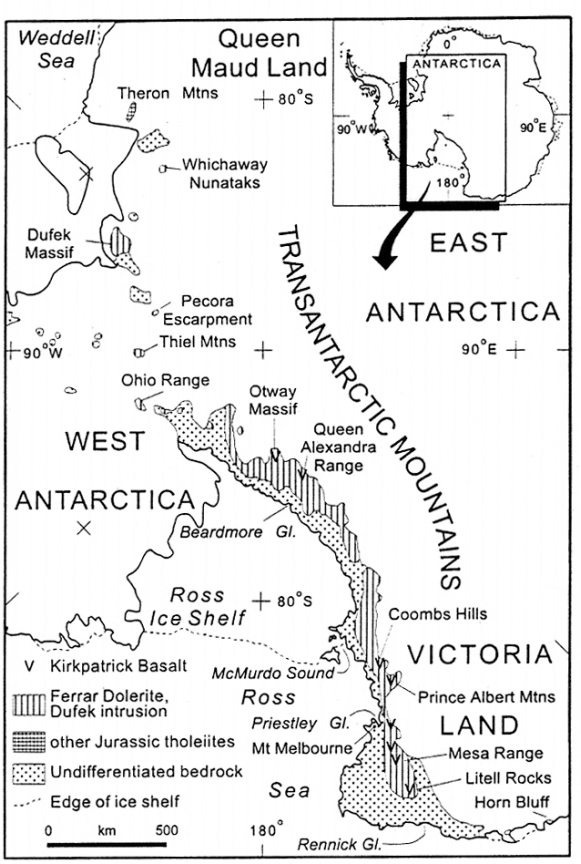

Figure 1. Map of the Transantarctic Mountains showing exposure of the Kirkpartick Basalt.

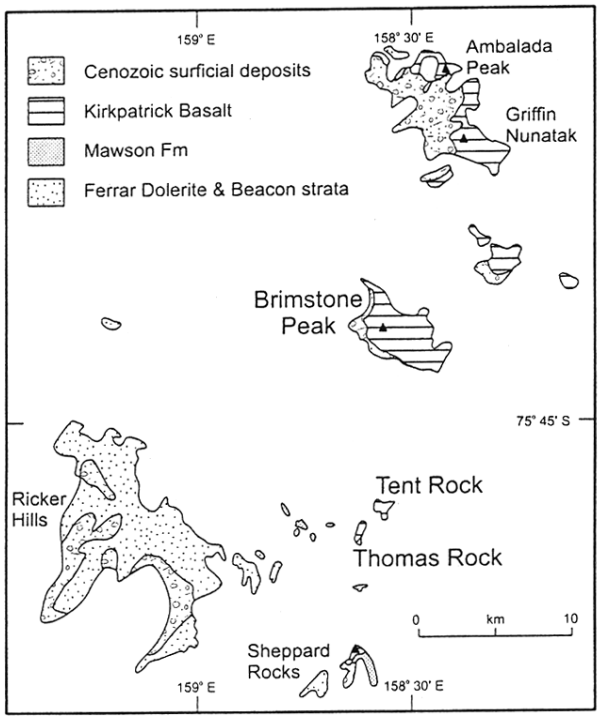

Figure 2. Map detail of the Prince Albert Mountains.

Secondary minerals are abundant in the upper and lower contact zones of the basalt flows where they commonly fill vesicles. They also occur in cavities and vugs, as well as in veins and on fracture surfaces. The secondary minerals identified include quartz, chalcedony, calcite, apophyllite, and the zeolite minerals stilbite, heulandite, mesolite, and scolecite. Notable associations of minerals are apophyllite-stilbite, heulandite-stilbite, and mesolite-scolecite. The mineral assemblage is similar to that observed in the Kirkpatrick Basalt in northern Victoria Land 200 kilometers to the north and the Beardmore Glacier region 700 kilometers to the south (Barrett, Elliot, and Lindsay 1986; Elliot, Haban, and Siders 1986).

In flood basalt provinces, secondary minerals often show a spatial arrangement, or zonation, developed in response to temperature and pressure trends. The classic work on zeolites in basaltic rocks is that of Walker (1960), who examined their distribution in the Tertiary basalt lavas of eastern Iceland and established a set of zeolite zones. Later, Kristmannsdóttir and Tómasson (1978) conducted a more detailed study of zeolitization in active geothermal areas in Iceland and recorded a similar set of zones, which they linked to increasing temperature with depth. In East Greenland, Neuhoff et al. (1997) mapped secondary minerals occurring through much of the Tertiary flood basalts and established low-temperature metamorphic mineral zones, which they also interpreted to reflect increasing temperature with depth.

Comparison of the secondary minerals in the Kirkpatrick Basalt with those in younger basalts elsewhere in the world provides insight into the significance of their occurrence. The zeolite assemblages found in the Prince Albert Mountains combined with observations of earlier workers suggest that a vertical zonation exists in Antarctica. Varva (1989) noted the presence of the zeolite minerals laumontite and heulandite in the Beacon sedimentary rocks beneath the Kirkpatrick Basalt. Laumontite and heulandite in a zone below the zeolite assemblages seen in the basalts is consistent with the zoning observed in Greenland and Iceland.

The secondary minerals in the Kirkpatrick Basalt have important implications. Assuming the pressure and temperature conditions implied for zeolite assemblages elsewhere also apply to Antarctica, then either considerable erosion has occurred or the geothermal gradient in Antarctica at the time of mineralization was different (that is, much higher) than in Iceland or Greenland. It is unlikely that the geothermal gradient in Antarctica at that time was higher than in Iceland, which has been an active volcanic center for the past 50 million years. The zoning in the antarctic zeolites suggests a burial depth much greater than that observed today, with possibly more than 1 kilometer of overburden at the time of zeolite formation. Preliminary dating of apophyllites from the Beardmore Glacier region and Victoria Land (Fleming, Foland, and Elliot 1993; Fleming, Elliot, and Foland 1994) suggests that at least some of the mineralization, including some minerals used to define zeolite zones, postdates extrusion of the basalts by 50 to 80 million years. These secondary minerals, apophyllite and the zeolite overgrowths, are interpreted as being formed in a hydrothermal system related to regional groundwater movement caused by uplift and erosion of the Transantarctic Mountains.

We thank J.S. Nicoll for laboratory assistance. This research was supported by

National Science Foundation grant OPP 94-20498 to D.H. Elliot.

References

Barrett, P.J., D.H. Elliot, and J.F. Lindsay. 1986. The Beacon Supergroup (Devonian-Triassic) and Ferrar Group (Jurassic) in the Beardmore Glacier area, Antarctica. In M.D. Turner and J.F. Splettstoesser (Eds.), *Geology of the central Transantarctic Mountains* (Antarctic Research Series, Vol. 36). Washington D.C.: American Geophysical Union.

Elliot, D.H. 1992. Jurassic magmatism and tectonism associated with Gondwanaland break-up: An antarctic perspective. In B.C. Storey, T. Alabaster, and R.J. Pankhurst (Eds.), *Magmatism and the causes of continental break-up* (Geological Society Special Publication No. 68). Boulder, Colorado: Geological Society of America.

Elliot, D.H., M.A. Haban, and M.A. Siders. 1986. The Exposure Hill Formation, Mesa Range. In E. Stump (Ed.), *Geological investigations in northern Victoria Land* (Antarctic Research Series, Vol. 46). Washington, D.C.: American Geophysical Union.

Fleming, T.H., D.H. Elliot, and K.A. Foland. 1994. Alteration events recorded in Jurassic Tholeiites (Kirkpatrick Basalt) from the Transantarctic Mountains: Evidence for Cretaceous tectonic activity. In T.J. Wilson and C.A. Finn (Eds.), *Geodynamic evolution of the Transantarctic Mountains and the west antarctic rift system* (Byrd Polar Research Center Report No. 9). Columbus, Ohio: Byrd Polar Research Center.

Fleming, T.H., K.A. Foland, and D.H. Elliot. 1993. Direct dating of mid-Cretaceous alteration of the Kirkpatrick Basalt in northern Victoria Land: Argon-40/argon-39 and rubidium/strontium ages of apophyllite. *Antarctic Journal of the U.S.*, 28(5), 38–40.

Hanson, R.E., and D.H. Elliot. 1996. Rift-related Jurassic basaltic phreatomagmatic volcanism in the central Transantarctic Mountains: Precursory stage to flood-basalt effusion. *Bulletin of Volcanology*, 58, 327–347.

Kristmannsdóttir, H., and J. Tómasson. 1978. Zeolite zones in geothermal areas in Iceland. In L.B. Sand and F.A. Mumpton (Eds.), *Natural zeolites: Occurrence, properties, and use*. New York: Pergamon Press.

Neuhoff, P.S., W.S. Watt, D.K. Bird, and A.K. Pedersen. 1997. Timing and structural relations of regional zeolite zones in basalts of the East Greenland continental margin. *Geology*, 25(9), 803–806.

Varva, C.L. 1989. Mineral reactions and controls on zeolite-facies alteration in sandstone of the central Transantarctic Mountains, Antarctica. *Journal of Sedimentary Petrology*, 59, 688–703.

Walker, G.P.L. 1960. Zeolite zones and dike distribution in relation to the structure of the basalts of eastern Iceland. *Journal of Geology*, 68, 515–528.

A report of field surveys for the Transantarctic Mountains Aerogeophysical Research Activities (TAMARA) Program

Carol Finn, *U. S. Geological Survey, Denver*,

Detlef Damaske, *Bundesanstalt für Geowissenschaften und Rohstoffe, Hannover, Germany*

Terry Wilson, *Ohio State University*

The Transantarctic Mountains (TAM) rift flank uplift has developed along the ancestral margin of the East Antarctic craton, and forms the boundary between the craton and the thinned lithosphere of the West Antarctic rift system. Geodynamic processes associated with the exceptionally large-magnitude uplift of the mountain belt remain poorly constrained, but may involve interaction of rift-related mechanical and thermal processes, and the inherited mechanical elements of the cratonic lithosphere. Our program proposes to document the regional structural architecture of a key segment of the Transantarctic Mountains in the region around the Royal Society Range (figure) where the rift flank is offset along a transverse accommodation zone.

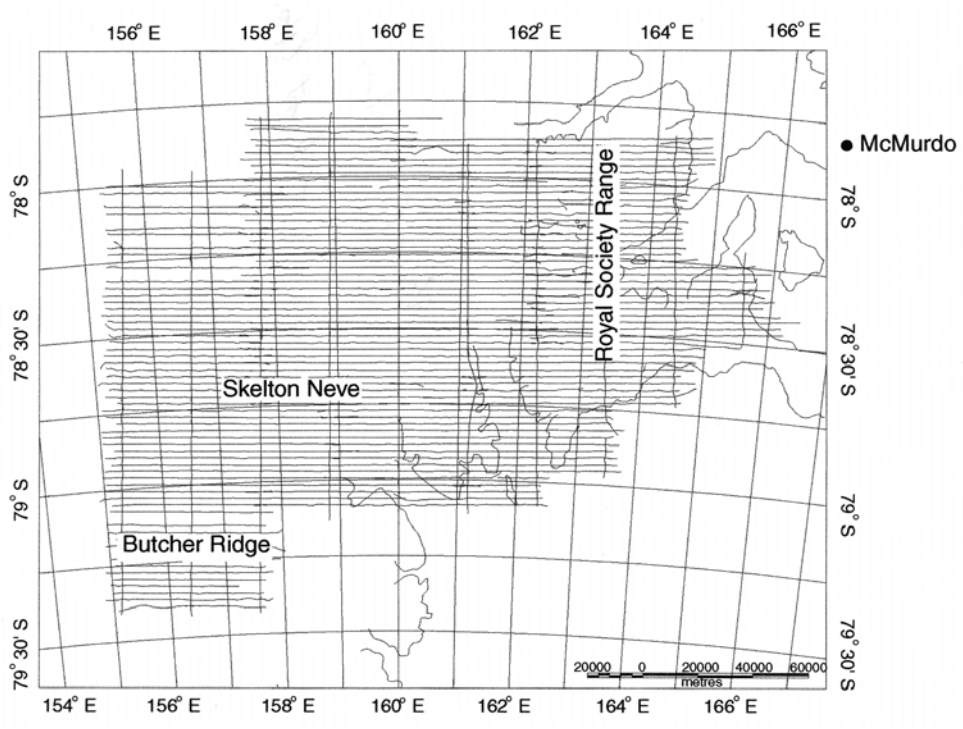

Map showing the location of lines flown for the survey.

In December and January 1998, we flew a helicopter magnetic survey and collected ground gravity data. We plan to integrate these data with other geologic and geophysical information from the region to map the large-scale structures along the Transantarctic Mountains to try to resolve the relationships between longitudinal and transverse structures along the rift flank can be resolved. This mapping campaign has three primary objectives:

- to delineate the Mesozoic-Cenozoic structural geometry of the TAM rift accommodation zone in the region around the Royal Society Range, including the Jurassic and Cenozoic magmatic architecture. To determine the plate-scale kinematics associated with continental breakup, the positions, orientations, and displacement patterns of faults oriented along the mountains must be mapped – along with transverse faults segmenting and offsetting the mountains along their length. To test Jurassic tectonic and magmatic models for Antarctica, it is necessary to document the regional extent of the Jurassic Ferrar Group magmatic rocks within East and West Antarctica, the position(s) of source bodies, and the regional geometry and interconnectivity of the Ferrar sheet intrusions along the Transantarctic Mountains. To define the geometry of neotectonic activity – and to provide constraints on the intraplate stress regime, rift kinematics, and Transantarctic Mountain uplift models – the extent and structural setting of Cenozoic magmatic rocks must be mapped.
- to map the continuity of petrotectonic elements that define the geometry of the ancestral Paleozoic Gondwana active margin in this sector of the Transantarctic Mountains. Geophysical delineation of the continuity, termination, or offset of the Granite Harbor Intrusive Complex, as well as adjacent Paleozoic terranes in the region could resolve important issues related to the evolution of the Ross orogen.
- to compare the Paleozoic and rift-related architecture to establish the role of structural ancestry in rift-flank development. Lithospheric structures formed during the Neoproterozoic and Paleozoic may have controlled the geometry of the superposed rift flank, and changes in character of Paleozoic lithospheric elements may have influenced the mechanical response of the lithosphere when it was reactivated by rift processes in the Mesozoic and Cenozoic. Geophysical mapping of a zone can determine whether rift-related and Paleozoic trends can be shown to either cross-cut or parallel each other. Such maps should be able to establish the role of inherited structures in rift-flank architecture and uplift for of this part of the Transantarctic Mountains.

The helicopter-borne magnetic operations started and ended in McMurdo, about 100 kilometers (km) northeast of the Royal Society Range (figure) with a 1 month period in January spent in a field camp on the Skelton Névé (figure). The aeromagnetic surveying was divided into targets based from McMurdo and Skelton Névé. Over most areas, magnetic data were collected with a 2.5 km line-spacing and tie lines every 25 km. The survey was flown with a terrain clearance of 300-500 meters (m).

The main target area was to the west of the Royal Society Range, covering all of

Skelton Névé to just beyond the westernmost outcrops. The area over the Butcher Ridge was also flown from the Skelton Névé field camp (figure). The portions of the survey from the eastern side of the Royal Society Range to the east were flown from McMurdo (figure).

The crew for the aeromagnetic helicopter-borne program consisted of three helo-support personnel (including two pilots and a helo-engineer) and six scientific staff (geophysicists, engineers, quality-control specialists). Bundesanstalt für Geowissenschaften und Rohstoffe (BGR) contributed one geophysicist, one engineer, and one quality control specialist. Three more scientific staff were contributed by the U.S. Geological Survey and Ohio State University. A general assistant for camp operations and a mountaineer were provided by U.S. Antarctic Program support contractor.

To isolate the field effects observed from the helicopter and to record the daily variations of the Earth's magnetic field, magnetic base stations were established in McMurdo and the Skelton Névé field camp to record the daily variations of the Earth's magnetic field for removal from the field observed from the helicopter. A cesium magnetometer was flown in a bird slung 30 m below the helicopter. Positioning was done with Trimble 4000 GPS receivers. Barometric altitudes were also recorded. The data from each flight was quality controlled. Lines with poor data were reflown.

During the 1997-1998 field season, the Transantarctic Mountains Aerogeophysical Research Activities (TAMARA) project collected about 14,100 line-kilometers of helicopter magnetic data, covering an area just under 30,000 square kilometers. One hundred twenty-five hours of helicopter time were used to complete the survey. When field work was completed, 92.5 percent of line-kilometers, 95 percent of the planned area, had been covered. In addition to the aeromagnetic data, 65 gravity stations were collected in profiles in the Skelton Névé region.

This research was supported by National Science Foundation grant OPP 96-18568. We thank Bea Csatho, Christie Demosthenous, Dieter Möller, Vera Marcinkowski, Kathy Young, Vince Langemann, Beez Bonner, Ethan Conner, Chris Dean, Richard Dipboye, Everett Fouts, Jack Hawkins, Scott Pentecost and Ed Sangurima for their help in the field. We thank Bill Smith and Bob Glover, Oivind Ruud and UNAVCO for GPS support. Robin Bell was instrumental in helping to plan the survey.

Testing the SWEAT hypothesis and studying Neoproterozoic-Cambrian deformation in the Nimrod Glacier area, central Transantarctic Mountains

John Encarnación, *Department of Earth and Atmospheric Sciences, Saint Louis University*

Timothy Paulsen, *University of Wisconsin*

Michael Watkeys, *School of Geological and Computer Sciences, University of Natal, South Africa*

The SWEAT (Southwest U.S.-East Antarctic) hypothesis places Laurentia against East Antarctica and Australia in the Neoproterozoic (Moores 1991). The SWEAT connection was broken when the Rodinia supercontinent broke apart about 750 million years ago. Recent work in the Transantarctic Mountains and in other sectors of Antarctica has eliminated previously considered Proterozoic rocks that might have been correlated with Laurentian geology or related to the Rodinia rifting event about 750 million years ago (Encarnación and Grunow 1996).

One of the main objectives of our study was to test the SWEAT hypothesis by studying basement rocks exposed in the Nimrod Glacier area, which is one of the two remaining locations in Antarctica that offers possible Neoproterozoic correlation with Laurentia. The Nimrod Glacier area also is a key area in the Ross orogen because here previously described structural relationships and a purported angular unconformity between the Neoproterozoic(?) Beardmore Group and the Early Cambrian Byrd Group offer possible evidence for an older Beardmore orogeny. Our second objective was to characterize the structural and stratigraphic relationships in the area to determine whether geologic relations are compatible with one or more orogenic events. To address these issues, our field party spent a month in the Nimrod Glacier area investigating the geology and structure of the area and sampling for U-Pb geochronology and paleomagnetism.

Our work was mainly based from a field camp ("Moody Camp") with two A-Star helicopters, shared with another science group from Southern Methodist University lead by John Goodge (NSF 97-25426). The camp was located just east of Moody Nunatak on the Marsh Glacier (figure 1). Moody Camp had a single polar haven used for meals and office space. Members of both field parties and the support personnel (two pilots, a mechanic, and a camp manager) slept in mountain tents. A Scott tent was set up to house the latrine. Along with the two helicopters, we had Alpine I and Skandec skidoos, and Nansen sleds.

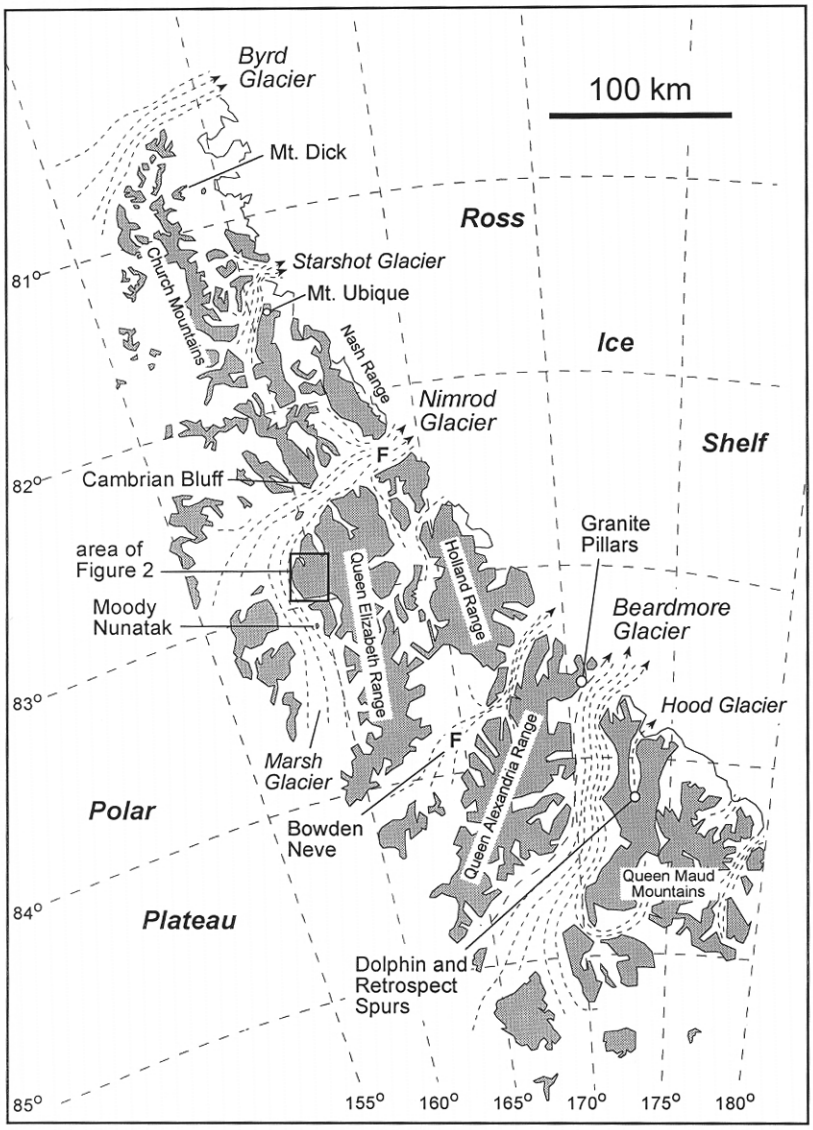

Figure 1. Map of the central Transantarctic Mountains showing location of various places mentioned in the text. Sites marked "F" are fuel caches. Shaded areas are areas of major outcrop. Area shown in Figure 2 is indicated by box.

Our field party consisted of three geologists — John Encarnación, Timothy Paulsen, and Michael Watkeys — and a mountaineer (Peter Braddock). Braddock was put in at Moody Camp on 1 December 1998, along with the two helicopters to help set up the camp. John Encarnación and Michael Watkeys were put in at Moody Camp on 3 December 1998, and Tim Paulsen on 7 December 1998, by LC-130.

After working primarily by helicopter from Moody Camp, both field parties were moved to the top of Cotton Plateau by helicopter on 9 December. The helicopter crew then returned to McMurdo Station. We set up a tent camp and traversed to the Panorama Point area by snowmobile and Nansen sleds (figure 2). On 17 December, we were picked

up at Cotton Plateau by helicopters, which had returned from McMurdo, and based ourselves once again at Moody Camp. Our field party pulled out by Twin Otter and the support personnel by helicopter on 30 December. Poor weather precluded landing by Twin Otter near Mt. Dick (figure 1) during our pull-out. These weather patterns prevented several later attempts to visit Mt. Dick from McMurdo Station.

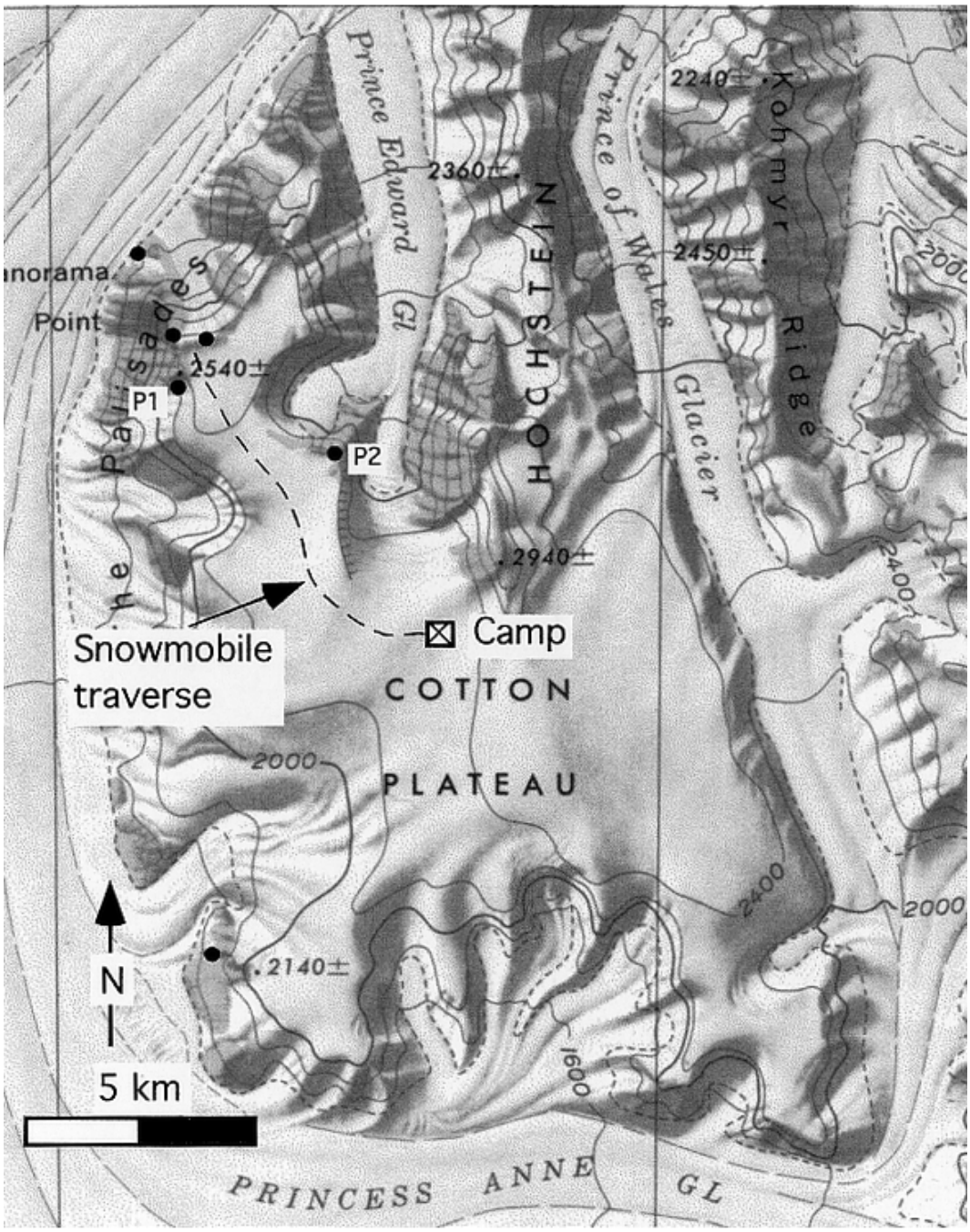

Figure 2. Map of Cotton Plateau area. Black dots are paleornagnetic drill sites; Pl and P2 are locations of mafic pillow lavas.

From Moody Camp we were able to access sites at Mt. Ubique (east side of the Starshot Glacier) and outcrops near the head of the Hood Glacier (Dolphin and Retrospect spurs, Mt. Harcourt and Granite Pillars) by refueling the helicopters at fuel caches on the lower Nimrod Glacier (82º 20.193'S, 163º 43.550'E) and Bowden Neve (at the old "Beardmore Camp"), respectively (figure 1). The helicopters were also able to land at two sites on the Palisades, west side of Cotton Plateau, which allowed us to do substantial work in that area.

Typical weather patterns consisted of clear skies during the evening and night, with low cloud banks coming up the Nimrod and Marsh Glaciers, occasionally enveloping Cotton Plateau and Moody Camp. We lost only about 4 days total to bad weather.

Structural work in the Cotton Plateau area was done in part with members of the Southern Methodist University field party; preliminary results of the field season are described in Goodge et al. (1999). The Goldie formation is deformed into tight northeast-plunging mesofolds associated with a penetrative northeast-dipping axial-plane cleavage and mineral lineations. These folds have been refolded during the formation of a subhorizontal north-northwest-trending, west-southwest-verging syncline in the Shackleton Limestone. At the base of the Shackleton Limestone on the western slopes of Cotton Plateau, the two units show a moderate-to-high angular discordance. Where observed, this contact is marked by ductile L-S tectonite fabrics in the basal quartzite of the Shackleton, rather than an angular unconformity as suggested by Stump (1995). Although a stretched quartz pebble conglomerate was identified at two localities along the contact suggestive of a basal conglomerate to the Shackleton Limestone, the clear evidence of shear along this boundary raises the question of the original nature of this contact and whether the Ross and Beardmore orogenies represent the same event or at least were closely related in time.

We collected approximately 200 paleomagnetic core samples from a 30 sites during the field season. We sampled granitoids, gabbro, pillow basalts, a felsite, and meta-sediments on Cotton Plateau; we also sampled granitoids near the Miller Range and the mouth of Beardmore Glacier. A total of 22 geochronology samples for zircon U-Pb dating were collected.

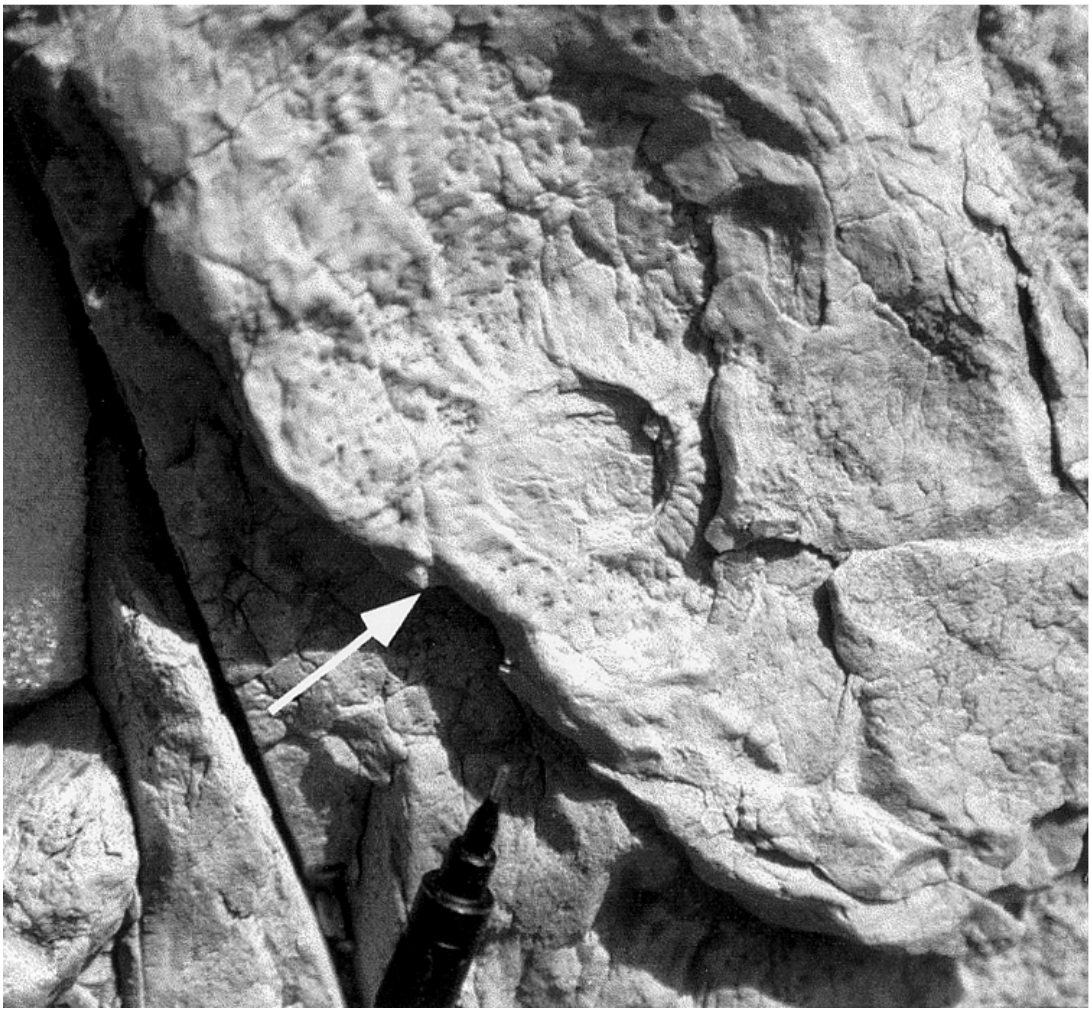

Figure 3. Photograph of Archaeocyathid from lower part of Shackleton Limestone on the west side of Cotton Plateau (photo by Peter Braddock).

Braddock found an *Archeocyathid* in the Shackleton limestone on the west side of Cotton Plateau (figure 3). The sample was found in the gray limestone layer beneath the massive white layer on the lower limb of the syncline. This is the first discovery of Archeocyathids in what is mapped as Shackleton limestone at Cotton Plateau and confirms a Lower Cambrian age of this unit.

Our field party found several relationships that apparently have been previously misidentified in the literature.

1. The "felsites" that have been reported at Dolphin Spur (Oliver 1972 and personnel communication to A. Grunow1998) are probably sills. We found only one that bifurcated along the crest of Dolphin Spur. Goldie Formation in contact with the top and lower contacts of the felsite contained a red to yellow staining, probably marking an intrusive-related alteration zone. No felsites were found at Retrospect spur, which is the next spur to the east.
2. The felsites reported as "orange bands" at Mt. Ubique (Laird 1963) are also probably

sills. We found granite dikes on the northern side of Mt. Ubique originating from a granite stock near glacier level. We also found at least three tabular sill-like bodies, possibly repeated by folding, with chilled margins and intruded into the Starshot Formation on the ridge on the south side of Mt. Ubique. The sills have a cleavage that is conformable with cleavage observed in the Starshot Formation and thus predate shortening.

3. The 'Holyoake Gabbro' (Laird 1963, 1971) is not post-tectonic. The gabbro at Cambrian Bluff has a subsolidus foliation parallel to the metamorphic foliation in the Shackleton limestone (now marble) and, thus, is pre- to syntectonic. Along one of the contacts elongate foliated fragments of gabbro are mixed in the marble. In some parts there are several irregular patches in the foliated gabbro that are pegmatitic and without the fabric in the host gabbro and marble, suggesting that the gabbro was not completely crystallized during deformation or that some gabbro intrusion locally postdated deformation.

We thank P. Braddock, S. Norman, and N. Juergens for their mountaineering assistance, the PFH helicopter crew, and Rosie for her delicious cooking. This work was supported by U.S. National Science Foundation grant OPP 97-25417 to Grunow and Paulsen and National Science Foundation grant OPP 97-26104 to Encarnación.

References

Encarnación, J. and A. Grunow. 1996. Changing magmatic and tectonic styles along the paleo-Pacific margin of Gondwana and the onset of early Paleozoic magmatism in Antarctica. *Tectonics,* 15, 1325-1341,.

Goodge, J.W., T. Paulsen, S.K. Deering, J. Encarnación, and M Watkeys. 1999. Progressive (?) Deformation of Supracrustal Rocks in the Ross Orogen, Central Transantarctic Mountains. Abstract, International Symposium on Antarctic Earth Sciences, Wellington, New Zealand, 1999.

Laird, M.G. 1963. Geomorphology and stratigraphy of the Nimrod Glacier-Beaumont Bay region, southern Victoria Land, Antarctica. *New Zealand Journal of Geology and Geophysics*, 6, 465-84.

Laird, M.G., G.D. Mansergh, and J.M.A. Chappell. 1971. Geology of the central Nimrod Glacier area, Antarctica. *New Zealand Journal of Geology and Geophysics*, 14, 427-68.

Moores, E.M. 1991. The southwest U.S.-East Antarctic (SWEAT) connection: A hypothesis. *Geology*, v. 19, p. 425-428.

Oliver, R.L. 1972. Geology of an area near the mouth of the Beardmore Glacier, Ross dependency. In R.J Adie (ed.) *Antarctic geology and geophysics.* Symposium on Antarctic and Solid Earth Geophysics, Oslo, 6-15 August 1970. Oslo, Norway: Universitetsforlaget. 379-385.

Stump, E. 1995. *Ross orogen of the Transantarctic Mountains.* New York, New York: Cambridge University Press. 284 p.

Origin of carbonates in Martian meteorite Allan Hills 84001

Edward R.D. Scott *and* Alexander N. Krot, *Hawaii Institute of Geophysics and Planetology, School of Ocean and Earth Science and Technology, University of Hawaii at Manoa*

The Allan Hills (ALH) 84001 meteorite, which was found in the Far Western Icefield of the Allan Hills area in Southern Victoria Land (Sandford 1992), is one of 13 meteorites from Mars. The carbonates in this rock contain features that McKay et al. (1996) claim are evidence for life on Mars — microfossil-shaped objects, polycyclic aromatic hydrocarbons and minerals that resembled those made by terrestrial microbes. McKay and his colleagues suggested that the carbonates — and the submicrometer iron oxide and sulfides in the carbonates — had been formed in cracks by Martian microorganisms, as aqueous solutions seeped slowly through the rock. Even before these controversial claims, ALH84001 was already one of the most intensely studied meteorites because it formed over 4 billion years ago and contains important clues to the abundance and location of water and carbon dioxide on Mars. These atmospheric volatiles controlled the evolution of the climate on Mars and its habitability for life.

We studied the carbonates in ALH84001, using optical and scanning electron microscopes and electron microprobe analysis to determine the chemical composition of the minerals. Our goal was to find out how the carbonates and other minerals had been affected by impact processes and what the rock looked like before it was battered and deformed.

The carbonates in ALH84001 differ from all other carbonates and their origin is still controversial — almost everyone who has studied them has come up with a different explanation for their formation. On fracture surfaces, the carbonates appear as disks (60-300 micrometers in diameter) with complex chemical and isotopic variations, especially near their rims (figure 1). The complex layering precludes the possibility that the carbonates could have formed slowly at high temperatures, however conventional geochemical techniques have not been able to constrain the temperature at which they formed.

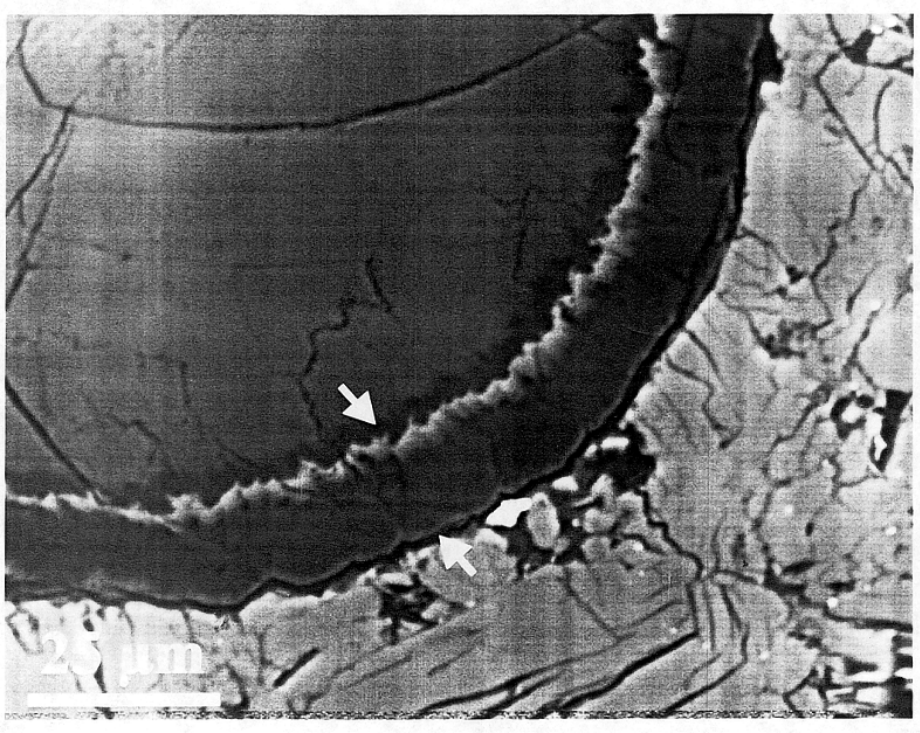

Figure 1. This scanning electron microscope image shows part of a carbonate disk (upper left) in fractured pyroxene (lower right) in the Martian meteorite ALH84001. The light and dark bands marked by arrows indicate chemical variations in the rim of the carbonate disk.

McKay et al. (1996) studied the carbonate disks and inferred that they had formed slowly, in fractures from percolating aqueous solutions. However, in thin sections, the disks and irregularly shaped carbonate grains appear to be embedded in pyroxene or plagioclase — as if they had formed by replacement of these phases. If this had happened, major amounts of silican and other aluminum-bearing silicates would also have formed. From their absence, we and most other researchers have inferred that the carbonate must have been deposited in open fractures and voids. The shapes of the carbonates vary, according to the nature of the host mineral and its impact fractures, but all carbonate grains have the same chemical variations, indicating they were formed by the same process.

We inferred that ALH84001 had been shocked to more than 35-45 gigaPascals during an impact that converted the plagioclase to glass and twisted and deformed the rock, creating fracture zones and numerous fractures. As in many other heavily shocked and deformed rocks, the fractures were resealed under impact pressure so that the rock now has a low porosity. Carbonates and smaller amounts of plagioclase glass are embedded in pyroxene fractures that were opened and then quickly resealed. These phases lack the fractures and extensive deformation present in the pyroxene and could not have formed before the impact that deformed the pyroxene. The carbonate, like the plagioclase glass, must have formed from a fluid that was present in the rock when the fractures were opened and then resealed. Thus, the carbonate could not have formed slowly from an aqueous fluid, but must have formed rapidly from a shock-formed fluid

during an impact on Mars (Scott, Yamaguchi, and Krot 1997; Scott, Krot, and Yamaguchi 1998) (figure 2).

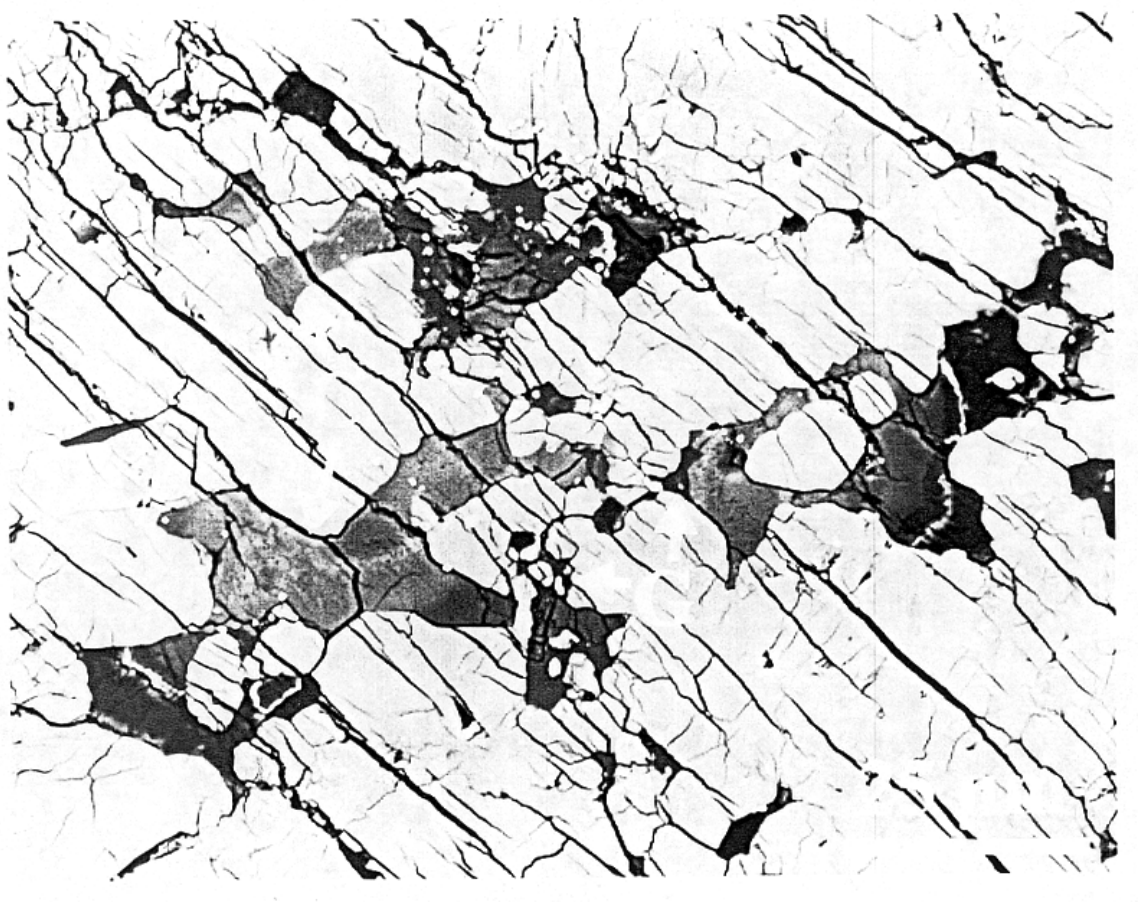

Figure 2. This scanning electron microscope image shows irregularly shaped grains of carbonate (C) and smaller grains of plagioclase glass (G) embedded in a part of a fractured and deformed pyroxene crystal. The wider black lines are fractures that formed after the carbonates crystallized. The glass and the carbonate both appear to have been formed in the pyroxene crystal during an impact on Mars.

The largest concentrations of carbonates are found at interstitial sites next to plagioclase glass, and in pyroxene fractures around such sites. We inferred that an earlier generation of carbonates and other secondary minerals were deposited in pores (at interstitial sites) from percolating fluids at low temperatures. These phases would have been heated and mobilized by the impact that melted plagioclase and created the fracture zones. The carbonates and their submicrometer iron oxide and sulfide minerals are unique, not because they were formed by microorganisms, but because ALH84001 is the only known, heavily shocked rock that contains a few percent (volume) of carbonate in a volatile-poor matrix of igneous silicates (Scott 1998).

The antarctic meteorite program has been responsible for some remarkable discoveries during the past 25 years, but Allan Hills 84001 has completely eclipsed the first lunar meteorite and the first meteorite found to contain trapped Martian gases. Studies of ALH84001 have helped to establish the new discipline of astrobiology and

have revitalized the exploration of Mars by spacecraft. What is truly astonishing about the antarctic meteorite program is that we can predict, with some confidence, that even more remarkable space rocks will soon be brought back from the icefields of Antarctica.

We thank our colleagues, Akira Yamaguchi, Tom Cooney, and Shiv Sharma for their assistance with analytical and spectroscopic studies of minerals. This work was supported by National Science Foundation grant 97-14012, the National Aeronautics Space Administration, the field work of William Cassidy and his team, and the curatorial expertise of Marilyn Lindstrom and her colleagues at the NASA Johnson Space Center.

References

McKay, D. S., E. K. Gibson Jr., K. L. Thomas-Keprta, H. Vali, C. S. Romanek, S. J. Clemett, X. D. F. Chiller, C. R. Maechling, and R. N. Zare. 1996. Search for past life on Mars: possible biogenic activity in Martian meteorite ALH84001. *Science, 273*, 924-930.

Sandford, S.A. 1992. The 1984-1985 Antarctic search for meteorites (ANSMET) field program. *Smithsonian Contributions to the Earth Sciences*, 30, 5-9.

Scott, E.R.D., A. Yamaguchi, and A.N. Krot. 1997. Petrologic evidence for shock melting of carbonates in Martian meteorite ALH84001. *Nature*, 387, 377-379.

Scott, E.R.D., A.N. Krot, and A. Yamaguchi. 1998. Carbonates in fractures in Martian meteorite Allan hills 84001: Petrologic evidence for impact origin. *Meteoritics and Planetary Science*, 33, 709-719.

Scott, E.R.D. 1999. Origin of carbonate-magnetite-sulfide assemblages in Martian meteorite ALH84001. *Journal of Geophysical Research*, in press.

Claystone breccias at the Permian-Triassic boundary in Antarctica

Gregory J. Retallack, *Department of Geological Sciences, University of Oregon*

The dramatic perturbation in isotopic composition of organic matter due to the Permian-Triassic mass extinction has recently been found in non-marine rocks of Antarctica and Australia (Morante 1996; Krull 1998). Remarkably, this method of locating the stratigraphic level of this important event has also pinpointed distinctive claystone breccias in localities at least 2,600 km apart, even at the closest approach allowed by Gondwanan reconstruction at the time of the Permian-Triassic boundary some 250 million years ago (figure 1). Graphite Peak in the central Transantarctic Mountains, Mt. Crean in southern Victoria Land (figures 2 and 3), and Wybung Head on central coast of New South Wales (Retallack 1999a) all have thin (6-10 cm) claystone breccia beds at the boundary between productive latest Permian coal measures and coal-less Triassic fluvial sandstones, representing the onset of a global coal gap (Retallack *et al.* 1996). The breccias are all dominated by grains of granule size and by clayey clasts that show signs of prior pedogenic modification. They are unusual lithologies for their sequences in which other claystone breccias are of much larger grain size (2-10 cm), lower sphericity, and greater angularity. Discovery of uncommon shocked quartz grains and faint iridium anomalies within and near the claystone breccias opens the possibility that these might be either ejecta of asteroid impact or products of landscape destabilization following the abrupt terminal Permian extinction of *Glossopteris*-dominated swamp forests (Retallack *et al.* 1998a). The second alternative seems most likely considering the lack of spherules, suevite, and other impact debris in the claystone breccias and a variety of local differences detailed below.

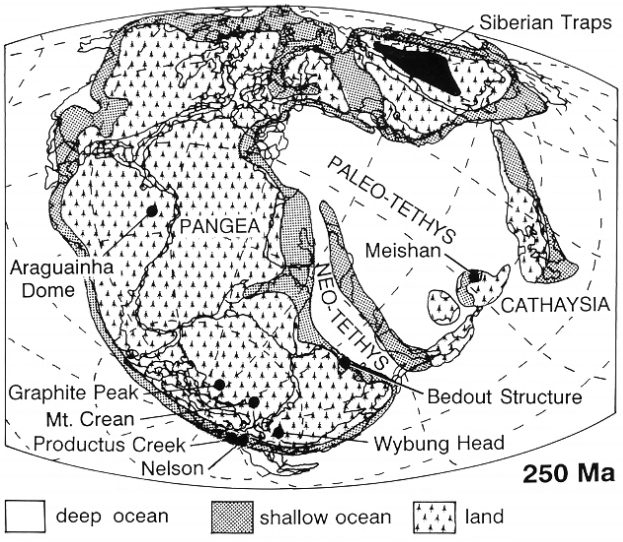

Figure 1. Mentioned localities in Antarctica and Australia on a continental reconstruction for the Permian-Triassic boundary (from Retallack* et al. *1998a, with permission of the Geological Society of America).

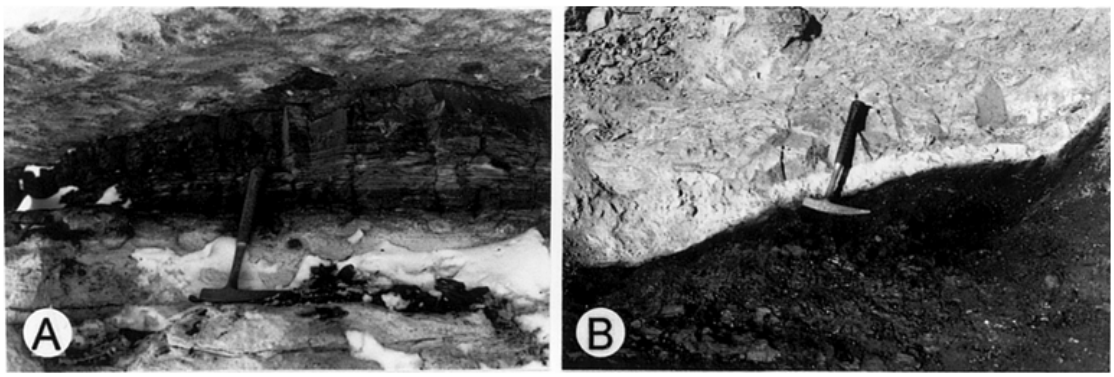

Figure 2. Field photographs of the claystone breccias at the horizon of carbon isotopic perturbation taken to be the Permian-Triassic boundary at Mt Crean, southern Victoria Land (A) and at Graphite Peak, central Transantarctic Mountains (B). Hammers for scale.

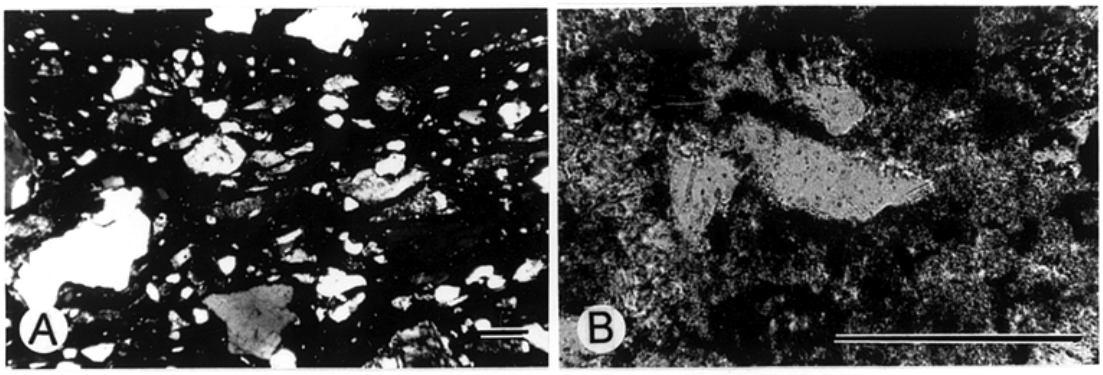

Figure 3. Petrographic appearance of claystone breccia with a dominance of opaque carbonaceous claystone clasts at Mt Crean, southern Victoria Land (A) and of pedogenically altered volcanic clasts at Graphite Peak, central Transantarctic Mountains (B). Scale bars are 0.1 mm.

The claystone breccia at Mt. Crean (77^{o} 52.4'S 159^{o} 32.0'E) commands attention in the field because it appears as if the large white quartz granules are floating in a matrix of black claystone (figure 2A). Thus, what would appear to be a grain size anomaly for hydrodynamic sorting is resolved on examination of thin sections, which show that the black matrix consists of carbonaceous claystone clasts also up to granule size (figure 3A; tables 1 and 2).

Table 1. Grain size of Permian-Triassic boundary breccias in Antarctica and Australia

Locality	Specimen	Percent Clay	Percent Silt	Percent Sand	Percent Gravel
Graphite Peak	R2060	35.2	30.8	27.4	6.6
Mount Crean	R1938	47.8	10.8	18.8	22.6
Wybung Head	R1667	29.6	8.8	30.0	31.6

Table 2. Petrographic composition of Permian-Triassic boundary breccias in Antarctica and Australia

Locality	Specimen	Clay	Hornblende	Feldspar	Mica	Rock Fragment	Opaque	Quartz
Graphite Peak	R2060	34.8	0.6	2.8	0.8	35.2	2.2	23.6
Mount Crean	R1938	49.2	0.6	1.2	6.6	3.8	0.0	38.6
Wybung Head	R1667	30.8	0.0	0.6	0.0	61.8	5.4	1.4

The claystone breccia here is stratigraphically near the top of the Permian Weller Coal Measures, overlain by 21 cm of gray carbonaceous siltstone and then massive sandstones of the overlying Feather Conglomerate (Askin *et al.* 1971; Retallack *et al.* 1997). A shift to lower isotopic values of organic carbon ($\delta^{13}C_{org}$) at the level of the claystone breccia suggests that this is the Permian-Triassic boundary and that the uppermost meter of Weller Coal Measures here is earliest Triassic in age (Krull 1998).

The claystone breccia from the Permian-Triassic boundary at Mt Crean is dominated by opaque claystone clasts rich in organic matter, like those in underclays of the underlying Weller Coal Measures. These probably came from erosion of local swamp soils. Other grains in the breccia include quartz granules, hornblende grains, and books of vermiculite (table 2). Large mafic grains include weathering rinds and inflation into books reflecting a period of weathering, presumably in soils of local granitic basement rocks of a hilly source land. The chemical composition of the claystone breccias indicates a relatively modest level of chemical weathering (tables 3 and 4), comparable to that found in paleosols of the Weller Coal Measures (Krull 1998). This also is indicated by their clay mineral composition, largely illite, with small amounts of smectite (Retallack *et al.* 1998a).

Table 3. Major element chemical composition of Permian-Triassic boundary breccias in Antarctica and Australia

Paleosol	Specimen	SiO_2	TiO_2	Al_2O_3	Fe_2O_3	FeO	MnO	MgO	CaO	Na_2O	K_2O	P_2O_5	LOI	Total
Graphite Peak	R2060	64.02	0.82	17.82	3.62	0.13	0.05	0.89	1.53	0.17	2.56	0.06	8.68	100.30
Mount Crean	R1938	30.78	0.80	13.32	<0.01	0.75	<0.01	0.23	0.34	<0.01	2.66	<0.03	49.27	98.17
Wybung Head	R1667	44.46	2.07	23.93	0.40	0.0	0.0	0.14	0.04	0.10	0.19	0.01	28.74	100.09

Note: Analyses are from inductively coupled plasma-atomic fusion by Bondar Clegg Inc, Vancouver. Errors were estimated from standards of 1989 CANMET SY-3 and CANMET SO-2 for ICP.

Table 4. Trace element chemical composition of Permian-Triassic boundary breccias in Antarctica and Australia

Location	Specimen	Ba	Cr_2O_3	Nb	Rb	Sr	Y	Zr	$g.cm^{-3}$
Graphite Peak	R2060	455	200	13	167	119	43	341	2.31
Mount Crean	R1938	946	200	18	119	70	45	274	-
Wybung Head	R1667	129	90	20	8	21	60	380	2.36

Note: Bulk density was calculated by weighing clods coated in paraffin of known bulk density (0.8639) in and out of water at the University of Oregon, Eugene, by Evelyn Krull. Chemical analyses as for table 3.

The claystone breccia at Graphite Peak (85° 2.99'S 172° 21.65'E) is a distinctive light olive bed overlying the last thick coal seam of the Buckley Formation and forming the base of the first green paleosol (Dolores pedotype) of the Fremouw Formation (figure 2B). In this case, carbon isotopic chemostratigraphy, palynology, paleobotany and vertebrate paleontology all provide supporting evidence that this claystone breccia at the formation boundary is also at the Permian-Triassic boundary (Retallack *et al.* 1998a). At a second area cleared of scree some 200 meters to the west, both the claystone breccia and coal are replaced by a thin (13 cm) vein of microspherulitic prehnite presumably emplaced with local Ferrar Dolerites (Retallack, 1999b).

Unlike the claystone breccia at Mt. Crean, the one at Graphite Peak is dominated by claystone clasts that show evidence of weathering in a non-swampy environment (tables 1 and 2). This includes non-carbonaceous claystones with wispy intersecting streaks of highly birefringent oriented clays of the kind that soil micromorphologists call climobimasepic plasmic fabric (figure 3B). Other grains have relict crystal outlines and appear to be volcanic rock fragments more or less weathered to clay (figure 3B). Both types of grains are common in paleosols of the underlying Permian Buckley Formation (especially Molly and Morton pedotypes, Retallack *et al.* 1998b). Their degree of chemical weathering is not great (tables 3 and 4), as indicated by alkali and alkaline earth content and by their illite-smectite composition (Retallack *et al.* 1998a). These observations also support the idea of a greater contribution of calcalkaline volcanics to this claystone breccia than the one at Mt. Crean.

Claystone breccias at Wybung Head in Australia have been described in comparable detail elsewhere (Retallack 1999a). Let it suffice to say that these breccias differ in provenance and degree of weathering from those at both Mt. Crean and Graphite Peak. The Australian claystone breccias reflect derivation from a mountainous metamorphic source and soils that were more deeply weathered chemically than those from Antarctica. The lack of chemical and mineralogical uniformity in these claystone breccias indicates that they do not represent parts of a widely distributed ejecta blanket from a single impact crater. The common thread to all three sites is inclusion of granule-sized fragments of local soils and minerals in a thin but persistent bed.

A tempting explanation for these breccias is that they represent a lag deposit at a major geological disconformity widely assumed to exist in Antarctica (Collinson *et al.*

1994). But such lag deposits consist of much larger grains of the most chemically resistant minerals available, such as quartz, chert, and siderite nodules. These are common constituents in both Permian and Triassic paleochannel-basal conglomerates at these localities, so were available to armor disconformities. In contrast, the dominance of clay granules is distinctive. The most similar modern analog in my experience is material delivered to creeks from soil erosion following clear cutting in Oregon. Granule size (2-10 mm) is common for clayey peds in the surface horizon of forested soils. Such an explanation gains force from the shape of the carbon-isotopic perturbation at these sites, which is gradual over several meters (Krull 1998) as in marine sequences assumed to be complete, and distinct from abrupt shifts seen in disconformable marine sequences such as that of the Canning Basin of Western Australia (Morante 1996). Additional arguments for completeness of the Permian-Triassic boundary sequence at Wybung Head in Australia come from palynology, sequence stratigaphy, and radiometric dating (Retallack 1999a), but few of these arguments can yet be applied effectively to the imperfectly known antarctic sections.

Although claystone breccias at the Permian-Triassic boundary in Antarctica and Australia appear to record a remarkable short-term soil destabilization following abrupt extinction of *Glossopteris* swamp forest, the search for possible impact debris in them should not be abandoned (Retallack *et al.* 1998a). This note is intended to draw attention to these rocks in the hope that additional occurrences in Antarctica and Australia will be reported and studied.

References

Askin, R.A., Barrett, P.J., Kohn, B.P. and McPherson, J.G., 1971. Stratigraphic sections of the Beacon Supergroup (Devonian and older(?) to Jurassic) in south Victoria Land. *Antarctic Data Series, Victoria University of Wellington* 2:88 p.

Collinson, J.W., Isbell, J.L., Elliot, D.H., Miller, M.F. and Miller, J.M.G., 1994. Permian-Triassic Transantarctic Basin. In: J.J. Veevers and C.Mc.A. Powell (eds.), Permian Triassic Pangean Basins and Foldbelts along the Panthalassan marine of Gondwanaland. *Geological Society of America Memoir* 184:173-222.

Krull, E.S., 1998. Paleoenvironmental and carbon isotopic studies ($\delta^{13}C_{org}$) from terrestrial and marine strata across the Permian-Triassic boundary in Antarctica and New Zealand. Unpublished PhD thesis, University of Oregon, 208 p.

Retallack, G.J., 1999a. Post-apocalyptic greenhouse paleoclimate revealed by earliest Triassic paleosols in the Sydney Basin, Australia. *Geological Society of America Bulletin* 111(1): 52-70.

Retallack, G.J., 1999b. A Jurassic prehnite vein intruding the Permian-Triassic boundary at Graphite Peak, Antarctica. *Antarctic Journal,* 30(5): 5-7.

Retallack, G.J., Veevers, J.J. and Morante, R., 1996. Global early Triassic coal gap between Late Permian extinction and Middle Triassic recovery of peat-forming plants. *Geological Society of America Bulletin* 108(2): 195-207.

Retallack, G.J., Krull, E.S. and Robinson, S.E., 1997. Permian and Triassic paleosols and paleoenvironments of southern Victoria Land, Antarctica. *Antarctica Journal,* 30(5): 33-36.

Retallack, G.J., Seyedolali, A., Krull, E.S., Holser, W.T., Ambers, C.A. and Kyte, F.T., 1998a. Search for evidence of impact at the Permian-Triassic boundary in Antarctica and Australia. *Geology* 26:979-982.

Retallack, G.J., Krull, E.S. and Robinson, S.E., 1998b. Permian and Triassic paleosols and paleoenvironments of the central Transantarctic Mountains, Antarctica. *Antarctica Journal,* 31(5): 29-32.

Alluvial architecture of the Feather Conglomerate, southern Victoria Land

Gregory J. Retallack, *Department of Geological Sciences, University of Oregon*

Massive fluvial sandstones commonly are interpreted as deposits of braided streams but can also be produced by meandering streams when the sediment accumulation rate is so low that channels rework most of the clayey overbank. The distinction between braided and meandering stream sandstones can be difficult, as illustrated by past study of the Early Triassic Feather Conglomerate of southern Victoria Land. Ballance (1977) interpreted it as a deposit of meandering streams, whereas Collinson *et al.* (1994) and Barrett and Fitzgerald (1985) proposed that it was deposited by low-sinuosity braided streams. A new approach to resolving these interpretive difficulties uses paleosols (Retallack 1990), which may be strongly developed between paleochannels of meandering streams but are weakly developed in braidplains (figure 1).

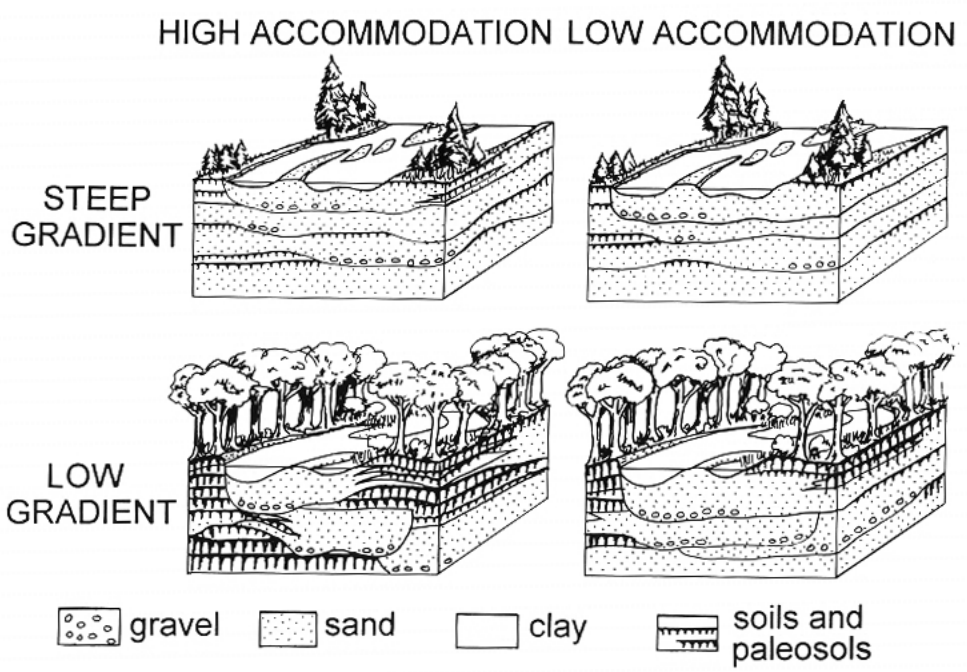

Figure 1. Four alternative alluvial architectures created by meandering and braided streams under different regimes of tectono-eustatic accommodation space (from Retallack 1990, with permission from Unwin Hyman).

During fieldwork in the central Allan Hills (76^{o} 42.2' 159^{o} 44.4'E), a detailed stratigraphic section was measured and its paleosols sampled for laboratory study (Retallack *et al.* 1997). In addition, a small part (175-202 m of Retallack *et al.* 1997) of the near-perfect exposures of the middle Feather Conglomerate was mapped to show lateral variation in sandstone and paleosol distribution (figure 2). This revealed several places where clayey units with moderately to strongly developed paleosols were

truncated by cut banks of fluvial paleochannels (figure 3). None of the cuts extend much below the shaley paleosols and were presumably prevented from further downcutting by the water table, which would not have been much farther down within these grey, little-oxidized paleosols. The cut banks are littered with claystone breccia derived from erosion of paleosols at the bank.

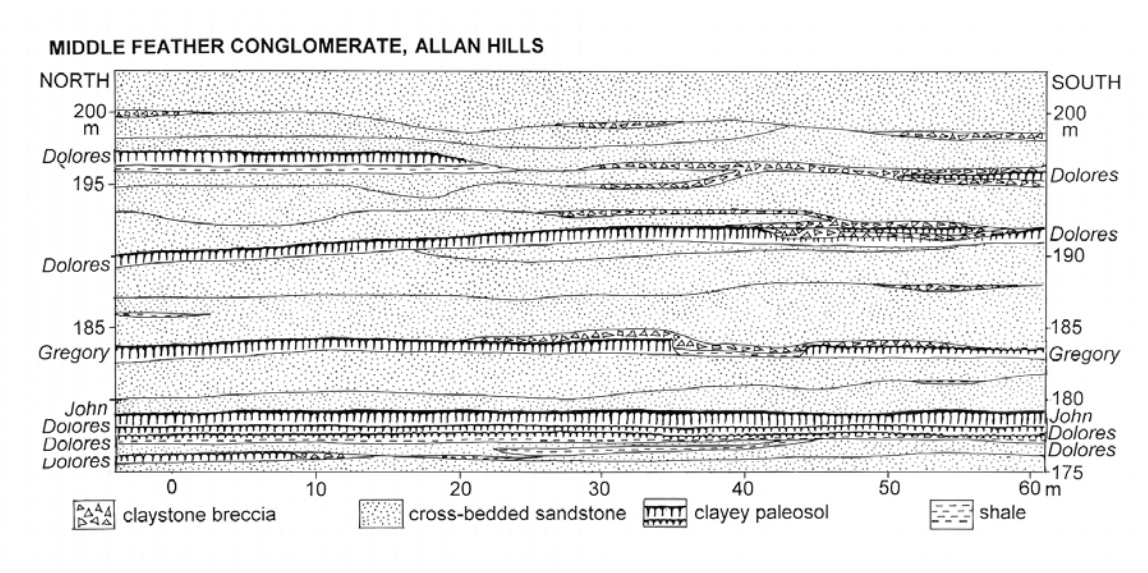

Figure 2. A scale drawing of the relationship between paleosols and channel sandstones in the middle Feather Conglomerate of the central Allan Hills (175-202 m of Retallack et al. 1997). Depth of the tick pattern on paleosols indicates degree of paleosol development, and in some cases strong development.

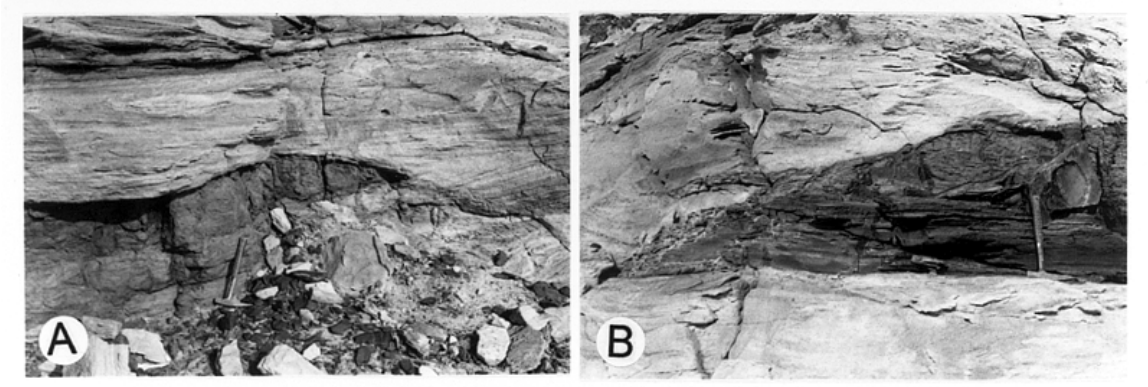

Figure 3. Erosionally truncated shaley paleosols in the middle Feather Conglomerate in the Allan Hills, southern Victoria Land. View A is at 176 m to the right in figure 2. View B is at the same stratigraphic level 20 m to the north of figure 2. Hammers give scale.

Paleosols of the Feather Conglomerate in the Allan Hills include sandy profiles riddled with *Skolithus* burrows (Edwin pedotype), weakly developed silty profiles with green chloritic nodules (Dolores), moderately developed profiles with distinctive columnar jointing (Gregory), and strongly developed paleosols with clay-enriched subsurface horizons (Retallack *et al.* 1997). Comparably developed paleosols have been

found in the Feather Conglomerate elsewhere in southern Victoria Land (Barrett and Fitzgerald 1985).

These observations of cut banks (figure 3) and of strongly developed paleosols (figure 2) support the interpretation of Ballance (1977) that the middle Feather Conglomerate in the Allan Hills was deposited by periodically-avulsing meandering streams under a tectono-eustatic regime of low accommodation space (figure 1).

These conclusions do not apply to the lower Feather Conglomerate in the Allen Hills, with its remarkable bioturbation by *Skolithus* and scattered very weakly developed clayey paleosols (Susanne pedotype of Retallack *et al*. 1997). Both observations are evidence of periodic sedimentary reworking of all of the floodplain as in a fluvial braidplain (Clemente and Perez-Arlucea 1993).

The upper Feather Conglomerate in the Allan Hills presents another case again because fine-grained interbeds and paleosols there consist only of premineralised peats and cherty paleosol fragments associated with fossil log rafts (Retallack 1997), comparable to occurrences in the stratigraphically-correlative Fremouw Formation of the central Transantarctic Mountains (Taylor *et al.* 1989). These indicate floodplains stable for hundreds of years, as opposed to thousands of years for the middle Feather Conglomerate and tens of years for the lower Feather Conglomerate paleosols. An intermediate model of loosely-sinuous and sparsely-interconnected channels in a regime of low tectono-eustatic accommodation in the upper Feather Conglomerate is also indicated by the thickness (3-9 m) of paleochannel sandstones.

The question of whether this sequence of lower, then higher, then lower accommodation space through the depositional history of the Feather Conglomerate is due to changes in subsidence rates or relative sea level is best addressed by comparison with the downstream portion of this enormous Gondwanan drainage basin in the Sydney Basin of Australia (Collinson *et al.* 1994). The lower Feather Conglomerate accumulated at the same time as the lower Narrabeen Group, during prolonged low sea level following basal Triassic marine transgression (Retallack *et al.* 1998). The middle Feather Conglomerate examined here (figures 2 and 3) was deposited at the same time as upper Narrabeen Group and the highest sea level of the Early Triassic (Retallack 1998). The uppermost Feather Conglomerate can be correlated using palynology with the Hawkesbury Sandstone, a remarkably high-energy braidplain deposit from a time of low sea level (Conaghan 1980; Retallack and Alonzo-Zarza 1996). Thus observed variation in accommodation space during deposition of the Feather Conglomerate is understandable in terms of changes in sea level rather than changes in tectonic subsidence or gradients.

References

Ballance, P.F., 1977. The Beacon Supergroup in the Allan Hills, central Victoria Land, Antarctica. *New Zealand Journal of Geology and Geophysics,* 20(6):1003-1016.

Barrett, P.J. and P.G. Fitzgerald. 1985. Deposition of the lower Feather Conglomerate, a Permian braided river deposit in southern Victoria Land, Antarctica, with notes on the regional paleogeography. *Sedimentary Geology,* 45(1/2):189-208.

Clemente, P. and M. Perez-Arlucea, . 1993. Depositional architecture of the Cuerda del Pozo Formation of the extensional Cameros Basin, north central Spain. *Journal of Sedimentary Petrology,* 63(3): 437-452.

Collinson, J.W., J.L. Isbell, D.H. Elliot, M.F. Miller, and J.M.G. Miller.1994. Permian-Triassic Transantarctic Basin. In J.J. Veevers and C.McA. Powell (eds.), Permian Triassic Pangean Basins and Foldbelts along the Panthalassan margin of Gondwanaland. *Geological Society of America Memoir* 184:173-222.

Conaghan, P.J. 1980. The Hawkesbury Sandstone: gross characteristics and depositional environment. In C. Herbert and R. Helby (eds.), A guide to the Sydney Basin. *New South Wales Geological Survey Bulletin,* 26:188-253.

Retallack, G.J. 1990. *Soils of the past.* Unwin Hyman, London, 521 p.

Retallack, G.J. 1997. Permian and Triassic driftwood from the Allan Hills, Antarctica. *Antarctic Journal of the United States,* 30(5):37-39.

Retallack, G.J. 1998. Discussion: Sequence stratigraphic analysis of Early and Middle Triassic alluvial and estuarine facies in the Sydney Basin, Australia. *Australian Journal of Earth Sciences* 45:653-655.

Retallack, G.J., E.S Krull, and S.E. Robinson. 1997. Permian and Triassic paleosols and paleoenvironments of southern Victoria Land, Antarctica. *Antarctic Journal of the United States,* 30(5): 33-36.

Retallack, G.J., A. Seyedolali, E.S. Krull, W.T. Holser, C.A. Ambers, and F.T., Kyte.1998. Search for evidence of impact at the Permian-Triassic boundary in Antarctica and Australia. *Geology,* 26(11): 979-982.

Retallack, G.J., and A.M. Alonso-Zarza.1996. Middle Triassic paleosols and paleoclimate of Antarctica. *Journal of Sedimentary Research,* 68(1): 169-184.

Taylor, E.L., T.N. Taylor, and J.W. Collinson. 1989. Depositional setting and paleobotany of Permian and Triassic premineralized peat from the central Transantarctic Mountains, Antarctica. *International Journal of Coal Geology* 12:657-679.

Uranium-234/ Thorium-23O dates of lacustrine carbonates at Lake Vida: Implications for the radiocarbon reservoir effect

Brenda L. Hall, *Institute for Quaternary Studies and Department of Geological Sciences, University of Maine, Orono, Maine and Department of Geology and Geophysics, Woods Hole Oceanographic Institution, Woods Hole, Massachusetts*

Gideon M. Henderson, *Department of Earth Sciences, Oxford University, United Kingdom*

Surficial geologic mapping indicates that lakes in the McMurdo Dry Valleys region of Antarctica have been much larger in the past than they are today. As most of these lakes exist in closed basins, a history of their water-level variations has paleoclimatic significance. A precise chronology for lacustrine sediments is the first step toward resolving this paleoclimate history. At present, the chronology hinges on radiocarbon dates of algae and carbonates. However, one potential problem is that CO_2 in the lake water may not have been in equilibrium with atmospheric CO_2, leading to a ^{14}C reservoir effect and erroneously old ^{14}C dates.

McMurdo Dry Valleys lakes may be susceptible to a ^{14}C reservoir effect because of perennial ice cover and, in many cases, strong stratification, both of which inhibit mixing. In addition, some lakes are proglacial and may receive old CO_2 from glacial meltwater. Despite the potential for problems, Doran et al. (1999) recently showed that algae living in the nine seasonally open moats on deltas yield modern ages and hence do not suffer from a ^{14}C reservoir effect. However, there are few data concerning the ^{14}C reservoir of deeper levels of the lakes. The available data suggest that it may range up to 10,000-15,000 years (Doran et al. 1999; Hendy et al. 1977).

Here, we present the first systematic use and comparison of thermal-ionization mass spectrometry (TIMS) uranium-thorium and accelerator mass spectrometry (AMS) radiocarbon dating of biogenically precipitated lacustrine carbonates in the McMurdo Dry Valleys for purposes of determining the former lake-bottom reservoir effect. We collected samples of algae and coprecipitated carbonate from the north shore of Lake Vida in Victoria Valley (figure 1). At the time these carbonates formed, Lake Vida was at least 20 meters above its present level but substantially lower than its last glacial maximum (LGM) highstand.

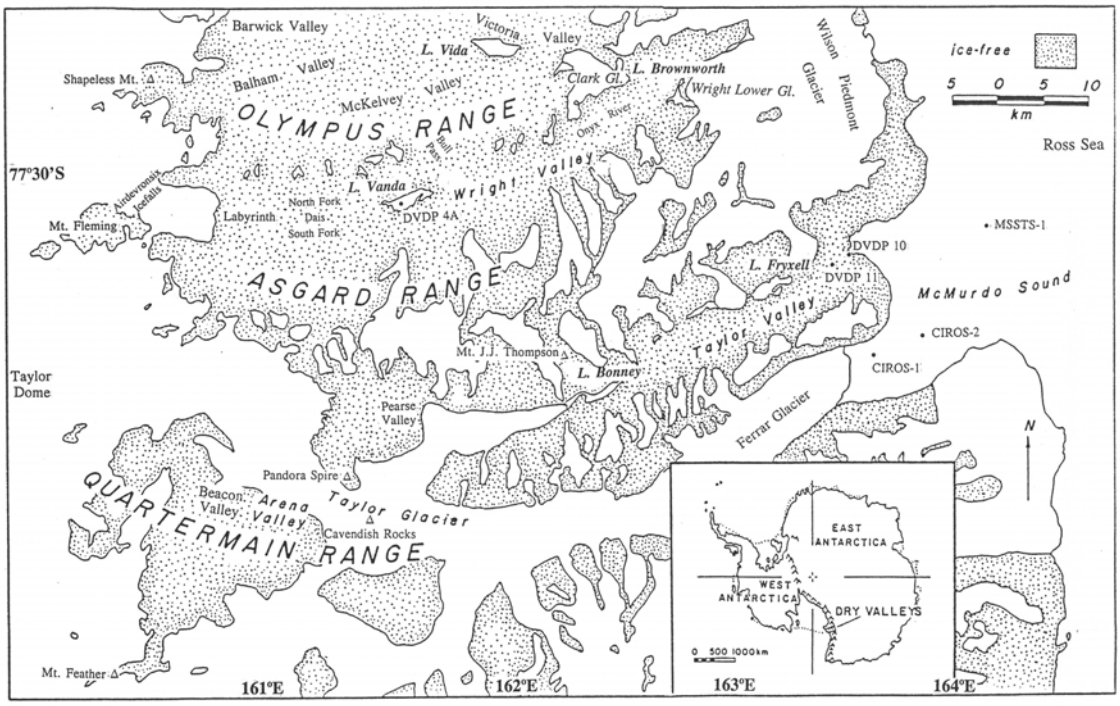

Figure 1. Index map showing the location of Lake Vida.

Over 50 algae and carbonate samples were dated by the AMS radiocarbon method. Twenty-one carbonates and one sample of algae also were dated by the TIMS Uranium-234/Thorium-230 ($^{234}U/^{230}Th$) disequilibrium method (Edwards et al. 1986). Based on radiocarbon ages that ranged from about 11,000 to 11,500 ^{14}C-years before present, all samples were assumed to be coeval. The varying percentage of detrital material within the carbonates afforded us an opportunity to construct U/Th isochron plots, both of which are linear, reinforcing our assumption that the samples are coeval (figure 2). Data from these plots indicate an initial $^{232}Th/^{230}Th$ of 232,000 ± 34,000. This value is typical of average upper crust material and shows that the samples do not contain significant quantities of authigenic or lake-water-derived ^{230}Th. The initial $d^{234}U$ is 734 ± 4, demonstrating the importance of alpha-recoil processes in controlling stream and lake-water uranium isotopes in this arid environment. The isochron yields an age of 9,547 ± 338 calendar years before present (2 sigma error; Ludwig and Titterington 1994).

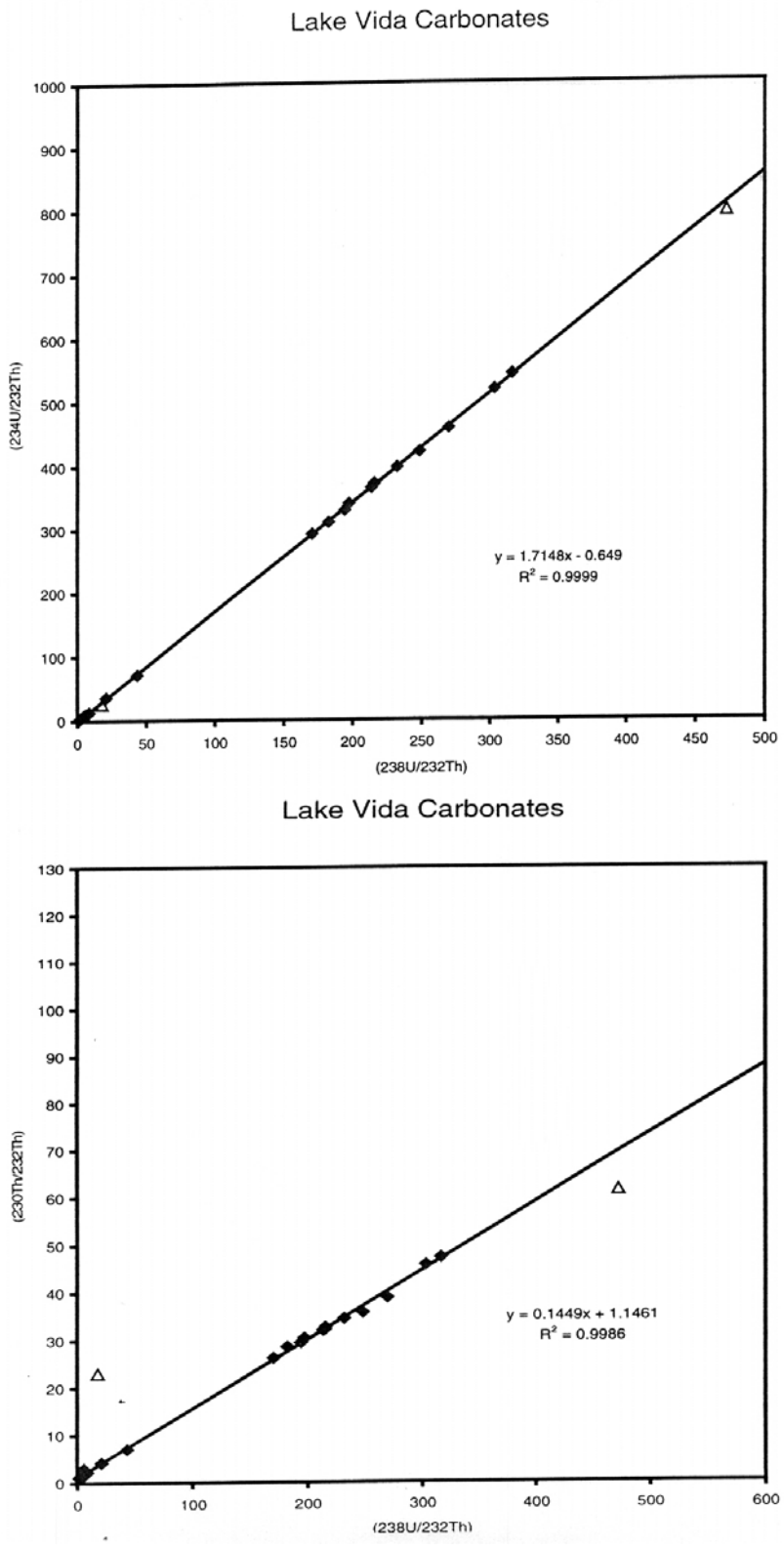

Figure 2. Rosholt-type isochron plots of the activity ratios of $^{230}Th/^{232}Th$ vs. $^{238}U/^{232}Th$ and $^{234}U/^{232}Th$ vs. $^{231}U/^{232}Th$ used to calculate the age of Lake Vida carbonates. Two of the 21 samples (triangles) clearly fall off the line and are not included in the age calculation.

Comparison of this age with radiocarbon ages [converted to calendar years using the Calib 4.2 program (http://depts.washington.edu/qil/calib/)] of the same samples yields an average offset of about 3,400 years, which is believed to be the ^{14}C reservoir age of Lake Vida bottom waters about 9,550 years ago. We suggest that this offset is due to perennial ice cover and perhaps to strong stratification of the water column, both of which would hinder mixing and CO_2 exchange. These data confirm work by Hendy et al. (1977) and Doran et al. (1999), suggesting the presence of a significant reservoir effect for deep-water lacustrine sediments, and allow the reservoir effect to be quantified. These results also show that the TIMS U-Th disequilibrium method can be used successfully to date lacustrine carbonates in the McMurdo Dry Valleys region.

This work was supported by the Office of Polar Programs of the National Science Foundation. B. Overturf assisted in the field. Uranium-thorium dating was carried out while the first author was a visiting postdoctoral scientist in the Department of Earth Sciences, Oxford University and an external postdoctoral fellow at Lamont-Doherty Earth Observatory.

References

Doran, P.T., G.W. Berger, W.B. Lyons, R.A. Wharton, M.L. Davisson, J. Southon, and J.E. Dibb. 1999. Dating Quaternary lacustrine sediments in the McMurdo Dry Valleys, Antarctica: *Palaeogeography, Palaeoclimatology, Palaeoecology,* 147: 223-239.

Edwards, R.L., J.H. Chen, and G.J. Wasserburg. 1986. ^{238}U-^{234}U-^{23O}Th-^{232}Th systematics and the precise measurement of time over the past 500,000 years. *Earth and Planetary Science Letters, 81: 175-192.*

Hendy, C.H., A.T. Wilson, K.B. Popplewell, and D.A. House. 1977. Dating of geochemical events in Lake Bonney, Antarctica, and their relation to glacial and climate changes. *New Zealand Journal of Geology and Geophysics,* 20: 1103-1122.

Ludwig, K.R., and D.M. Titterington. 1994. Calculation of $^{230}Th/U$ isochrons, ages, and errors. *Geochimica et Cosmochimica Acta,* 58: 5031-5042.

Antarctic mapping, geodesy, GIS and the U.S. Antarctic Resource Center (USARC)

Tony K. Meunier, and Jerry L. Mullins, *National Mapping Division,*

U.S. Geological Survey, Reston Virginia 20192

The National Science Foundation (NSF), through the U.S. Geological Survey (USGS), conducts geodesy and mapping in Antarctica. During the 1997-1998 season, the USGS's National Mapping Division (NMD) concentrated on antarctic mapping and geodetic activities using global positioning system (GPS) mapping control for topographic and satellite image mapping. In addition, the USGS manages the United States Antarctic Resource Center (USARC) as the U.S. official depository for U.S. Antarctic mapping reference material.

Antarctic geodetic field programs support national and international research in defining the Earth's geoid and to provide the basis for spatial reliability in producing accurate maps. The ability to obtain accurate horizontal and vertical positions using GPS is now available to the scientific community for accurately mapping their disciplines surficial data. Recently, the Scientific Committee on Antarctic Research (SCAR) working group on Geodesy and Geographic Information recommended the use of GPS satellite surveying technology to tie previously obtained conventional survey networks to a common Earth-centered datum. Accuracies attainable using the GPS can be used in monitoring deformation of the solid Earth, variations in sea level and tides, ice sheet dynamics, ionospheric change, the geodynamics of the Antarctic and its adjoining tectonic plates.

The 1997-1998 USGS NMD field team included William J. Smith, Robert P. Glover, Jerry L. Mullins, Michael L. Prentice (University of New Hampshire), Jean-Claude Thomas and James D. Williams (National Oceanic and Atmospheric Administration/National Geodectic Survey). The USGS continued its geodetic program to determine the relative motions of bedrock in the Transantarctic Mountains of southern Victoria Land to validate models for predicting tectonism. This effort of investigator Larry Hothem (Mullins, et al 1997) and others is also improving the accuracy of models for change in global sea level. The geodetic scientists from the USGS, in cooperation with geophysicists and geologists from Byrd Polar Research Center, Ohio State University, occupied 23 sites where rock-based monuments were placed in the Transantarctic Mountains Deformation (TAMDEF) project, including new sites at Beaufort and Franklin Islands. Most of the sites are located along the Transantarctic Mountains within helicopter range of McMurdo Station. Accuracies at the millimeter level of vertical and horizontal motion between bedrock points are being determined by use of dual-frequency, high-quality GPS receiver systems. Combined with the "precise" ephemerides provided by the International GPS for Geodynamics System (IGS), the USGS in cooperation with NOAA/NGS established absolute gravity values to improve the gravity model of the region.

The USGS geodetic survey personnel in coordination with the University Navstar Consortium (UNAVCO) ran permanent GPS continuously operating reference stations (CORS) at McMurdo. The station collects highly accurate geodetic data for use by the geodetic and scientific community to improve the accuracy of GPS field mapping activities that would otherwise require time-consuming site visits and stateside post processing of data.

Thirteen GPS geodetic control stations were established in support of the Satellite Image mapping program. This control is being used to rectify five 100,000-scale satellite image maps using Landsat images, one 1:250,000-scale Landsat Thematic Mapper (TM) mosaic of the South Ross Sea region, and fifty 1:25,000-scale satellite image maps of McMurdo Dry Valley region. The 50 quadrangles are products created by merging Landsat TM data with Systeme Probatoire d'Observation de la Terra (SPOT) panchromatic data.

In January 1998, the USGS conducted a GPS geodetic survey to establish the actual position of true geographic South Pole. Based on this season's observations and data from previous surveys, the team determined that the ice sheet at Amundsen-Scott Pole Station is moving towards the northwest at 9.98 meters per year. The USGS installed a permanent brass geodetic marker identifying the 1997-98 austral summer position.

The USGS NMD manages the United States Antarctic Resource Center at the USGS National Center in Reston, Virginia. The ARC is the official U.S. depository of antarctic maps, charts, publications, geodetic control and approximately 450,000 mostly black and white prints and negatives which constitutes all U.S. antarctic aerial mapping photography since the United States Antarctica Service Expedition (1939-41). It is also the depository of all material received from the other Antarctic Treaty nations as part of a Standing Resolution for the Exchange of Information between countries. In addition, the USARC is the depository for the NSF archival collection of antarctic slides, photographs, and videos.

The USGS's antarctic mapping program is producing 1:50,000-scale topographic maps for areas in the McMurdo Dry Valleys. The mapping is being conducted in cooperation with Land Information New Zealand. Under this cooperative program, the USGS obtains the aerial photographs, establishes the geodetic control, and performs the aerotriangulation. New Zealand performs the stereo compilation, collects digital cartographic data, prepares shaded relief, and provides color separates. The USGS print the maps. These 1:50,000-scale, 15-minute topographic maps have 50-meter contour intervals and 25-meter supplemental contours using the World Geodetic System-84 (WGS84) geodetic datum. The maps include existing and new place names approved by the U.S. Board on Geographic Names. Five maps covering part of the Royal Society Range were published in 1993, and seven additional maps were published in 1998.

Dr. Cheryl Hallam (NMD) continues to provide GIS support to the antarctic scientific community and has begun an *Atlas of Antarctic Research*, which is accessible on the USGS Website at http://usarc.usgs.gov/antarctic_atlas/. The McMurdo Dry Valley region GIS, extending from the Convoy Range to the Upper Skeleton Neve uses the 1:50,000-scale digital satellite images as the base map. Mr. Angel Gonzalez at the

Antarctic Resource Center developed and maintained the USARC Webpage at http://usarc.usgs.gov/.

The USGS continues to manage antarctic geographic names using the computer-based geographic names information system (GNIS), which are available through the USGS Antarctic Geographic Names Website http://mapping.usgs.gov/www/gnis/antform.html.

These programs were funded by National Science Foundation grant OPP 91-14787.

References

Mullins, J., L. Hothem and C. Hallam, 1997, *Antarctic geodesy and mapping:* Antarctic Journal of the United States, 32(5), p.209-210.

Mullins, Jerry L., 1994, *The global positioning system, surveying, aerial photography, and mapping program of the United States in* Antarctica: Antarctic Journal of the United States, 29(5), p. 44-45.